UNIVERSITY OF CALIFORNIA
RIVERSIDE

Stirred Suspension Culture for Scalable Production and Differentiation of Human Pluripotent Stem Cells

A Dissertation submitted in partial satisfaction
of the requirements for the degree of

Doctor of Philosophy

in

Bioengineering

by

Daniel Pareza Nampe

March 2017

Dissertation Committee:
Dr. Hideaki Tsutsui, Chairperson
Dr. Nicole zur Nieden
Dr. Prudence Talbot

The Dissertation of Daniel Nampe is approved:

_____

_____

_____

Committee Chairperson

University of California, Riverside

ACKNOWLEDGEMENTS

I would like to use this page to extend my deepest appreciation to the many people who made this work and my development in the program a success.

First, I would like to express my sincere gratitude to my advisor and mentor, Dr. Hideaki Tsutsui. I am extremely grateful that he took a chance on me despite the lack of training I had in the field. He taught me how to be meticulous and critical in my research so that I may produce quality results. He encouraged me to keep moving forward in my research and allowed me to grow as a research scientist. His knowledge and mentorship was paramount in providing me with the necessary skills to be independent. Without his guidance, support and patience, this dissertation and my success in the program would not have been possible, and for this, I am truly grateful.

I would also like to show gratitude to my committee members, Dr. Nicole zur Nieden and Dr. Prue Talbot.

I am deeply indebted to Dr. zur Nieden for being tremendously supportive throughout my time as a graduate student. She is encouraging, insightful, and honest, and it is because of that I know I need to present her quality work, and she expected no less of me. I can honestly say without her intellectual contributions and collaborative effort from her lab group, I would not have been able to propel my research and provide the work I present in this dissertation.

I am also deeply thankful to Dr. Talbot for serving as a committee member and a mentor through my qualifying exam. She gave me the opportunity to be a contributor to the Stem Cell Core training course and the Inland Empire Stem Cell Consortium organizing

committee. Her support, encouragement and expertise have influenced me to be a more well-rounded stem cell researcher and for that I am grateful.

I would also like to give special thanks to Dr. Hyle Park in the Department of Bioengineering. Dr. Park was my more than my graduate student advisor, but the first person that supported me through the fire and not letting me slip through the crack. I am very thankful for everything he did because I would not be here without his help.

In addition, I would like to thank Kevin Keller for his collaborative support. His contribution was the key to the success of this dissertation. Also, to my undergrads Ronak Joshi, Josh Karam, and Maribel Gonzalez, I am very grateful for all of their time and efforts into helping me. I wish you all the best in your endeavors.

To my lab colleagues Carlos Castro, Brent Kalish, and Jessica Wen. The respect I have for them is due to their amazing attitude, intelligence and willingness to lend a hand. It was truly an honor to work with you all and I am grateful for the bond that we developed throughout the years. Also, to all of my first-year colleagues in Bioengineering, thank you for making the start of graduate school more enjoyable. In particular, I would like to thank Soroush, Harry, Zied, Leo, Dieanira, Karen, and Lauren for their support and keeping me sane through the adventures that we had. My attitude and experience in graduate school would not have been as fulfilling without them. I would also like to thank Dr. Duncan Liew and Maria Valle for their invaluable contributions to my work.

Lastly, I would like to give special thanks to Dr. Steve Mullen. He was my supervisor and first mentor before graduate school. It was through his guidance, encouragement, and support that I wanted to pursue a higher education.

DEDICATION

This dissertation is dedicated to my family.

To my beloved parents, thank you for always supporting me and being the epitome of a hard worker. Most of all, thank you for sacrificing so much just for a better life.

To my grandparents, thank you for always believing in me.

To my five sisters, thank you for the support and for giving me patience.

To my nieces and nephews, I hope this will inspire you to try and do more than what is expected from us.

To all of my cousins, thank you for always being there. We have never moved.

Haganup do tarpatupa ahu marhiteihon bana na margogohi ahu. Horas!

ABSTRACT OF THE DISSERTATION

Stirred Suspension Culture for Scalable Production and Differentiation of Human Pluripotent Stem Cells

by

Daniel Pareza Nampe

Doctor of Philosophy, Graduate Program in Bioengineering
University of California, Riverside, March 2017
Dr. Hideaki Tsutsui, Chairperson

The success of human pluripotent stem cells (hPSCs) as a source of future cell therapies hinges in part on the availability of a robust scalable culture system that can readily produce clinically relevant number of cells and their derivatives. Stirred suspension culture has been identified as one of such promising platforms due to its ease of use, scalability, and widespread use in the pharmaceutical industry (e.g., CHO cell-based production of therapeutic proteins) among others. However, culture of undifferentiated hPSCs in stirred suspension is a relatively new development in the past several years, and little is known beyond empirically optimized culture parameters. The goal of this study was to elucidate the impact of fluidic agitation on hPSCs in stirred suspension culture. In particular, we systematically investigated various agitation rates to characterize their impact on cell yield, viability, and maintenance of pluripotency. Additionally, we closely examined the

distribution of cell aggregates and how the observed culture outcomes are attributed to their size distribution. Our results showed that moderate agitation maximized the propagation of hPSCs by controlling the cell aggregates below the critical size, beyond which the cells suffer from diffusion limitation, while limiting cell death caused by excessive fluidic forces. Furthermore, we observed that fluidic agitation could regulate not only cell aggregation, but also expression of some key signaling proteins in hPSCs. Upon discovering this mechanosensitive effector enabled a novel approach for linking expansion and cardiac differentiation to generate over 90% cardiomyocytes. In addition, these cardiomyocytes displayed highly organized sarcomere structure which suggests an improved maturation in their morphology. Altogether, results presented in this study indicate the new possibility of guiding stem cell fate determination by fluidic agitation in stirred suspension cultures.

Table of Contents

List of Tables

List of Figures

CHAPTER 1:

INTRODUCTION

Recent development in human pluripotent stem cells (hPSCs) culture, including embryonic stem cells (hESCs) and induced pluripotent stem cells (iPSCs), has the potential to revolutionize the fields of tissue engineering and regenerative medicine. The importance of hPSCs lies in their capability to self-renew indefinitely while retaining their pluripotent capacity to form into any derivatives from all three germ layers: ectoderm, mesoderm, and endoderm [1-3]. This unique characteristic is the reason why many regard these cells to be the most versatile and promising renewable cell source for cell-based therapy, disease modeling, and drug discovery and screening (Figure 1.1) [4-6]. However, bringing their promising potential closer to clinical relevance is met with many challenges. At the forefront of these challenges is the strategy to deliver a clinically relevant quantity of hPSC-derivatives [7]. The issue is partly due to the lack of a robust, scalable and cost-effective culture system that could readily meet the demands of anticipated clinical applications [8].

For clinical applications, providing a particular number of high-quality cells is of utmost importance. The number of cells needed depends on the specific application, which can range from 10^5 to 10^9 specialized cells [8, 9]. For cell-based therapy, treatment to target diseases such as myocardial infarction, type I diabetes, and hepatic failure, would require transplantation of approximately 10^9 cardiomyocytes [9], insulin-producing β-cells [10],

and hepatocytes [11], respectively. Treatments for Parkinson's disease, Stargardt's macular dystrophy, and age-related macular degeneration will require at least 10^5 cells [12, 13]. The simplest strategy to produce such large number of specialized cells is first to exploit the self-renewal capacity of hPSCs and expand the undifferentiated population to such a high degree before differentiation towards a functional derivative. However, given the relatively low efficiency and cell yield of *in vitro* differentiation, not to mention *in vivo* survival of transplanted cells, supplying high-quality hPSC-derivatives on the order of $10^8 – 10^{10}$ could be necessary to satisfy the requirements of many cell-based therapies [14]. Consequently, expanding and maintaining undifferentiated hPSC culture would require a culture platform with greater scalability and reproducibility.

To date, 2D monolayer culture systems are the gold standard and most widely used method for the expansion of hPSCs. However, this approach may not be ideal for the mass production of hPSCs and their derivatives. Nevertheless, it is through the discovery from 2D monolayer cultures that have given researchers insight to controlling hPSCs' fate and enabled an alternative solution for a more scalable culture platform in 3D suspension systems. As such, we will briefly discuss key developments in monolayer systems that have led to the discovery of a multifaceted network that controls hPSC culture outcomes.

Development of hPSC Cultures in 2D Monolayer System

Since the discovery of hESCs, 2D monolayer systems have been widely used to support the growth and pluripotent characteristics of these cells. Initially, the best condition for self-renewal and maintenance of pluripotency were on mouse embryonic fibroblasts (MEF) feeder layers (Figure 1.2Ai) [1]. However, the use of MEF feeder layers presents a risk for clinical applications because feeder-cells can be a source of pathogens for hPSCs. Therefore, the need for a feeder-free system has led to using specific extracellular matrix (ECM) to facilitate the attachment and growth of hPSCs. Matrigel is an animal-derived basement membrane matrix and was the first development of a feeder-free system that is still one of the most commonly used adherent substrates for hPSC cultures to date (Figure 1.2Aii). Matrigel is comprised of various ECM proteins, proteoglycans, and undefined growth factors harvested from the Engelbreth–Holm–Swarm mouse sarcoma cells [15-17]. Unfortunately, similar to MEF feeder layers, Matrigel cannot be used for clinical applications due to safety concerns with xenogeneic components comprised in the substrate. As such, researchers have focused on developing a more defined xeno-free growth substrates from humanized protein mixture, peptide–polymer conjugate, recombinant protein, or polymeric substrates (Figure 1.2Aiii & 1.2Aiv) [18-22]. Nevertheless, such advances towards a feeder-free and xeno-free growth substrate would be impractical if the culture medium does not meet the same stringent requirement. For this reason, considerable efforts have also focused on developing a defined growth medium to truly eliminate xenogeneic elements for the ultimate goal of using hPSCs for biomedical purposes.

The growth medium is an essential component in hPSC culture. The first development of growth medium typically included fetal bovine serum (FBS) and MEF-conditioned medium (MEF-CM), undefined secretory growth factors from MEF-feeder cells [17, 23]. In the past decade, researchers have identified key growth factors such as Activin A, Nodal, and FGF-2, to support the propagation of undifferentiated hESCs and establish a better-defined culture medium [24, 25]. The most significant development for a more defined culture medium was in 2006, when Thomson and colleagues developed the most widely published and recognized feeder-free growth medium, mTeSR1 [26, 27]. The formulation of mTeSR1 is a complex combination of soluble factors and chemical signals to support the continuous expansion and long-term maintenance of hPSCs (Figure 1.2B). Although not completely free of xenogeneic elements, mTeSR1 is a powerful growth medium that has been successfully demonstrated to support hundreds of hPSC lines in many different parts of the world. More recently, Thomson and colleagues further improved their chemically defined growth medium by developing the Essential 8 (E8) medium, which is a derivative of the mTeSR1 but contained only the essential eight components without the addition of both serum albumin and β-mercaptoethanol [28, 29]. The development of this growth medium has become the gold standard to support hPSCs maintenance in various culture platforms.

Besides the ECM and soluble factors, the cellular microenvironment is also an important component that is worth consideration in hPSC cultures. In 2D monolayer cultures, it was found that environmental cues such as the physiological environment and physical forces could also influence hPSC fate decision for apoptosis, self-renewal or

differentiation. For instance, hPSCs are typically cultured under standard normoxic conditions (37°C, pH of 7.4, and 20% oxygen tension). But a study suggests that hPSC culture performs much better in an environment that recapitulates embryonic development such as low oxygen tension (hypoxia, 2-6% oxygen). The study reports that hPSCs self-renewal was enhanced while the likelihood of spontaneous differentiation and chromosomal abnormalities decreased in long-term cultures [30]. Similarly, numerous reports have also indicated that physical cues and stimulation, which mimic early developmental stages, are known to be a critical factor for hPSC fate determination [31]. For instance, physical cues such as fluid shear or tensile and compressive strain via surface modification could have a significant impact on hPSC culture outcome (Figure 1.2C) [32-34]. We will discuss more on how such forces influence stem cell physiology and molecular mechanisms in chapter 2. Nevertheless, these environmental factors have been extensively studied in 2D monolayer cultures, and these studies have provided great insight into regulating hPSCs' behavior *in vitro*.

Monolayer-based strategies have given researchers a foundation to control the stem cell's unique properties to yield a promising product for clinical benefits. However, there are still many challenges ahead in bridging the gap between research discoveries and therapeutic applications. For instance, improving differentiation efficiency for the desired cell type, maintaining long-term genetic stability, ensuring higher purity of clinical grade cells, and attaining scalability for mass production are some issues that need to be resolved before widespread clinical use. Fortunately, research in these aspects is in full swing, but

the limited scalability of 2D monolayer cultures is one major challenge that may not be addressed easily.

Limitation of 2D Monolayer Cultures for Scalable hPSC Bioprocesses

Monolayer cultures of hPSC have evolved quickly over the last decade to a point where many protocols have been established for the propagation and direct differentiation of hPSCs to a variety of cell lineages such as, but not limited to, hPSC-derived cardiomyocytes, pancreatic β-cells, hepatocytes and motor neurons. A number of these established protocols still depend on monolayer-based strategies for cell expansion and differentiation, but for scaling up to produce large numbers of specialized quality cells, monolayer-based strategies themselves could be the limiting factor for a more rapid implementation of hPSC-derived products [35]. Monolayer-based systems are known for its lack of scalability because the process to produce large cell number is achieved by increasing the 2D surface area for growth. Therefore, for hPSC cultures, surface enlargement also require an increase in candidate growth substrate as well as culture flask to accommodate the attachment and propagation of hPSCs without compromising their pluripotent characteristics [36]. Consequently, processing of many culture flasks in order generate large cell number would be time-consuming, labor intensive and an expensive process (Figure 1.3) [37]. Not to mention that the candidate growth substrate should be defined, xenogeneic-free, and serum-free for safer use in clinical applications [36]. Although such substrates have been commercially developed for safer use in clinical applications, Celiz et al. report that the cost of using these candidate substrates to produce

1 billion hPSCs alone is expensive (Table 1.1) [38]. In addition, despite considerable efforts in developing an inexpensive polymer substrate to reduce material cost, synthetic growth substrates still have significant limitations in production and cost for scalable manufacturing process [38]. These limitations present a bottleneck for 2D monolayer cultures to succeed as a real working platform for clinical-scale productions.

3D Suspension Cultures Enable Scalable Production of hPSCs

Alternatively, 3D suspension cultures provide a more promising scalable platform for the mass production of hPSCs than 2D monolayer-based systems [35]. What makes suspension methods more suitable for large-scale production is that 3D systems are not restricted to a 2D surface area to accommodate the propagation of cells [36]. Therefore, production of hPSCs could be scaled-up in volume with relative ease, as opposed to scaling out to multiple culture flasks [37]. Also, discoveries from 2D monolayer systems have benefited greatly for 3D suspension cultures, such as the use of growth medium and ECM substrates to support self-renewal and maintenance of pluripotency of hPSCs in suspension. Over the past decade, a variety of 3D suspension culture methods have been successfully established to facilitate the survival of cells in suspension: Cells immobilized on microcarriers [39-41], microencapsulation of cells [42-44], or self-aggregated hPSCs spheroids (Figure 1.4A) [45-47]. Also, these methods could be cultured under static suspension or various forms of dynamic suspension cultures including rotary orbital shakers, slow-turning lateral vessels (STLV), or spinner flask/tank bioreactors to name a few (Figure 1.4B). There is no standard approach to culturing hPSCs in 3D suspension

because every method has its benefits and pitfalls. Therefore, an understanding of the features in each culture method would provide us with some insight into its practical applications in generating large quantities of cells at a reasonable cost.

Microcarriers are small spherical particles that facilitate attachment of anchorage-dependent cells to be grown in suspension (Figure 1.4Ai). Although typically kept in suspension by stirring or other dynamic mechanisms, microcarriers enable a simple process to control cellular aggregation of hPSCs. The carriers enhance surface area attachment to volume ratio and allow options for different coating matrices or porous properties to improve hPSC expansion without compromising their differentiation potential [48, 49]. However, limitations of this approach are the material cost needed to optimize microcarriers with specific matrices and porous properties as well as additional labor for the cell-carrier separation process. Also, the shear stress experienced by the cells in dynamic microcarriers culture is a concern and will require additional studies to understand the cell's response to the hydrodynamic environment and physical properties of the microcarrier.

The development of microencapsulation technology enables a strategy to tightly control cell clump size and still provide a high surface-to-volume ratio for cell growth (Figure 1.4Aii). Microencapsulation also protects the cells from excessive shear force related damage in dynamic suspension systems and could facilitate an integrated strategy for expansion with cryopreservation of hPSCs [43]. One study has successfully demonstrated this integrated process and has reported a recovery rate greater than 70%

after cryopreservation [50]. The biomaterial to encapsulate the cells could also be engineered to improve culture performance as well as reproducibility. However, the physical properties of encapsulation allow limited flexibility to monitor the cell growth or characterize molecular diffusion inside the capsule. Notably, similar to microcarriers, the cost associated with the biomaterial and process to harvest the cells by decapsulation are some shortcomings of this method.

Without the use of microcarriers or encapsulation, hPSCs could adhere together and form free-floating cell aggregate spheroids (Figure 1.4Aiii). This default aggregate formation is vital for the survival and growth of hPSCs in suspension. Typically, the 3D spherical structure comprised of hPSCs is known as embryoid bodies (EBs). In this discussion, we characterize EBs as cell aggregate spheroids undergoing spontaneous differentiation in suspension [51], whereas hPSCs aggregates are the 3D spherical structure where the cells maintain their undifferentiated and pluripotent state [45]. Culturing hPSCs as aggregates allow the cells to retain their high differentiation efficiency because the 3D cell-cell contact is preserved to sustain endogenous signaling within the cell aggregate [35]. In recent years, aggregate cultures have been successfully demonstrated to enable the long-term expansion of hPSCs without the need of costly substrates and microcarriers to maintain their pluripotent characteristics in suspension [36]. However, controlling the aggregate size and preventing excessive agglomeration are common issues that could significantly affect the culture outcome [52]. To minimize agglomeration, hPSCs aggregates cultured in dynamic suspension systems have proved to be more effective in producing uniform aggregate size and improve cell production yield than static suspension

conditions [47]. Unfortunately, similar to microcarriers, the lack of knowledge in how the hydrodynamic shear force effects hPSC self-renewal or lineage determination is a concern that leads to many uncertainties in controlling the culture outcome.

Although each method has its own benefits and shortcomings that need to be addressed, the high surface-to-volume ratio in 3D suspension cultures enables a scalable platform for meeting the ultimate goal of generating clinically relevant quantities of cells with relative ease. Ultimately, the development of a fully automated and controllable bioprocess systems will be required for the industrial scale-up production of cells. Stirred tank bioreactors have been the standard for chemical engineering and bioprocessing industries because of the numerous flexibility to fully automate, monitor and control specific culture parameters. Also, using the hPSCs aggregate approach, and integrating the process for expansion with differentiation in stirred suspension culture would be the simplest, cost-effective and ideal method for the scalable production of hPSCs and their derivatives (Figure 1.5). However, in order for stirred-tank bioreactors to be considered as a viable alternative for stem cell bioprocessing, understanding the impact of hydrodynamic conditions on stem cell physiology is one major issue that needs to be addressed for future development.

Benefits and Drawbacks of Aggregate Suspension Culture of hPSCs

In the past few years, studies on hPSCs aggregates cultured in stirring vessels have shown great results in generating a large number of cells for future applications. In fact,

across various reports, stirred suspension cultures proved to be more effective in the expansion of undifferentiated hPSCs than static suspension conditions [36]. Static suspension culture is often subject to agglomeration, whereby individual aggregates clump together in a stochastic manner and form large clusters that result in an increase in growth rates variability, apoptosis, and heterogeneity [53-55]. On the other hand, spinner flasks and stirred-tank bioreactors apply agitation via impeller to induce fluid motion and assure sufficient mixing of chemicals and dissolved gasses in the culture media. Indeed, applying agitation was beneficial to minimize agglomeration and heterogeneous growth conditions, thereby promoting higher cell yield as previous reports indicate. The question now arising is how the hydrodynamic shear force imparted by fluid agitation affects hPSCs in regards to controlling the culture for survival, self-renewal, or directed differentiation in dynamic suspension systems.

At present, there is a lack of consensus for the optimal growth conditions in stirred suspension protocols. For instance, the optimal agitation rate for the expansion of hPSCs often varies from one system to another [56, 57]. The main reason for this is due to the complexity of hydrodynamic motions present in different designs of the culture vessels. Therefore, tailoring protocols for specific purposes is difficult because the key parameters that control the culture outcome have not yet been fully understood [58]. Development of analytical technologies such as particle-image-velocimetry (PIV) measurements (Figure 1.6A) and computational fluid dynamics (CFD) (Figure 1.6B) have at least provided a quantitative characterization on how the hydrodynamic forces, such as fluid shear, could affect the cells in dynamic suspension cultures [59, 60]. From these studies, it was found

that the magnitude of shear stress could spatially vary 10-100 times within the culture vessel. Also, internal fluid friction known as eddy viscosity (μ_T) can also have a significant impact on the local shear stress the cells experienced in culture [61]. Thus, drawing comparisons from separate studies to establish a standard optimal protocol presents a challenge in itself because the complexity of hydrodynamic forces depends on the specific culture parameters (e.g. medium properties, agitation rates, and inoculation density) and the design of the vessel.

How hPSCs respond to the hydrodynamic environment is another key topic that requires more investigation. Specifically, knowledge of how the mixing conditions impact cells' survival, aggregation, and phenotype with respect to their signaling mechanisms will be extremely beneficial for a more standard approach to controlling the culture outcome of hPSCs in stirred suspension systems. Clearly, viability will depend on the thresholds of shear stress that the cells can tolerate. However, the aggregate size is also known to have an effect on the cells viability and phenotype. As such, there should be a fine balance between the mixing condition that is necessary for aggregation and to produce uniformed sized aggregates of a particular size while limiting excessive force-related cell death. More importantly, understanding of core signaling pathways and how they are influenced by suspension cultures is important for the control of hPSCs fate in stirred suspension systems (Figure 1.6C). Insight into signaling pathways that are modulated by fluidic agitation will provide huge implications to tailoring protocols for specific purposes. Altogether, it is expected that such knowledge will enable a more standardized process to controlling the culture outcome of hPSCs in stirred suspension systems.

Objective and Significance

Our long-term goal is to develop a scalable manufacturing culture system that can produce a clinically relevant number of hPSCs and its derivatives for clinical applications. For this reason, we explore how the dynamic fluid microenvironment impacts cellular responses manifested by the propagation, viability, aggregation and phenotype of hPSCs in stirred suspension cultures. Since these responses are inter-related and attributed by multiple parameters – such as medium properties, agitation rates, and inoculation density – we use the optimal growth medium for the propagation of hPSCs in suspension and focus on investigating the impact of different agitation rates on cellular responses of hPSCs. In addition, cellular responses of hPSCs are dictated by their signaling pathways, so we also evaluate possible molecular mechanisms that are modulated due to fluidic agitation. Our principle hypothesis is that hPSCs are sensitive to stirring-induced shear force, thereby altering signaling mechanisms to promote survival, self-renewal or differentiation. The basis of our hypothesis is from our literature study of micromechanical cues affecting hPSC regulation and fate (Chapter 2), and our preliminary data using a conventional spinner flask to assess the impact of fluidic agitation on hPSCs (Chapter 3). The rationale for the research is that, once candidate mechanosensitive signaling proteins governed by fluid agitation are identified, they can be leveraged to steer cell fate decisions along with or in place of chemical cues. Altogether, by gaining some insight into both cellular responses and molecular mechanism, we report the effective parameters to enhance the scalable production and differentiation of hPSCs in stirred suspension culture.

Table & Figures

I Table 1.1. Development of defined growth substrates for hPSC expansion in 2D monolayer cultures. Growth substrate, culture medium, and price of scalability are given to get an estimated total cost of producing 1 billion hPSCs. The estimated cost is based on (a & b) using 100 coated T75 flasks, (c) 150 kits to coat a sufficient number of 6-well plates, and (d) considering it to be equal to or more expensive than similar recombinant protein-based substrate such as StemAdhere. Adapted from Celiz et al., 2014 [38].

Growth Substrate	Culture medium	Cost/scalability	Cost per 10^9 hPSCs	Defined	Synthetic	Xeno-free
Matrigel	mTeSR1	$15 per T75	(a) ~$1,500			
Synthemax (peptide-polymer conjugate)	X-VIVO 10, 80 ng/ml hrbFGF, 0.5 ng/ml hrTGF-β	$380 per 10 mg $80 per 6-well plate $100 per T75 $295 per T225	(b) ~$10,000	x	x	x
StemAdhere (recombinant E-cadherin)	mTeSR1	$100 per kit $22 per 0.5 mg	(c) ~$15,000	x	x	x
Peptide-SAM (synthetic peptide)	mTeSR1 + ROCKi	Expensive	(d) >$15,000	x	x	x

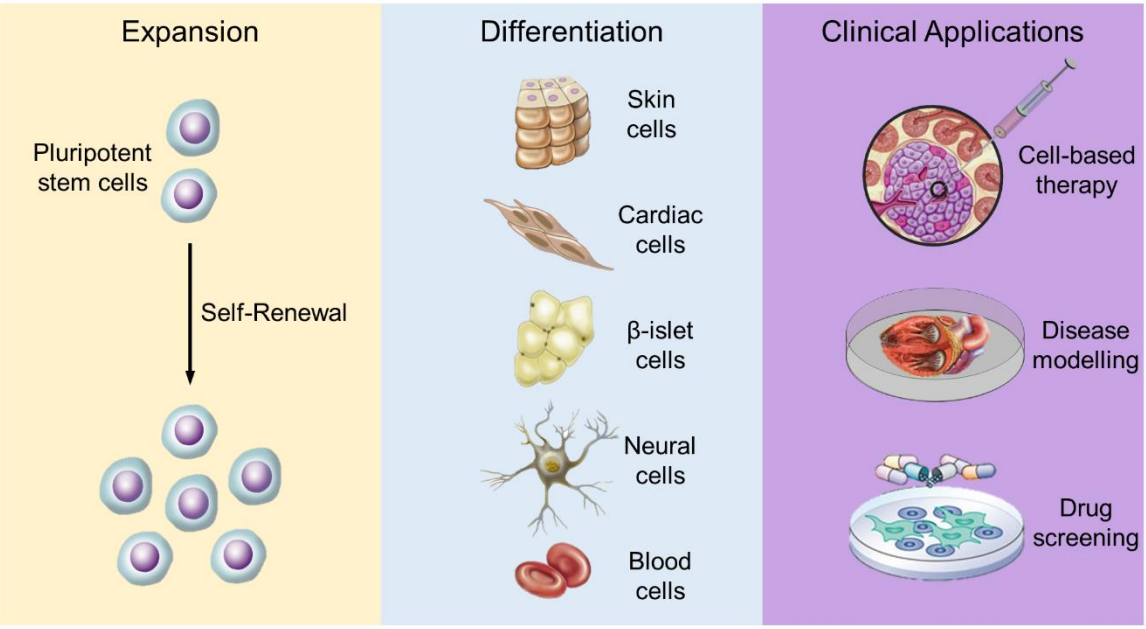

Figure 1.1. Overview of human pluripotent stem cells (hPSCs) bioprocess for clinical applications. Self-renewal capacity of hPSCs are first exploited for expansion to large numbers, followed by differentiation into specific functional derivatives, and lastly, clinical applications for cell-based therapy, disease modeling, and drug screening [63].

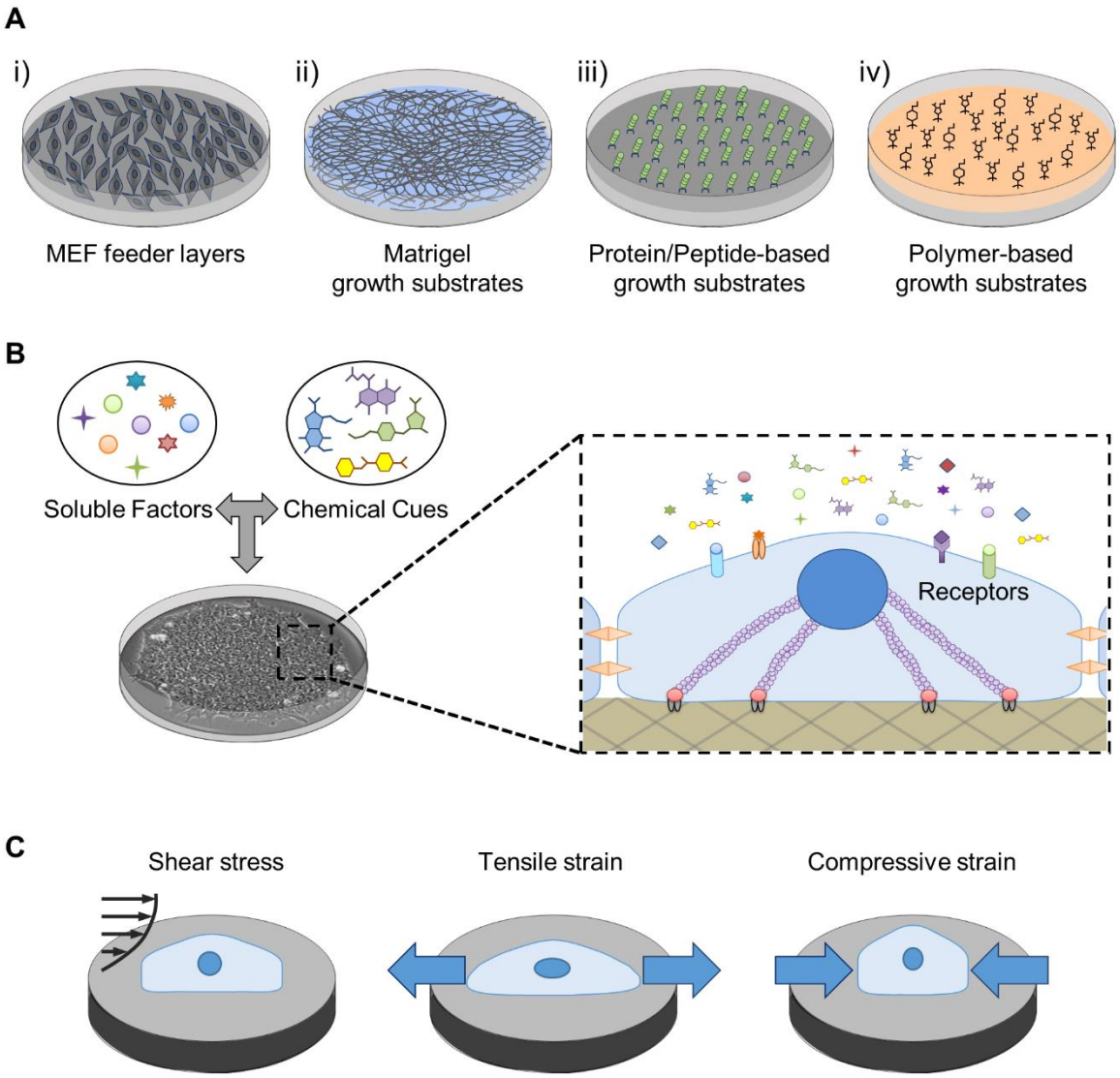

Figure 1.2. Development of 2D monolayer cultures of hPSCs. (A) The progress of growth substrates from (i) MEF feeder layers to (ii) Matrigel, (iii) Protein/peptide-based, and (iv) Polymer-based growth substrates. (B) Enacting soluble factors and chemical cues in culture media have paved the way to control hPSCs fate for optimal growth and differentiation. (C) Other cues such as mechanical stimulation in the microenvironment were also found to affect stem cell fate in 2D cultures.

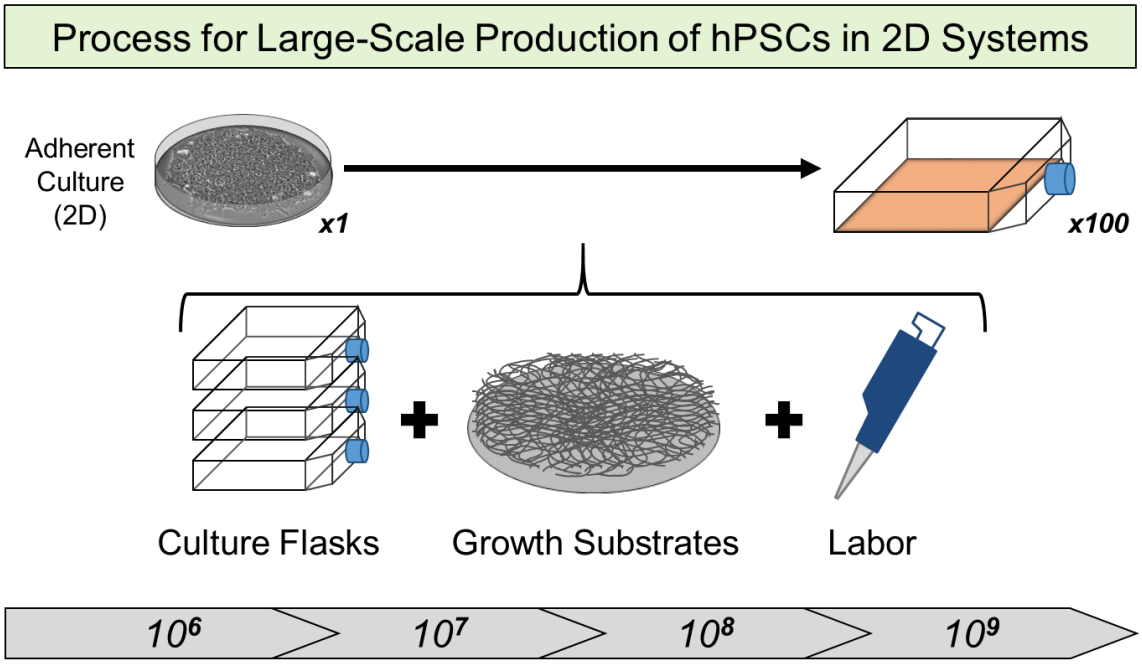

Figure 1.3. 2D process strategy to produce 1 billion hPSCs requires multiple culture flask coated with growth substrates and labor-intensive uptake and handling.

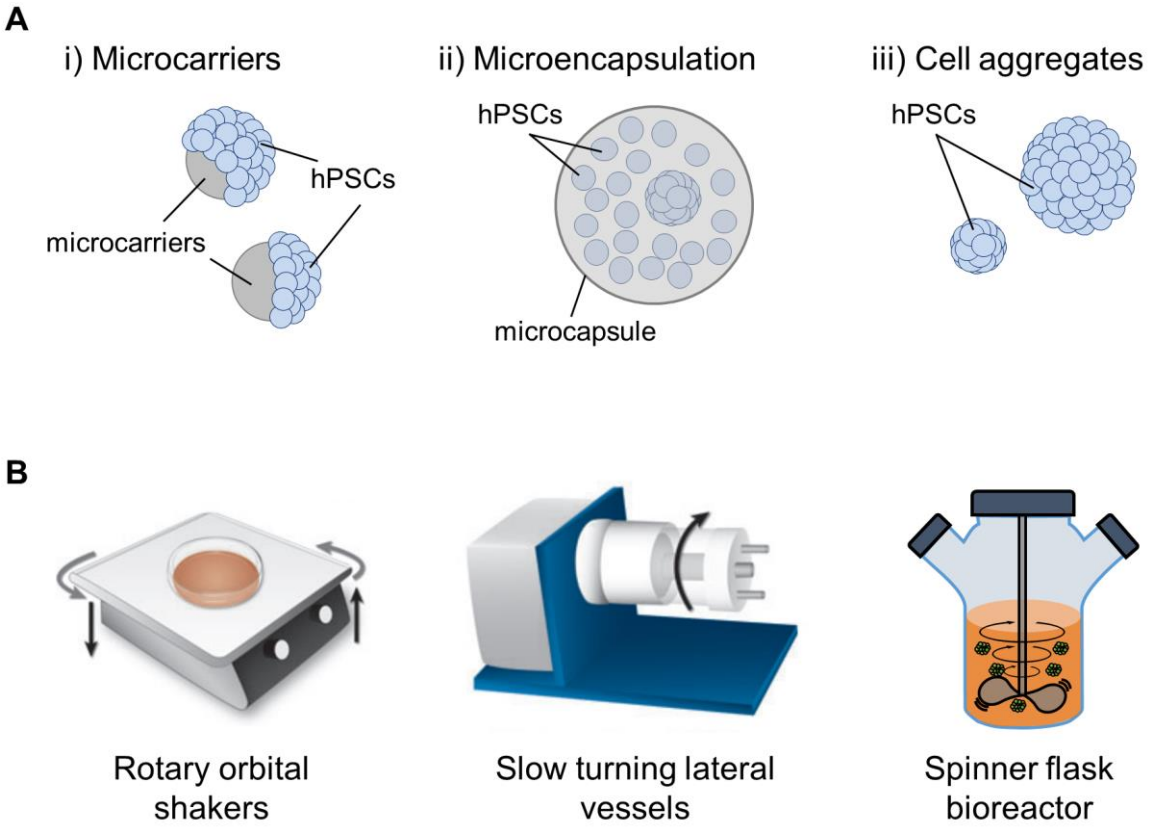

Figure 1.4. 3D suspension cultures enable the easily scalable production of hPSCs. (A) hPSCs could be cultured in suspension by i) microcarriers, ii) microencapsulation, or iii) as cell aggregates. Adapted from Serra et al., 2012 [35]. (B) These methods could also be cultured in various dynamic suspension platforms such as Rotary orbital shakers [62], slow turning lateral vessels [62], and spinner flask bioreactor.

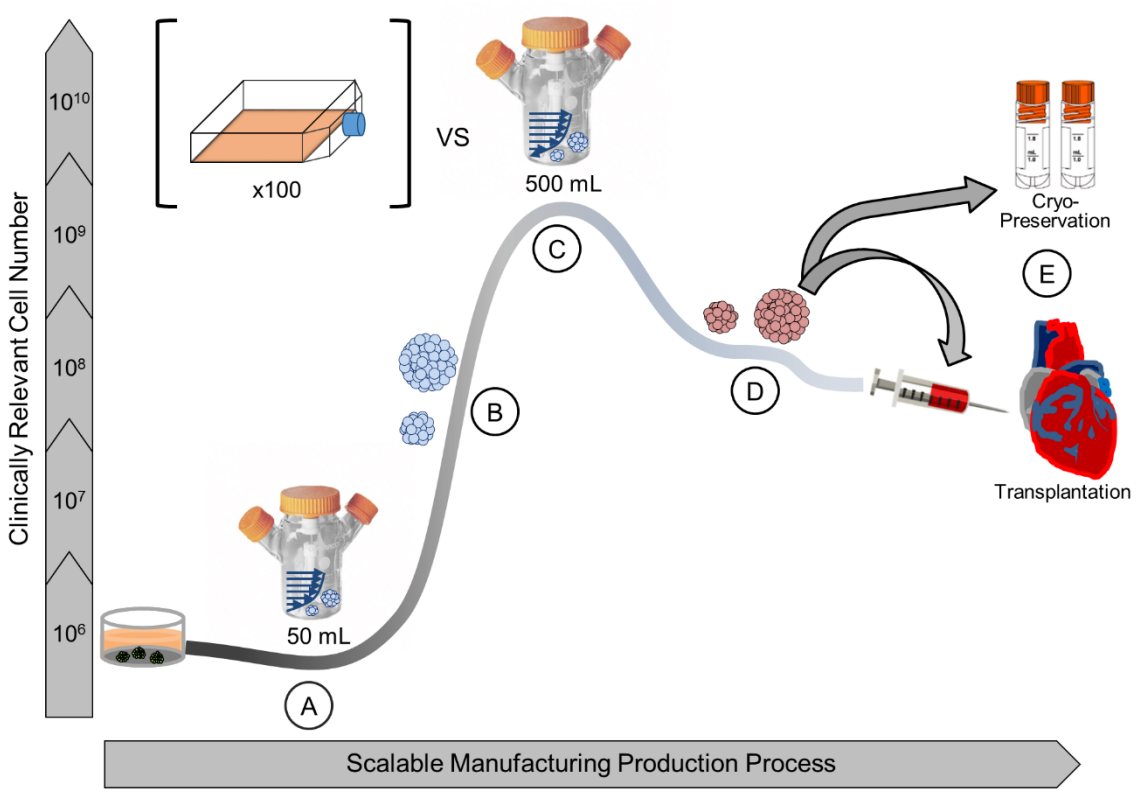

Figure 1.5. Overview of hPSC bioprocess strategy in 3D dynamic suspension culture vs. 2D monolayer based methods. (A) Transitioning from a monolayer to aggregate suspension culture using a spinner flask does not require costly substrates for growth. (B) Expanding hPSCs in suspension requires (C) scaling up in volume with relative ease. (D) Integrated process for hPSC expansion and differentiation will be extremely useful to (E) store and readily provide a large number of desired cell type for transplantation.

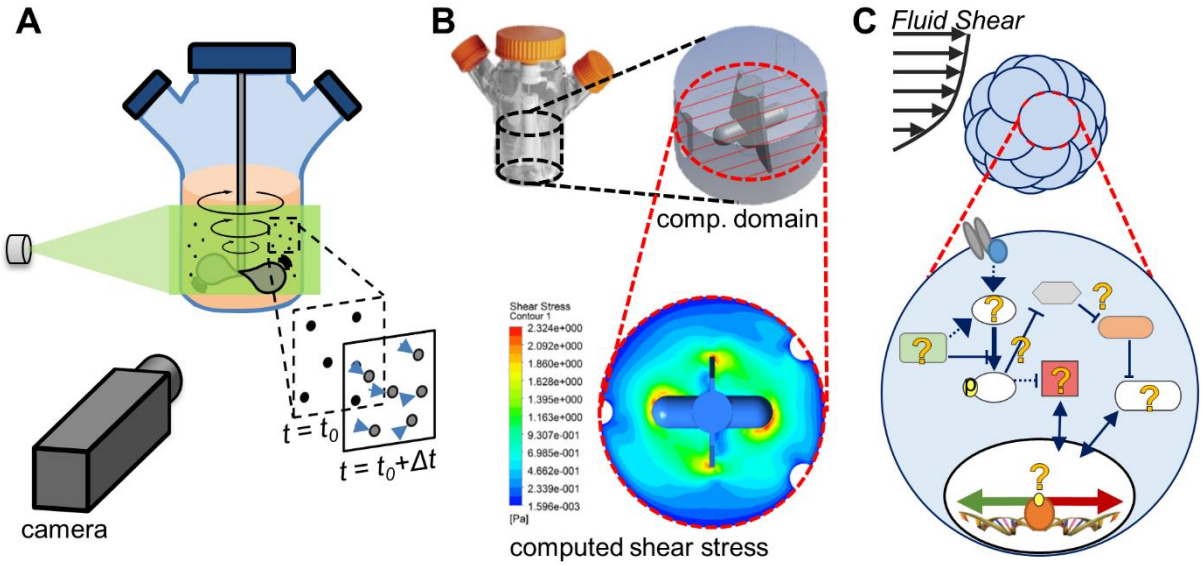

Figure 1.6. (A) PIV overview. Laser source and a cylindrical lens are used to create a thin illuminated image plane as the camera captures sequential images of moving particles in the fluid. (B) CFD could illustrate the flow characteristics and shear stress distribution at varying agitation rates. (C) Uncovering potential signaling pathways that are modulated by fluid shear in 3D dynamic suspension cultures.

References

1. Thomson, J.A., *Embryonic Stem Cell Lines Derived from Human Blastocysts.* Science, 1998. **282**(5391): p. 1145-1147.
2. Burdon, T., I. Chambers, C. Stracey, et al., *Signaling mechanisms regulating self-renewal and differentiation of pluripotent embryonic stem cells.* Cells Tissues Organs, 1999. **165**(3-4): p. 131-143.
3. Amit, M., M.K. Carpenter, M.S. Inokuma, et al., *Clonally derived human embryonic stem cell lines maintain pluripotency and proliferative potential for prolonged periods of culture.* Dev Biol, 2000. **227**(2): p. 271-8.
4. Sterneckert, J.L., P. Reinhardt, and H.R. Scholer, *Investigating human disease using stem cell models.* Nature Reviews Genetics, 2014. **15**(9): p. 625-639.
5. Robinton, D.A. and G.Q. Daley, *The promise of induced pluripotent stem cells in research and therapy.* Nature, 2012. **481**(7381): p. 295-305.
6. Saha, K. and R. Jaenisch, *Technical challenges in using human induced pluripotent stem cells to model disease.* Cell Stem Cell, 2009. **5**(6): p. 584-95.
7. Murry, C.E. and G. Keller, *Differentiation of embryonic stem cells to clinically relevant populations: Lessons from embryonic development.* Cell, 2008. **132**(4): p. 661-680.
8. Lipsitz, Y.Y., N.E. Timmins, and P.W. Zandstra, *Quality cell therapy manufacturing by design.* Nature Biotechnology, 2016. **34**(4): p. 393-400.
9. Segers, V.F. and R.T. Lee, *Stem-cell therapy for cardiac disease.* Nature, 2008. **451**(7181): p. 937-42.
10. Lock, L.T. and E.S. Tzanakakis, *Stem/Progenitor cell sources of insulin-producing cells for the treatment of diabetes.* Tissue Eng, 2007. **13**(7): p. 1399-412.
11. Tzanakakis, E.S., D.J. Hess, T.D. Sielaff, et al., *Extracorporeal tissue engineered liver-assist devices.* Annual Review of Biomedical Engineering, 2000. **2**: p. 607-632.
12. Lindvall, O. and Z. Kokaia, *Stem cells for the treatment of neurological disorders.* Nature, 2006. **441**(7097): p. 1094-6.
13. Dantuma, E., S. Merchant, and K. Sugaya, *Stem cells for the treatment of neurodegenerative diseases.* Stem Cell Research & Therapy, 2010. **1**.
14. Lei, Y. and D.V. Schaffer, *A fully defined and scalable 3D culture system for human pluripotent stem cell expansion and differentiation.* Proc Natl Acad Sci U S A, 2013. **110**(52): p. E5039-48.

15. Kleinman, H.K., M.L. Mcgarvey, L.A. Liotta, et al., *Isolation and Characterization of Type-Iv Procollagen, Laminin, and Heparan-Sulfate Proteoglycan from the Ehs Sarcoma.* Biochemistry, 1982. **21**(24): p. 6188-6193.

16. Vukicevic, S., H.K. Kleinman, F.P. Luyten, et al., *Identification of Multiple Active Growth-Factors in Basement-Membrane Matrigel Suggests Caution in Interpretation of Cellular-Activity Related to Extracellular-Matrix Components.* Experimental Cell Research, 1992. **202**(1): p. 1-8.

17. Xu, C.H., M.S. Inokuma, J. Denham, et al., *Feeder-free growth of undifferentiated human embryonic stem cells.* Nature Biotechnology, 2001. **19**(10): p. 971-974.

18. Mei, Y., K. Saha, S.R. Bogatyrev, et al., *Combinatorial development of biomaterials for clonal growth of human pluripotent stem cells.* Nature Materials, 2010. **9**(9): p. 768-778.

19. Miyazaki, T., S. Futaki, K. Hasegawa, et al., *Recombinant human laminin isoforms can support the undifferentiated growth of human embryonic stem cells.* Biochemical and Biophysical Research Communications, 2008. **375**(1): p. 27-32.

20. Villa-Diaz, L.G., H. Nandivada, J. Ding, et al., *Synthetic polymer coatings for long-term growth of human embryonic stem cells.* Nature Biotechnology, 2010. **28**(6): p. 581-583.

21. Braam, S.R., L. Zeinstra, S. Litjens, et al., *Recombinant vitronectin is a functionally defined substrate that supports human embryonic stem cell self-renewal via alpha V beta 5 integrin.* Stem Cells, 2008. **26**(9): p. 2257-2265.

22. Rodin, S., A. Domogatskaya, S. Strom, et al., *Long-term self-renewal of human pluripotent stem cells on human recombinant laminin-511.* Nature Biotechnology, 2010. **28**(6): p. 611-U102.

23. Amit, M., C. Shariki, V. Margulets, et al., *Feeder layer- and serum-free culture of human embryonic stem cells.* Biology of Reproduction, 2004. **70**(3): p. 837-845.

24. Li, Y., S. Powell, E. Brunette, et al., *Expansion of human embryonic stem cells in defined serum-free medium devoid of animal-derived products.* Biotechnology and Bioengineering, 2005. **91**(6): p. 688-698.

25. Vallier, L., M. Alexander, and R.A. Pedersen, *Activin/Nodal and FGF pathways cooperate to maintain pluripotency of human embryonic stem cells.* Journal of Cell Science, 2005. **118**(19): p. 4495-4509.

26. Ludwig, T.E., V. Bergendahl, M.E. Levenstein, et al., *Feeder-independent culture of human embryonic stem cells.* Nature Methods, 2006. **3**(8): p. 637-646.

27. Ludwig, T.E., M.E. Levenstein, J.M. Jones, et al., *Derivation of human embryonic stem cells in defined conditions.* Nat Biotechnol, 2006. **24**(2): p. 185-7.

28. Chen, G.K., Z.G. Hou, D.R. Gulbranson, et al., *Actin-Myosin Contractility Is Responsible for the Reduced Viability of Dissociated Human Embryonic Stem Cells.* Cell Stem Cell, 2010. **7**(2): p. 240-248.

29. Chen, G.K., D.R. Gulbranson, Z.G. Hou, et al., *Chemically defined conditions for human iPSC derivation and culture.* Nature Methods, 2011. **8**(5): p. 424-U76.

30. Ezashi, T., P. Das, and R.M. Roberts, *Low O-2 tensions and the prevention of differentiation of hES cells.* Proceedings of the National Academy of Sciences of the United States of America, 2005. **102**(13): p. 4783-4788.

31. Buxboim, A., I.L. Ivanovska, and D.E. Discher, *Matrix elasticity, cytoskeletal forces and physics of the nucleus: how deeply do cells 'feel' outside and in?* Journal of Cell Science, 2010. **123**(3): p. 297-308.

32. Nampe, D. and H. Tsutsui, *Engineered Micromechanical Cues Affecting Human Pluripotent Stem Cell Regulations and Fate.* Jala, 2013. **18**(6): p. 482-493.

33. Sun, Y., C.S. Chen, and J. Fu, *Forcing stem cells to behave: a biophysical perspective of the cellular microenvironment.* Annu Rev Biophys, 2012. **41**: p. 519-42.

34. DuFort, C.C., M.J. Paszek, and V.M. Weaver, *Balancing forces: architectural control of mechanotransduction.* Nat Rev Mol Cell Biol, 2011. **12**(5): p. 308-19.

35. Serra, M., C. Brito, C. Correia, et al., *Process engineering of human pluripotent stem cells for clinical application.* Trends Biotechnol, 2012. **30**(6): p. 350-9.

36. Chen, K.G., B.S. Mallon, R.D. McKay, et al., *Human pluripotent stem cell culture: considerations for maintenance, expansion, and therapeutics.* Cell Stem Cell, 2014. **14**(1): p. 13-26.

37. Jenkins, M.J. and S.S. Farid, *Human pluripotent stem cell-derived products: Advances towards robust, scalable and cost-effective manufacturing strategies.* Biotechnology Journal, 2015. **10**(1): p. 83-95.

38. Celiz, A.D., J.G.W. Smith, R. Langer, et al., *Materials for stem cell factories of the future.* Nature Materials, 2014. **13**(6): p. 570-579.

39. Fok, E.Y.L. and P.W. Zandstra, *Shear-controlled single-step mouse embryonic stem cell expansion and embryoid body-based differentiation.* Stem Cells, 2005. **23**(9): p. 1333-1342.

40. Nie, Y., V. Bergendahl, D.J. Hei, et al., *Scalable Culture and Cryopreservation of Human Embryonic Stem Cells on Microcarriers.* Biotechnology Progress, 2009. **25**(1): p. 20-31.

41. Phillips, B.W., R. Horne, T.S. Lay, et al., *Attachment and growth of human embryonic stem cells on microcarriers.* Journal of Biotechnology, 2008. **138**(1-2): p. 24-32.

42. Murua, A., A. Portero, G. Orive, et al., *Cell microencapsulation technology: Towards clinical application.* Journal of Controlled Release, 2008. **132**(2): p. 76-83.

43. Siti-Ismail, N., A.E. Bishop, J.M. Polak, et al., *The benefit of human embryonic stem cell encapsulation for prolonged feeder-free maintenance.* Biomaterials, 2008. **29**(29): p. 3946-3952.

44. Dang, S.M., S. Gerecht-Nir, J. Chen, et al., *Controlled, scalable embryonic stem cell differentiation culture.* Stem Cells, 2004. **22**(3): p. 275-282.

45. Steiner, D., H. Khaner, M. Cohen, et al., *Derivation, propagation and controlled differentiation of human embryonic stem cells in suspension.* Nat Biotechnol, 2010. **28**(4): p. 361-4.

46. Amit, M., J. Chebath, V. Margulets, et al., *Suspension culture of undifferentiated human embryonic and induced pluripotent stem cells.* Stem Cell Rev, 2010. **6**(2): p. 248-59.

47. Krawetz, R., J.T. Taiani, S.Y. Liu, et al., *Large-Scale Expansion of Pluripotent Human Embryonic Stem Cells in Stirred-Suspension Bioreactors.* Tissue Engineering Part C-Methods, 2010. **16**(4): p. 573-582.

48. Heng, B.C., J. Li, A.K.L. Chen, et al., *Translating Human Embryonic Stem Cells from 2-Dimensional to 3-Dimensional Cultures in a Defined Medium on Laminin- and Vitronectin-Coated Surfaces.* Stem Cells and Development, 2012. **21**(10): p. 1701-1715.

49. Chen, A.K.L., X.L. Chen, A.B.H. Choo, et al., *Critical microcarrier properties affecting the expansion of undifferentiated human embryonic stem cells.* Stem Cell Research, 2011. **7**(2): p. 97-111.

50. Serra, M., C. Correia, R. Malpique, et al., *Microencapsulation Technology: A Powerful Tool for Integrating Expansion and Cryopreservation of Human Embryonic Stem Cells.* Plos One, 2011. **6**(8).

51. Itskovitz-Eldor, J., M. Schuldiner, D. Karsenti, et al., *Differentiation of human embryonic stem cells into embryoid bodies compromising the three embryonic germ layers.* Mol Med, 2000. **6**(2): p. 88-95.

52. Singh, H., P. Mok, T. Balakrishnan, et al., *Up-scaling single cell-inoculated suspension culture of human embryonic stem cells.* Stem Cell Res, 2010. **4**(3): p. 165-79.

53. Valamehr, B., S.J. Jonas, J. Polleux, et al., *Hydrophobic surfaces for enhanced differentiation of embryonic stem cell-derived embryoid bodies.* Proc Natl Acad Sci U S A, 2008. **105**(38): p. 14459-64.

54. Olmer, R., A. Haase, S. Merkert, et al., *Long term expansion of undifferentiated human iPS and ES cells in suspension culture using a defined medium.* Stem Cell Res, 2010. **5**(1): p. 51-64.

55. Ungrin, M.D., G. Clarke, T. Yin, et al., *Rational bioprocess design for human pluripotent stem cell expansion and endoderm differentiation based on cellular dynamics.* Biotechnol Bioeng, 2012. **109**(4): p. 853-66.

56. Abbasalizadeh, S., M.R. Larijani, A. Samadian, et al., *Bioprocess development for mass production of size-controlled human pluripotent stem cell aggregates in stirred suspension bioreactor.* Tissue Eng Part C Methods, 2012. **18**(11): p. 831-51.

57. Hunt, M.M., G. Meng, D.E. Rancourt, et al., *Factorial experimental design for the culture of human embryonic stem cells as aggregates in stirred suspension bioreactors reveals the potential for interaction effects between bioprocess parameters.* Tissue Eng Part C Methods, 2014. **20**(1): p. 76-89.

58. Kehoe, D.E., D.H. Jing, L.T. Lock, et al., *Scalable Stirred-Suspension Bioreactor Culture of Human Pluripotent Stem Cells.* Tissue Engineering Part A, 2010. **16**(2): p. 405-421.

59. Ismadi, M.Z., P. Gupta, A. Fouras, et al., *Flow Characterization of a Spinner Flask for Induced Pluripotent Stem Cell Culture Application.* Plos One, 2014. **9**(10).

60. Liovic, p., I.d. Šutalo, R. Stewart, et al., *Fluid Flow and Stresses on Microcarriers in Spinner Flask Bioreactors.* Ninth International Conference on CFD in the Minerals and Process Industries, 2012.

61. Papoutsakis, E.T., *Fluid-Mechanical Damage of Animal-Cells in Bioreactors.* Trends in Biotechnology, 1991. **9**(12): p. 427-437.

62. Kinney, M.A., C.Y. Sargent, and T.C. McDevitt, *The multiparametric effects of hydrodynamic environments on stem cell culture.* Tissue Eng Part B Rev, 2011. **17**(4): p. 249-62.

63. Bellin, M., M.C. Marchetto, F.H. Gage, et al., *Induced pluripotent stem cells: the new patient?* Nature Reviews Molecular Cell Biology, 2012. **13**(11): p. 713-726.

CHAPTER 2:

ENGINEERED MICROMECHANICAL CUES AFFECTING HUMAN PLURIPOTENT STEM CELL REGULATIONS AND FATE

Abstract

The survival, growth, self-renewal, and differentiation of human pluripotent stem cells (hPSCs) are influenced by their microenvironment, or so-called "niche," consisting of particular chemical and physical cues. Previous studies on mesenchymal stem cells and other stem cells have collectively uncovered the importance of physical cues and have begun to shed light on how stem cells sense and process such cues. In an attempt to support similar progress in mechanobiology of hPSCs, we review mechanosensory machinery, which plays an important role in cell–extracellular matrix interactions, cell-cell interactions, and subsequent intracellular responses. In addition, we review recent studies on the mechanobiology of hPSCs, in which engineered micromechanical environments were used to investigate effects of specific physical cues. Identifying key physical cues and understanding their mechanism will ultimately help in harnessing the full potential of hPSCs for clinical applications.

Introduction

For every cell type, its microenvironment, consisting of chemical cues and physical cues, is essential for regulating and maintaining cellular functions and fate [1-4]. Although early studies suggest chemical cues, such as growth factors, cytokines, hormones, and extracellular matrix (ECM) ligands, are the major factors that regulate cellular activity [5-8], recent studies on a wide range of cell types collectively indicate the importance of physical cues, such as intercellular forces, matrix mechanical properties, and surface topography, to further influence cellular regulation [9-11]. These factors are most evident particularly, during embryogenesis and organogenesis, where chemical cues deliver a direct signal to stem cells and progenitors via paracrine, autocrine, or endocrine signaling for an intracellular command, and physical cues set the stage for morphogenesis and guide the process during development [12-14]. Observation and identification of such factors and their spatiotemporal changes led to a number of effective protocols for maintenance and differentiation of stem cells in vitro [15, 16]. Human pluripotent stem cells (hPSCs), including embryonic stem cells (hESCs) [17] and induced pluripotent stem cells (hiPSCs) [18, 19], are no exception, although these artificially established cell lines do not exist naturally in an adult body.

Over the past 15 years, hPSC culture has advanced significantly thanks to identification of essential growth factors and specific substrate coatings that allow for cellular growth, survival, and maintenance of the undifferentiated state [20-22]. For instance, adherent substrate coatings, such as Matrigel, purified ECM proteins, and even

fully synthetic polymers, in combination with a chemically defined growth medium, such as mTeSR, can now sustain long-term maintenance of hPSC under serum- and feeder-free condition [20, 23-25]. Such chemically defined culture systems further enabled discovery of a vast array of imperative regulations and signaling cues of stem cells. For example, specific growth factors in the transforming growth factor–β (TGF-b) superfamily, basic fibroblast growth factor, and insulin-like growth factors are essential for hESC maintenance, survival, and proliferation (reviewed extensively by Avery et al. [26] and Oshimori and Fuchs [27]). In addition, control of stem cell fate by specific inhibition of certain kinases such as the glycogen synthase kinase (GSK), mitogen-activated protein kinase (MAPK), and Rho-associated protein kinase (ROCK) has been demonstrated recently [28, 29]. On the other hand, understanding physical cues influencing hPSC regulations has been left behind until very recently. In one notable example, when subjected to cyclic biaxial mechanical strain, the TGF-β/Activin/Nodal pathways were activated and effectively inhibited differentiation of hESCs even without cytokines TGF-β1 and Activin A, suggesting that mechanical cues are capable of regulating certain pathways [30, 31]. Clearly, detailed knowledge of the chemical and physical factors, as well as their synergistic effects, is necessary to emulate the complexity of the *in vivo* niche that controls cell transformation during the embryological process [32, 33].

Recent advances in micro- and nano-fabrication technology and materials science has made engineered tools and platforms available for investigating effects of micromechanical cues on stem cell regulations. For example, specialized biomaterials have been used in hPSC cultures to mimic ECM properties of live tissue models [34-36].

Furthermore, effects of physical cues such as matrix stiffness, surface texture, and surface topography on hPSCs and adult stem cells have been explored [37-41]. These studies have successfully observed how stem cells responded to these cues and started shedding light on pathways that dictate their fate for survival, self-renewal, and lineage commitment [33, 42]. It is now evident that stem cells are capable of detecting various physical aspects of their microenvironment and translate such cues into intracellular biochemical signals that modulate cellular activity [43, 44]. Nevertheless, the complete mechanisms governing so-called mechanotransduction of hPSCs by physical cues are far from being understood. In this review, to continue this progress, we will first summarize how stem cells, in general, can sense different physical cues in their environment by referring to previous mechanobiology studies. Interpreting results obtained from different cell types, particularly human mesenchymal stem cells (hMSCs), can segue into understanding hPSC regulations in engineered micromechanical environments. We will then survey recent studies that have begun to show the effects of engineered microenvironments in determining the fate of hPSCs for survival, self-renewal, or differentiation. Finally, we will conclude by offering what we envision in the future progress of this emerging field.

Mechanosensory Machinery and Force Transmitter

The distinction between chemical cues and physical cues is how stem cells detect them and process the information subsequently [44, 45]. Extrinsic chemical cues are detected by binding to and activating specific membrane protein receptors, which then transmit internal signals to activate (or inactivate) protein activators and co-activators for

gene regulation. On the other hand, specific mechanisms by which stem cells sense physical cues, particularly mechanical stimuli, are not fully understood. However, accumulated evidence suggests that the peripheral transmembrane proteins, such as integrins and cadherins, and nonmuscle myosin II (NMMII) play an active role in detecting and responding to the physical changes of the microenvironment [46]. Integrins and cadherins function as the mechanosensory machinery and NMMII is a complex motor protein that binds to cytosol's actin filaments to form the actomyosin cytoskeleton (Figure 2.1). As a result, cellular activity for motility, morphogenesis, and gene transcription could be regulated in the process of adapting to their physical micromechanical environment. An excellent review of mechanotransduction machinery and transcriptional regulators of both stem cells and non–stem cells was recently published by Mammoto et al. [47]. In our current article, because of limited space, we focus on the suspected major players including integrins, cadherins, and NMMII.

Integrin: Cell-ECM Mechanical Sensor

For every adherent cell, anchorage to the ECM is made by cell membrane–bound integrin-complex proteins at the focal adhesion site [48]. On the internal side of the membrane, the integrin proteins are also integrated with the actomyosin cytoskeleton (Figure 2.1) [49]. Therefore, the link between the cell membrane and the ECM goes far beyond the attachment site and is actually the start point of a communication network between the cell and microenvironment [50-52]. CellECM communication is vital for hPSC function and activity as it provides essential signals for maintenance of pluripotency, self-renewal, and survival [53]. However, little is known about mechanical cues induced

by the ECM that control stem cell regulation and fate [54, 55]. One certain thing is that the properties of the ECM and underlying substrates such as elasticity, porosity, and spatiotemporal geometry and topography are among the physical stimuli that a cell, in essence, can "feel" [56, 57]. When the integrin complex binds to the ECM, the cell tends to conform to its microenvironment by modulating its intracellular mechanics. For instance, when murine or human MSCs were attached to a rigid substrate, they generated more traction force and consequently increased their cytoskeletal tension, emulating the substrate's rigidity [38]. Conversely, when murine ESCs were attached to a substrate whose stiffness was similar to its normal cytoplasmic value, it sustained survival, self-renewal, and the undifferentiated state [58, 59]. It is speculated that integrin adjustment and clustering is responsible for the increase in traction force and subsequent cytoskeletal tension [60-63]. Nevertheless, many studies point to NMMII activity and the Rho/ROCK pathway as the major players that generate cytoskeletal tension. The Rho/ROCK pathway is a molecular feedback mechanism known to be associated with the mechanosensory machinery that regulates NMMII activity (see "NMMII: Mechanical Motor Modulating Cellular Function and Cytoskeleton"). Importantly, the formation of focal adhesion up-regulates Rho/ROCK and consequently induces NMMII activity to increase traction force as well as cytoskeletal tension.

Integrin-mediated adhesion pathways are vital for stem cell function and activity. For instance, researchers observed that an elevated activity of the Rho/ROCK pathway was consistent with hyperactivation of NMMII, followed by an instability and destruction of the cytoskeletal structure [64, 65]. This is now thought to be the main cause of dissociation-

induced apoptosis of hESCs. As such, inhibition of the Rho/ ROCK pathway results in a higher percentage of hESC survival upon enzymatic dissociation into single cells [66]. Similarly, the phosphoinositide 3-kinase/Akt (PI3K/Akt) pathway and MAPK/extracellular-signal-regulated kinase (MAPK/ERK) pathway are the other integrin-mediated adhesion pathways critical for cell survival and maintenance of pluripotency [67-71]. Particularly, studies suggest that Akt negates apoptotic signals for sustaining continuous survival or delays the onset of cell death when single cell dissociation occurs [72, 73].

However, identifying an exact molecular mechanism through which extrinsic forces command stem cell regulations has proven to be difficult due to cross-talk among many defined and undefined factors in the microenvironment. In an attempt to decouple mechanical factors, Huebsch et al. [74] engineered a substrate with defined mechanical properties and studied their effects on MSCs' lineage commitment. By using a three-dimensional (3D) hydrogel-based, synthetic ECM conjugated with integrin-binding RGD (Arg-GlyAsp)–modified ligands, they observed that differentiation correlated with the traction-dependent reorganization of integrins and the adhesive ligands in response to matrix elasticity and 3D architecture [74]. In addition, some have suggested that mechanical cues may cause tension-induced conformational changes of membrane proteins to expose sites that favor ligand interactions. For instance, Friedland et al. [75] showed that integrin-complex receptors could alter their affinity strength in response to cytoskeleton tension and stress. The same physical force may also present dormant growth factors in an active form when stress is involved [76]. In addition, there are numerous examples of ion

channels, membrane receptor proteins, and intracellular proteins being constantly regulated when mechanical forces are applied [77-80]. It is, however, still debatable how exactly mechanical stimuli influence changes in transcriptional regulation. Nevertheless, integrin-ECM binding provides crucial inputs for chemical and physical signal transduction [81].

Cadherin: Cell-Cell Mechanical Sensor

Similar to the integrins complex on the focal adhesion site, transmembrane glycoprotein cadherins in the adherens junction has also been shown to function as a sensor for many cellular activities [82]. Besides mediating cell-cell interactions via a cadherin-cadherin bond as a form of communication among neighboring cells, the adherens junction is capable of detecting external forces in its peripheral surroundings, independent of the ECM [83]. Figuratively, the integrin complex acts as a foot to feel its platform, whereas the cadherin acts as a hand to sense its lateral microenvironment (Figure 2.1). This mechanism is essential for hESCs because organogenesis depends on cell-cell communication during the embryological process [84]. For instance, E-cadherin is highly expressed in undifferentiated hESCs, whereas an increase in expression of N-cadherin and VE-cadherin is required for neural formation and angiogenesis, respectively [85, 86].

The adherens junction is also linked to the cytoskeletal architecture of the cell via cadherin binding to β-catenin in the cytoplasm (Figure 2.1). Therefore, when cadherin-cadherin binding forms between two cells, the cytoskeletal backbone is also connected together. Consequently, each cell can affect the cytoskeletal tension of the other in the presence or absence of an external force. For example, Liu et al.[87] observed that the

adherens junctions between two endothelial cells changed in size and strength in response to cell-cell contact force under mechanical loading. Using a micromechanical force sensor, they measured traction force generated by the cells and quantified local contact force at the cell-cell adhesion site. This entails that the cadherin feedback mechanism is similar to that of integrins, where force-induced cellular functions are mediated by myosin activity [82]. It is important to note that even though Liu's work was based on endothelial cells, integrin-based adhesion, and cadherin-based adhesion are vital anchorage mechanisms that link to the actomyosin cytoskeleton in hPSCs. Consequently, both adhesion complexes may have the ability to mediate force-dependent regulation for survival, growth, morphology, and function of stem cells. Recent studies demonstrated that an excessive perturbation of cell-cell contact in hESCs resulted in the collapse of the intracellular architecture, leading to cell blebbing and eventually dissociation-induced apoptosis [64, 65]. This process was likely mediated by the Rho/ROCK pathway and NMMII hyperactivation.

Even though both the focal adhesion and adherens junction function as mechanosensory machinery, it is said their signaling mechanism can have different effects on hPSC fate and activity [71]. For instance, some reports suggest that the focal adhesion mechanism is necessary for cell migration and differentiation of hPSCs [88], whereas cadherin binding is necessary for colony formation, pluripotency maintenance, and long-term survival. The cadherin-mediated regulation was evidenced in a study by Li et al. [89] on short-term and long-term inhibition of NMMII using blebbistatin, a NMMII ATPase inhibitor. Temporal inhibition of NMMII using blebbistatin increased single cell survival of hESCs after enzymatic dissociation; however, prolonging inhibition attenuated cell-cell

contact and gradually increased apoptosis [89, 90]. Importantly, they demonstrated that an overexpression of E-cadherin in NMMII-depleted hESCs was able to recover cell-cell contact and overall colony formation as well as to reverse the downregulation of pluripotency markers [89]. This suggests that cell-cell contact and colony formation are beneficial to long-term survival and maintenance of the pluripotent state of hESCs.

NMMII: Mechanical Motor Modulating Cellular Function and Cytoskeleton

NMMII is known as the critical mechanical motor of a cell because of its integral role in remodeling the cytoskeletal architecture for cellular adhesion, motility, morphology, and overall modulation of polarity [46]. The actomyosin cytoskeleton is intricately connected throughout the cytoplasm, from the membrane to the nucleus (Figure 2.1) [91]. Consequently, when physical cues from the ECM or adjacent cells are sensed by the mechanosensory machinery, pathways such as Rho/ROCK are up-regulated to activate NMMII, which then helps reorganize the cytoskeleton architecture (Figure 2.2) [92, 93]. It is hypothesized that altering the cytoskeleton architecture affects organelle localization and nuclear conformation, thus mediating transcription regulations vital for the fate of stem cells [47, 94].

Earlier studies that evidenced critical involvement of NMMII and pioneered the field of stem cell mechanobiology were conducted using hMSCs. McBeath et al. [37] examined how directed cell shapes contributed to hMSCs' commitment to osteoblast or adipocyte. Using a surface micropatterning technique to control cell shape and the degree of cytoskeletal tension, the group observed that cytoskeletal tension was the driving force

of lineage commitment [37]. Furthermore, cell shape and tension were highly regulated by Rho/ROCK activity on the actomyosin cytoskeleton; in fact, it was the NMMII-mediated spreading and contracting mechanism that controlled differentiation pathways regardless of soluble differentiation factors [39]. Engler et al. [38] also showed that NMMII activity directed naive hMSC lineage commitment, but in this case, it was the matrix elasticity that dictated cell morphology by modulating NMMII activity and consequently cytoskeletal structure. This cytoskeletal remodeling coincided with a dramatic change in transcriptional regulation, resulting in lineage commitment toward a cell type whose elastic modulus was similar to that of the underlying substrate [38].

Micromechanical Control of hPSC Fate

Given the multifaceted factors influencing stem cell regulations, numerous strategies have been explored to efficiently control cellular function for proliferation and differentiation [95-98]. Certainly, the lack of efficiency has always been a major issue for stem cell culture. Accordingly, researchers have been and are still developing methods to efficiently expand and/or differentiate stem cells with a high purity of the desired phenotype [99-104]. At an early stage, hESC culture relied on feeder cells and serum-supplemented media for continuous self-renewal. Since then, many chemically defined culture systems have been developed, eliminating exogenous undefined factors and animal products that are potentially problematic for clinical applications [98, 105-108]. For instance, Saha et al. [108] engineered ultraviolet/ozone modified polystyrene surface patterns, which in combination with human serum or recombinant vitronectin coating

improved long-term growth of hPSCs. By controlling colony size with the developed technology, the group was able to achieve at least a threefold increase in cell number compared with a conventional culture employing feeder cells [108]. Although the physically controlled colony size likely modulated exposure to soluble factors and cell-cell interactions, detailed mechanisms explaining the observed effects were not fully understood.

Unlike murine ESCs, which reportedly favor a soft substrate whose stiffness is close to the intrinsic cytoplasmic value (~0.6 kPa) for sustaining self-renewal [58, 59], hPSCs seem to favor stiff ones. Musah et al. [109] sought to determine an optimal mechanical property of engineered substrates for supporting pluripotency and robust proliferation of hESCs. By using a stiff polyacrylamide hydrogel (10 kPa) conjugated with glycosaminoglycans (GAG)-binding peptides, the group saw more robust attachment, growth, and maintenance of pluripotency compared with hydrogels of identical stiffness (10 kPa) conjugated with integrin-binding RGD peptides or a softer hydrogel substrate (0.7 kPa) conjugated with the GAG-binding peptides. In addition, they speculated that activation of YAP/TAZ in the nucleus was essential for pluripotency; as such, they saw a higher YAP/TAZ activation on the stiffer hydrogel than on the softer hydrogel. Interestingly, when plated on hydrogels with an intermediate stiffness (3 kPa), the cells attached and formed colonies in a similar manner as on the stiffest hydrogel (10 kPa) but began to detach from the substrate in the middle region of the colony in subsequent days. This suggests that although the intermediate stiffness can facilitate cell anchoring and colony formation, it is not supportive of cell spreading and continuous self-renewal [109].

Lee et al. [110] also demonstrated that substrate properties could significantly affect hESC culture through a survey of multiple permeable membranes whose surface hardness was dictated by their material and pore density. They reported that a polyethylene terephthalate membrane with a pore density of 4×10^6 pores/ cm^2 and hardness of 0.3 GPa was able to support cell attachment and growth of undifferentiated hESCs [110]. However, because the mechanical property of the membrane was coupled with the pore density and thus its permeability, one cannot conclude that hardness alone was the cause of the observed hESCs' response. In an attempt to decouple mechanical properties of the substrate, Sun et al. [111] employed a polydimethylsiloxane micro-post array, which allowed for tuning effective Young's moduli by changing the post height without altering contact surface area, matrix porosity, or surface chemistry. In this study, they showed that rigid substrates (>15 kPa) promoted growth, colony formation, and maintenance of undifferentiated hESCs (Figure 2.3A) [111]. In a different study, the same group explored the ability of hESCs to feel nanotopography by culturing the cells on a smooth surface or a rough surface [112]. Results from their nanotopography tests showed that hESCs alter the patterns of their focal adhesion formation in response to the underlying surface texture. Specifically, hESCs cultured on a smooth surface resulted in a focal adhesion formation on the periphery of the cell, whereas a random distribution of focal adhesion was observed for hESCs cultured on the rough surface (Figure 2.3B). Moreover, hESCs cultured on a smooth surface were able to spread, form colonies, and self-renewal, whereas hESCs cultured on rough surface exhibited a decrease in adhesion rate, colony size, and pluripotency [112]. These results collectively show that defined physical properties of the ECM and substrates can cause a

cellular response, which critically affects hPSC growth, undifferentiation, and colony formation. In addition, these processes are mediated by the mechanosensory machinery and NMMII activity in hPSC, as is the case in hMSC. Similarly, differentiation of hPSCs could be influenced by the substrate's mechanical properties. Recently, Keung et al. demonstrated that a soft polyacrylamide hydrogel substrate up-regulated early neural marker SOX1 in the absence of extrinsic neural inducers [113, 114]. However, the effect was limited to the first stage of differentiation, and further downstream differentiation required soluble neural factors. Interestingly, they observed that at different substrate stiffness, the cells' proliferation rate and pluripotency did not vary during the first 3 days of culture, although colonies were significantly smaller and more compact on the softer ECM (0.1 kPa) than on the more rigid one (75 kPa). Nevertheless, the soft microenvironment promoted neural differentiation better than the rigid substrate, suggesting that the compact colony formation had a higher impact on differentiation than spread colonies did as seen on the rigid substrate [114, 115].

During embryogenesis, mechanical forces are particularly important for lineage specification to the primary germ layer: mesoderm, endoderm, and ectoderm [14, 32]. Zoldan et al. [116] studied how mechanical properties of a variety of 3D porous polymer scaffolds in vitro can guide hESCs into either one of the germ layers. The group reported hESCs remained undifferentiated in the scaffold with the highest elasticity (>6 MPa), suggesting it supports maintenance of pluripotency. In addition, the group observed that hESCs cultured on substrates with high (1.5–6 MPa), intermediate (0.1–1 MPa), and low (<0.1 MPa) elasticity expressed gene markers specific for mesodermal, endodermal, and

ectodermal differentiation, respectively. They speculated that the scaffold elasticity affected the motility, traction force, and cytoskeletal tension and that the modulation of such cellular conditions could result in changes in morphology, adhesion to the ECM, cell-cell contact, and transcription relevant to differentiation, thus allowing hESCs to adjust to the microenvironment [116].

Other engineered micromechanical environments have been employed to explore optimal mechanical conditions to direct hPSC fate. For instance, Chan et al. [117] demonstrated how a specific topography could influence neural differentiation of hPSCs, even in the absence of chemical differentiation factors. They cultured hESCs on a 2 μm pitch, linear grating and observed cell and colony morphology being elongated along the grating direction, mimicking a neural lineage state even in a chemical condition promoting the undifferentiated state (Figure 2.3C). When cultured in differentiation-inducing media, hPSCs quickly committed to a neural lineage, showing the collaborative effect of both physical and chemical cues [117]. The synergistic role of chemical cues and physical cues presents great potential for leveraging control of hPSCs by the engineered microenvironment; however, identifying optimal cross-talk brings the need for screening multiple physical cues that support differentiation into many cell types [41, 118]. For this reason, Ankam et al. [119] developed a multiarchitecture chip (MARC) to screen multiple combinations of topography designs specifically for ectoderm differentiation. The multitude of topography designs in the MARC varies in geometry such as gratings, pillars, and wells, as well as their 3D dimension. Overall, they observed that neuronal fate was highly favored on anisotropic geometries, such as linear gratings, where cell morphology

was aligned and elongated along the grating direction, inducing neuronal differentiation. In contrast, they observed that glial fate was promoted on isotropic geometries such as pillars and wells, where the cells stayed round and spread along all direction of the patterned substrate (Figure 2.3C) [119]. The spreading morphology of hESCs on pillars was also observed by Kong et al. [120], however, in this study, a higher percentage of OCT4 (a marker of undifferentiated state) was observed in cells cultured under hexagonal and honeycomb pillar lattice configuration. It was suggested that the pillar patterns attenuated focal adhesion formation to shift dependency on cell-cell contact for survival and self-renewal [120]. Altogether, physical cues such as substrate stiffness and topography have a profound impact on hPSC regulation, which in turn can dictate its survival, self-renewal, or differentiation. Recent demonstrations of hPSC control using micromechanical environments are summarized in Table 2.1.

Summary and Future Perspective

With help from recent progress in micro- and nanotools and technologies, researchers are beginning to understand the mechanobiology of hPSCs and specific physical cues associated with cellular regulations. For instance, similar to hMSCs, it is now evident that hPSCs are equipped with molecular machinery for sensing various physical cues in their surroundings. These mechanosensors are essential interpreters of cell-ECM and cell-cell physical interactions and translate physical cues into intracellular biochemical signals. Subsequently, the biochemical signals can direct many cellular activities such as regulating cell polarity for cell migration, contraction, or expansion. Changes in cell

polarity are regulated by the NMMII activity. In addition, the cytoskeletal tension produced by hPSCs can dictate regulations for survival, self-renewal, pluripotency, and lineage specification. For this reason, some have tried to characterize the intracellular mechanics of hPSCs and their differentiated derivatives to uncover mechanical phenotypes indicative of hPSC lineage specification [121-123]. Nevertheless, investigation of hPSC mechanobiology is still at an early stage, and much remains to be uncovered. For example, the majority of work done so far has only probed the effects of physical cues on either maintenance of pluripotency or initial commitment to differentiation lineages but not on long-term, terminal differentiation into fully mature cells. As the core value of hPSCs is their ability to differentiate into many, if not all, types of human tissues, understanding roles of physical cues in downstream differentiation will be particularly important for basic science as well as for clinical applications in which such knowledge is required to fully exploit differentiation potential of the cells.

To further investigate the impact of individual physical cues, new tools that allow for decoupling of physical properties and high-throughput screening methods will be desired. Innovative platforms such as the MARC [119] and TopoChip [124] have shown great promise by enabling high-throughput screening of defined topography on a single platform. However, as the density of test beds on chip increases, precise fluid handling (e.g., media exchange without chemical cross-talk among neighboring test sites) analytical measurement technique beyond simple immunostaining and fluorescence measurement on-chip needs to be developed. In particular, passaging cells in a multistep differentiation process, in which chemical stimulants are sequentially changed according to specific stages

down the lineage commitment, will be extremely challenging in a high-throughput array format. Furthermore, upon successfully identifying potent physical factors that affect hPSC fate, screening of combinatorial cues of both physical and chemical factors should take place. Given that the in vivo stem cell niche comprises dynamic signaling of chemical and physical cues, an optimal microenvironment in vitro would most likely require a combination of multiple factors to unleash the full potential of the stem cell by maximizing synergistic effects. However, the factorial of multiple chemical and physical parameters suffers from an exponentially large combinatorial problem. To make matters worse, factoring timing as one of the parameters will inevitably make the challenge almost impossible. Therefore, new innovations, perhaps as a combination of nanofabrication, fluid handling, molecular imaging, automation, and an optimization algorithm, will be necessary to complete such an extremely daunting task.

In addition, from the point of view of hPSC-based cell therapy, culture methods need to be scaled up to supply a clinically relevant number of transplantable cells. Three-dimensional cultures in which hPSCs are cultured within a scaffold or suspended as clusters with or without microcarriers in a culture medium are the likely solutions to meet such demands at a reasonable cost. However, on such a platform, implementing physical cues such as defined surface topography or matrix stiffness would be difficult and require the development of a whole new set of engineered tools and technologies to harness physical cues to control of stem cell fate.

All of these requirements highlight the fact that mechanobiology of hPSCs is a truly multidisciplinary field and offers a unique opportunity for exciting collaborations among stem cell biologists, chemists, materials scientists, physicists, engineers, and more.

Table & Figures

II Table 2.1. List of engineered micromechanical cues affecting human pluripotent stem cells

Mechanical Environment	Effects on hPSC Fate	Cell Lines	Reference
Surface Roughness	Nanoscale surface roughness induced spontaneous differentiation, whereas a smooth surface promoted self-renewal and long-term pluripotency.	hESC (H9)	112
Substrate Elasticity and Stiffness	Polyethylene terephthalate (PET) membrane with a defined porous density at 4 x 10^6 pores/cm^2 and stiffness at 0.3 GPa promoted self-renewal and growth, in addition to uniform colony formation.	hESC (HSF6, H9, Miz4, Miz6)	110
	Rigid polyacrylamide hydrogel (10 kPa) coated with GAG-binding peptides supported optimal hESC adhesion, self-renewal, proliferation and long-term maintenance of pluripotency.	hESC (H9)	109
	Higher stiffness of PDMS micropost arrays resulted in increased hESC traction force, cellular adhesion and maintenance of pluripotency.	hESC (H1, H9)	111
	Soft polyacrylamide hydrogel substrate (0.1 kPa) promoted early differentiation to neural lineages.	hESC (H1), hiPSC (MSC-iPS)	114
	3D scaffolds with low (<0.1 MPa), intermediate (0.1-1 MPa) and high elasticity (1.5-6 MPa) promoted expression of ectoderm, endoderm, and mesoderm markers, respectively.	hESC (H9)	116
Topographical Patterns	350 nm ridge/groove patterns directed differentiation to neural lineage without biochemical differentiation factors.	hESC (H9)	41
	2 µm grating patterns increased the rate and efficiency of early and mature neural differentiation.	hESC (HES-3, H7), hiPSC (iPS-IMR90)	117
	Surface grating promoted neuronal differentiation, whereas pillars and wells promoted glial differentiation.	hESC (H1, H9)	119
	Nanopillar lattices with hexagonal or honeycomb configuration maintained high expression of pluripotent marker OCT4 even in the absence of bFGF.	hESC (H1)	120
Directed Colony Shape and Size	Size-controlled colonies at 300 µm diameter expanded faster and showed higher expression of pluripotency markers compared to colonies on feeder layers.	hESC (BG01, WIBR1, WIBR3), hIPSC (C1-iPS)	108
	Size-controlled colonies resulted in higher percentage of population that are double-positive against TRA 1-81 and each of OCT4, NANOG and SOX2 compared to colonies on feeder layers.	hESC (HSF1, H9)	104

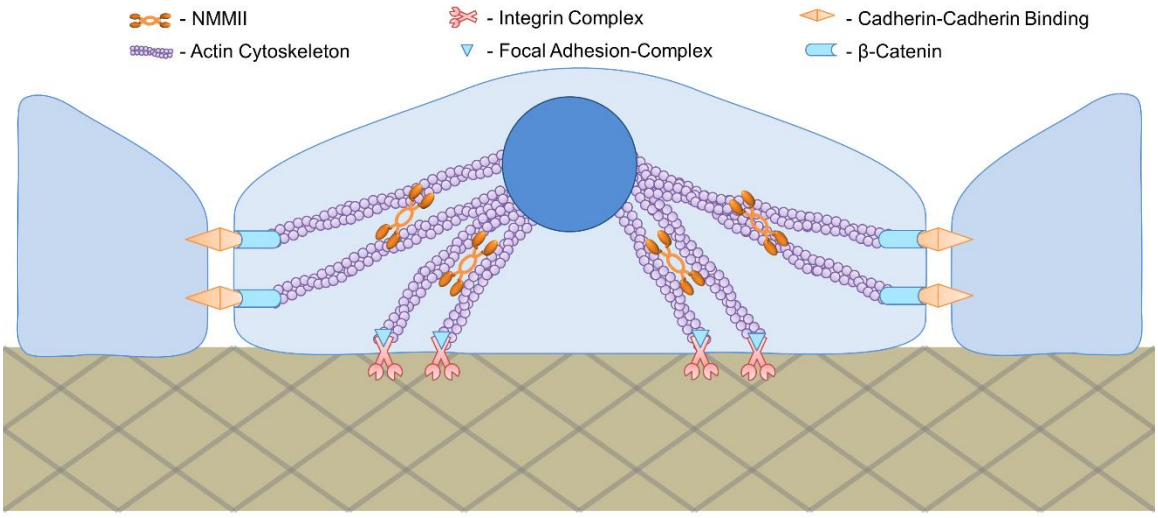

Figure 2.1. Cell mechanical regulations simplified. Cellular adhesion to extracellular matrix and adjacent cells are regulated by integrins at the focal adhesion and by cadherins at the adherens junction, respectively. Inside the cell, both integrin and cadherin are integrated with the actin cytoskeleton mediated by other proteins such as focal adhesion complex for integrins and b-catenin for cadherins. The actin cytoskeleton supports the cell structure and shape throughout the cytoplasm. When intracellular activity signals to alter cell polarity, nonmuscle myosin II (NMMII) mediates reorganization of actin cytoskeletal tension and induces changes in cell morphology.

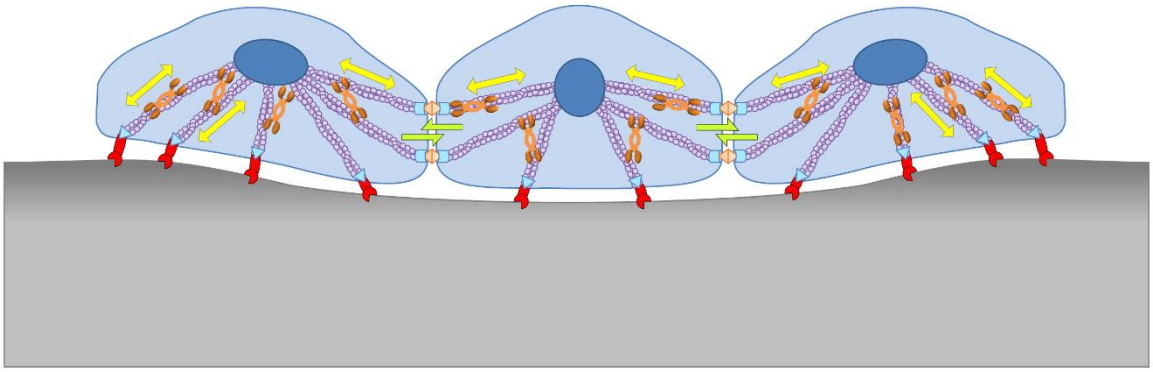

Figure 2.2. Mechanics of cell–extracellular matrix (ECM) and cell-cell interactions. Mediated by nonmuscle myosin II (NMMII), forces exerted by the ECM and neighboring cells can affect contraction or elongation. In turn, local deformation of the cell and the ECM can be dictated by their mechanical properties and number of cell-ECM and cell-cell force interactions.

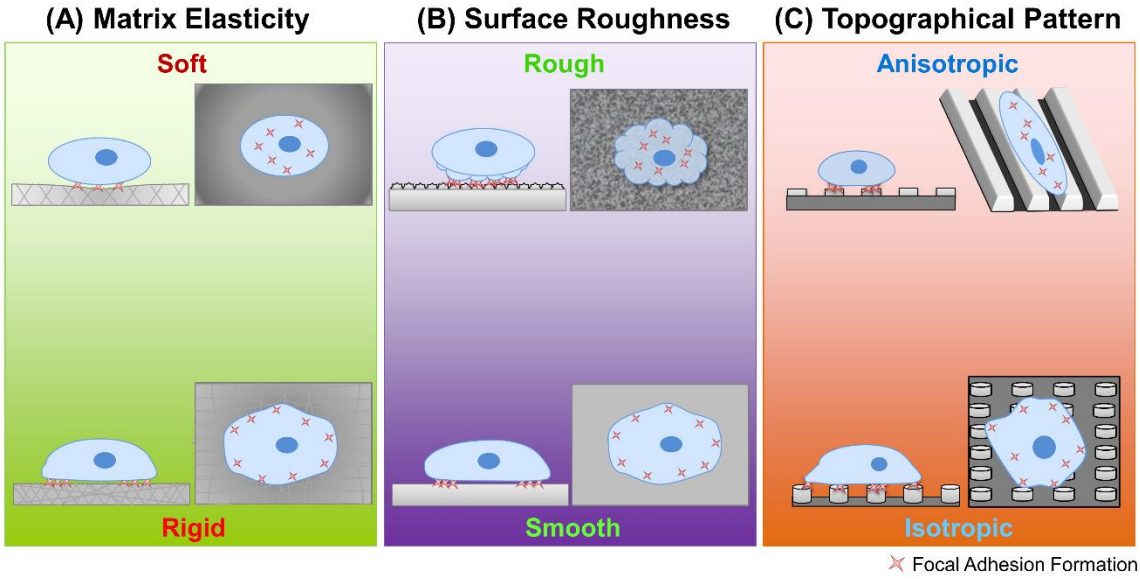

Figure 2.3. Substrate mechanical properties affecting the behavior of human pluripotent stem cells. (A) Soft substrates lead to a decrease in traction force and compact single-cell and colony morphologies (top), whereas rigid substrates lead to an increase in traction force at the peripheral regions of the cell, resulting in an increased single-cell and colony spreading (bottom). (B) Nanoscale rough surfaces result in compact single-cell and colony morphologies due to randomly distributed focal adhesion formations and decreased cellular adhesion to the extracellular matrix (top). On the other hand, smooth surfaces result in increased single-cell and colony spreading where focal adhesion formations are distributed along the periphery of the cells (bottom). (C) Anisotropic topographical patterns influence single-cell and colony morphologies to elongate along the feature direction (top), whereas isotropic patterns, result in rounded morphologies with fewer focal adhesion formations (bottom). (Illustrations made based on findings in refs. 109, 111, 112, 114, 117, 119, and 120).

References

1. Berridge, M.J. and R.F. Irvine, *Inositol Phosphates and Cell Signaling.* Nature, 1989. **341**(6239): p. 197-205.
2. Ullrich, A. and J. Schlessinger, *Signal Transduction by Receptors with Tyrosine Kinase-Activity.* Cell, 1990. **61**(2): p. 203-212.
3. Cantley, L.C., K.R. Auger, C. Carpenter, et al., *Oncogenes and Signal Transduction.* Cell, 1991. **64**(2): p. 281-302.
4. Hynes, R.O., *Integrins - Versatility, Modulation, and Signaling in Cell-Adhesion.* Cell, 1992. **69**(1): p. 11-25.
5. Jones, J.I. and D.R. Clemmons, *Insulin-Like Growth-Factors and Their Binding-Proteins - Biological Actions.* Endocrine Reviews, 1995. **16**(1): p. 3-34.
6. Johe, K.K., T.G. Hazel, T. Muller, et al., *Single factors direct the differentiation of stem cells from the fetal and adult central nervous system.* Genes & Development, 1996. **10**(24): p. 3129-3140.
7. Niwa, H., T. Burdon, I. Chambers, et al., *Self-renewal of pluripotent embryonic stem cells is mediated via activation of STAT3.* Genes & Development, 1998. **12**(13): p. 2048-2060.
8. Burdon, T., I. Chambers, C. Stracey, et al., *Signaling mechanisms regulating self-renewal and differentiation of pluripotent embryonic stem cells.* Cells Tissues Organs, 1999. **165**(3-4): p. 131-143.
9. Chen, C.S., M. Mrksich, S. Huang, et al., *Geometric control of cell life and death.* Science, 1997. **276**(5317): p. 1425-1428.
10. Xia, Z.G., M. Dickens, J. Raingeaud, et al., *OPPOSING EFFECTS OF ERK AND JNK-P38 MAP KINASES ON APOPTOSIS.* Science, 1995. **270**(5240): p. 1326-1331.
11. Kyriakis, J.M., P. Banerjee, E. Nikolakaki, et al., *THE STRESS-ACTIVATED PROTEIN-KINASE SUBFAMILY OF C-JUN KINASES.* Nature, 1994. **369**(6476): p. 156-160.
12. Gumbiner, B.M., *Cell adhesion: The molecular basis of tissue architecture and morphogenesis.* Cell, 1996. **84**(3): p. 345-357.
13. Ashkenazi, A. and V.M. Dixit, *Death receptors: Signaling and modulation.* Science, 1998. **281**(5381): p. 1305-1308.
14. Ingber, D.E., *Mechanical control of tissue morphogenesis during embryological development.* International Journal of Developmental Biology, 2006. **50**(2-3): p. 255-266.

15. Lee, O.K., T.K. Kuo, W.M. Chen, et al., *Isolation of multipotent mesenchymal stem cells from umbilical cord blood.* Blood, 2004. **103**(5): p. 1669-75.

16. Jiang, Y.H., B.N. Jahagirdar, R.L. Reinhardt, et al., *Pluripotency of mesenchymal stem cells derived from adult marrow.* Nature, 2002. **418**(6893): p. 41-49.

17. Thomson, J.A., *Embryonic Stem Cell Lines Derived from Human Blastocysts.* Science, 1998. **282**(5391): p. 1145-1147.

18. Takahashi, K., K. Tanabe, M. Ohnuki, et al., *Induction of pluripotent stem cells from adult human fibroblasts by defined factors.* Cell, 2007. **131**(5): p. 861-72.

19. Yu, J.Y., M.A. Vodyanik, K. Smuga-Otto, et al., *Induced pluripotent stem cell lines derived from human somatic cells.* Science, 2007. **318**(5858): p. 1917-1920.

20. Xu, C.H., M.S. Inokuma, J. Denham, et al., *Feeder-free growth of undifferentiated human embryonic stem cells.* Nature Biotechnology, 2001. **19**(10): p. 971-974.

21. Mohammadi, M., S.K. Olsen, and O.A. Ibrahimi, *Structural basis for fibroblast growth factor receptor activation.* Cytokine Growth Factor Rev, 2005. **16**(2): p. 107-37.

22. Androutsellis-Theotokis, A., R.R. Leker, F. Soldner, et al., *Notch signalling regulates stem cell numbers in vitro and in vivo.* Nature, 2006. **442**(7104): p. 823-6.

23. Ludwig, T.E., V. Bergendahl, M.E. Levenstein, et al., *Feeder-independent culture of human embryonic stem cells.* Nature Methods, 2006. **3**(8): p. 637-646.

24. Ludwig, T.E., M.E. Levenstein, J.M. Jones, et al., *Derivation of human embryonic stem cells in defined conditions.* Nat Biotechnol, 2006. **24**(2): p. 185-7.

25. Chen, G., D.R. Gulbranson, Z. Hou, et al., *Chemically defined conditions for human iPSC derivation and culture.* Nat Methods, 2011. **8**(5): p. 424-9.

26. Avery, S., K. Inniss, and H. Moore, *The regulation of self-renewal in human embryonic stem cells.* Stem Cells and Development, 2006. **15**(5): p. 729-740.

27. Oshimori, N. and E. Fuchs, *The harmonies played by TGF-beta in stem cell biology.* Cell Stem Cell, 2012. **11**(6): p. 751-64.

28. Tsutsui, H., B. Valamehr, A. Hindoyan, et al., *An optimized small molecule inhibitor cocktail supports long-term maintenance of human embryonic stem cells.* Nat Commun, 2011. **2**: p. 167.

29. Hanna, J., A.W. Cheng, K. Saha, et al., *Human embryonic stem cells with biological and epigenetic characteristics similar to those of mouse ESCs.* Proceedings of the National Academy of Sciences of the United States of America, 2010. **107**(20): p. 9222-9227.

30. Saha, S., L. Ji, J.J. de Pablo, et al., *Inhibition of human embryonic stem cell differentiation by mechanical strain.* J Cell Physiol, 2006. **206**(1): p. 126-37.

31. Saha, S., L. Ji, J.J. de Pablo, et al., *TGFbeta/Activin/Nodal pathway in inhibition of human embryonic stem cell differentiation by mechanical strain.* Biophys J, 2008. **94**(10): p. 4123-33.

32. Farge, E., *Mechanotransduction in Development.* Forces and Tension in Development, 2011. **95**: p. 243-265.

33. Keung, A.J., S. Kumar, and D.V. Schaffer, *Presentation counts: microenvironmental regulation of stem cells by biophysical and material cues.* Annu Rev Cell Dev Biol, 2010. **26**: p. 533-56.

34. Place, E.S., N.D. Evans, and M.M. Stevens, *Complexity in biomaterials for tissue engineering.* Nature Materials, 2009. **8**(6): p. 457-470.

35. Burdick, J.A. and G. Vunjak-Novakovic, *Engineered Microenvironments for Controlled Stem Cell Differentiation.* Tissue Engineering Part A, 2009. **15**(2): p. 205-219.

36. Fisher, O.Z., A. Khademhosseini, R. Langer, et al., *Bioinspired Materials for Controlling Stem Cell Fate.* Accounts of Chemical Research, 2010. **43**(3): p. 419-428.

37. McBeath, R., D.M. Pirone, C.M. Nelson, et al., *Cell shape, cytoskeletal tension, and RhoA regulate stem cell lineage commitment.* Developmental Cell, 2004. **6**(4): p. 483-495.

38. Engler, A.J., S. Sen, H.L. Sweeney, et al., *Matrix elasticity directs stem cell lineage specification.* Cell, 2006. **126**(4): p. 677-89.

39. Ruiz, S.A. and C.S. Chen, *Emergence of patterned stem cell differentiation within multicellular structures.* Stem Cells, 2008. **26**(11): p. 2921-7.

40. Dalby, M.J., N. Gadegaard, R. Tare, et al., *The control of human mesenchymal cell differentiation using nanoscale symmetry and disorder.* Nat Mater, 2007. **6**(12): p. 997-1003.

41. Lee, M.R., K.W. Kwon, H. Jung, et al., *Direct differentiation of human embryonic stem cells into selective neurons on nanoscale ridge/groove pattern arrays.* Biomaterials, 2010. **31**(15): p. 4360-6.

42. Hoffman, B.D. and J.C. Crocker, *Cell mechanics: dissecting the physical responses of cells to force.* Annu Rev Biomed Eng, 2009. **11**: p. 259-88.

43. Eyckmans, J., T. Boudou, X. Yu, et al., *A hitchhiker's guide to mechanobiology.* Dev Cell, 2011. **21**(1): p. 35-47.

44. Hoffman, B.D., C. Grashoff, and M.A. Schwartz, *Dynamic molecular processes mediate cellular mechanotransduction.* Nature, 2011. **475**(7356): p. 316-23.

45. Costa, P., F.V. Almeida, and J.T. Connelly, *Biophysical signals controlling cell fate decisions: how do stem cells really feel?* Int J Biochem Cell Biol, 2012. **44**(12): p. 2233-7.

46. Conti, M.A. and R.S. Adelstein, *Nonmuscle myosin II moves in new directions.* Journal of Cell Science, 2008. **121**(1): p. 11-18.

47. Mammoto, A., T. Mammoto, and D.E. Ingber, *Mechanosensitive mechanisms in transcriptional regulation.* J Cell Sci, 2012. **125**(Pt 13): p. 3061-73.

48. Miyamoto, S., S.K. Akiyama, and K.M. Yamada, *Synergistic Roles for Receptor Occupancy and Aggregation in Integrin Transmembrane Function.* Science, 1995. **267**(5199): p. 883-885.

49. Burridge, K. and M. ChrzanowskaWodnicka, *Focal adhesions, contractility, and signaling.* Annual Review of Cell and Developmental Biology, 1996. **12**: p. 463-518.

50. Giancotti, F.G., *Integrin Signaling.* Science, 1999. **285**(5430): p. 1028-1033.

51. Geiger, B., A. Bershadsky, R. Pankov, et al., *Transmembrane extracellular matrix-cytoskeleton crosstalk.* Nature Reviews Molecular Cell Biology, 2001. **2**(11): p. 793-805.

52. Hynes, R.O., *Integrins: Bidirectional, allosteric signaling machines.* Cell, 2002. **110**(6): p. 673-687.

53. Prowse, A.B., F. Chong, P.P. Gray, et al., *Stem cell integrins: implications for ex-vivo culture and cellular therapies.* Stem Cell Res, 2011. **6**(1): p. 1-12.

54. Sun, Y., C.S. Chen, and J. Fu, *Forcing stem cells to behave: a biophysical perspective of the cellular microenvironment.* Annu Rev Biophys, 2012. **41**: p. 519-42.

55. Kshitiz, J. Park, P. Kim, et al., *Control of stem cell fate and function by engineering physical microenvironments.* Integrative Biology, 2012. **4**(9): p. 1008.

56. Buxboim, A., I.L. Ivanovska, and D.E. Discher, *Matrix elasticity, cytoskeletal forces and physics of the nucleus: how deeply do cells 'feel' outside and in?* Journal of Cell Science, 2010. **123**(3): p. 297-308.

57. DuFort, C.C., M.J. Paszek, and V.M. Weaver, *Balancing forces: architectural control of mechanotransduction.* Nat Rev Mol Cell Biol, 2011. **12**(5): p. 308-19.

58. Chowdhury, F., Y.Z. Li, Y.C. Poh, et al., *Soft Substrates Promote Homogeneous Self-Renewal of Embryonic Stem Cells via Downregulating Cell-Matrix Tractions.* Plos One, 2010. **5**(12).

59. Chowdhury, F., S. Na, D. Li, et al., *Material properties of the cell dictate stress-induced spreading and differentiation in embryonic stem cells.* Nat Mater, 2010. **9**(1): p. 82-8.

60. Maheshwari, G., G. Brown, D.A. Lauffenburger, et al., *Cell adhesion and motility depend on nanoscale RGD clustering.* Journal of Cell Science, 2000. **113**(10): p. 1677-1686.

61. Roca-Cusachs, P., N.C. Gauthier, A. del Rio, et al., *Clustering of alpha(5)beta(1) integrins determines adhesion strength whereas alpha(v)beta(3) and talin enable mechanotransduction.* Proceedings of the National Academy of Sciences of the United States of America, 2009. **106**(38): p. 16245-16250.

62. Boettiger, D., *Mechanical control of integrin-mediated adhesion and signaling.* Curr Opin Cell Biol, 2012. **24**(5): p. 592-9.

63. Cluzel, C., F. Saltel, J. Lussi, et al., *The mechanisms and dynamics of (alpha)v(beta)3 integrin clustering in living cells.* J Cell Biol, 2005. **171**(2): p. 383-92.

64. Ohgushi, M., M. Matsumura, M. Eiraku, et al., *Molecular pathway and cell state responsible for dissociation-induced apoptosis in human pluripotent stem cells.* Cell Stem Cell, 2010. **7**(2): p. 225-39.

65. Chen, G., Z. Hou, D.R. Gulbranson, et al., *Actin-myosin contractility is responsible for the reduced viability of dissociated human embryonic stem cells.* Cell Stem Cell, 2010. **7**(2): p. 240-8.

66. Watanabe, K., M. Ueno, D. Kamiya, et al., *A ROCK inhibitor permits survival of dissociated human embryonic stem cells.* Nat Biotechnol, 2007. **25**(6): p. 681-6.

67. Armstrong, L., O. Hughes, S. Yung, et al., *The role of PI3K/AKT, MAPK/ERK and NFkappabeta signalling in the maintenance of human embryonic stem cell pluripotency and viability highlighted by transcriptional profiling and functional analysis.* Hum Mol Genet, 2006. **15**(11): p. 1894-913.

68. Teramura, T., T. Takehara, Y. Onodera, et al., *Mechanical stimulation of cyclic tensile strain induces reduction of pluripotent related gene expressions via activation of Rho/ROCK and subsequent decreasing of AKT phosphorylation in human induced pluripotent stem cells.* Biochem Biophys Res Commun, 2012. **417**(2): p. 836-41.

69. Li, J., G. Wang, C. Wang, et al., *MEK/ERK signaling contributes to the maintenance of human embryonic stem cell self-renewal.* Differentiation, 2007. **75**(4): p. 299-307.

70. Comoglio, P.M., C. Boccaccio, and L. Trusolino, *Interactions between growth factor receptors and adhesion molecules: breaking the rules.* Current Opinion in Cell Biology, 2003. **15**(5): p. 565-571.

71. Xu, Y., X. Zhu, H.S. Hahm, et al., *Revealing a core signaling regulatory mechanism for pluripotent stem cell survival and self-renewal by small molecules.* Proc Natl Acad Sci U S A, 2010. **107**(18): p. 8129-34.

72. Downward, J., *PI 3-kinase, Akt and cell survival.* Seminars in Cell & Developmental Biology, 2004. **15**(2): p. 177-182.

73. Ohgushi, M. and Y. Sasai, *Lonely death dance of human pluripotent stem cells: ROCKing between metastable cell states.* Trends Cell Biol, 2011. **21**(5): p. 274-82.

74. Huebsch, N., P.R. Arany, A.S. Mao, et al., *Harnessing traction-mediated manipulation of the cell/matrix interface to control stem-cell fate.* Nature Materials, 2010. **9**(6): p. 518-526.

75. Friedland, J.C., M.H. Lee, and D. Boettiger, *Mechanically Activated Integrin Switch Controls alpha(5)beta(1) Function.* Science, 2009. **323**(5914): p. 642-644.

76. Wipff, P.J., D.B. Rifkin, J.J. Meister, et al., *Myofibroblast contraction activates latent TGF-beta1 from the extracellular matrix.* J Cell Biol, 2007. **179**(6): p. 1311-23.

77. Yamamoto, K., T. Sokabe, T. Watabe, et al., *Fluid shear stress induces differentiation of Flk-1-positive embryonic stem cells into vascular endothelial cells in vitro.* American Journal of Physiology-Heart and Circulatory Physiology, 2005. **288**(4): p. H1915-H1924.

78. Saretzki, G., T. Walter, S. Atkinson, et al., *Downregulation of multiple stress defense mechanisms during differentiation of human embryonic stem cells.* Stem Cells, 2008. **26**(2): p. 455-64.

79. Kim, T.J., J.H. Seong, M.X. Ouyang, et al., *Substrate Rigidity Regulates Ca2+ Oscillation Via RhoA Pathway in Stem Cells.* Journal of Cellular Physiology, 2009. **218**(2): p. 285-293.

80. Matthews, B.D., C.K. Thodeti, J.D. Tytell, et al., *Ultra-rapid activation of TRPV4 ion channels by mechanical forces applied to cell surface beta 1 integrins.* Integrative Biology, 2010. **2**(9): p. 435-442.

81. Geiger, B., J.P. Spatz, and A.D. Bershadsky, *Environmental sensing through focal adhesions.* Nat Rev Mol Cell Biol, 2009. **10**(1): p. 21-33.

82. Li, L., S.A. Bennett, and L. Wang, *Role of E-cadherin and other cell adhesion molecules in survival and differentiation of human pluripotent stem cells.* Cell Adh Migr, 2012. **6**(1): p. 59-70.

83. Azarin, S.M., X. Lian, E.A. Larson, et al., *Modulation of Wnt/beta-catenin signaling in human embryonic stem cells using a 3-D microwell array.* Biomaterials, 2012. **33**(7): p. 2041-9.

84. Wong, V.W., S. Akaishi, M.T. Longaker, et al., *Pushing back: wound mechanotransduction in repair and regeneration.* J Invest Dermatol, 2011. **131**(11): p. 2186-96.

85. Takeichi, M., H. Inuzuka, K. Shimamura, et al., *Cadherin-mediated cell-cell adhesion and neurogenesis.* Neuroscience research. Supplement : the official journal of the Japan Neuroscience Society, 1990. **13**: p. S92-6.

86. Wang, F., K. Dumstrei, T. Haag, et al., *The role of DE-cadherin during cellularization, germ layer formation and early neurogenesis in the Drosophila embryo.* Developmental Biology, 2004. **270**(2): p. 350-363.

87. Liu, Z.J., J.L. Tan, D.M. Cohen, et al., *Mechanical tugging force regulates the size of cell-cell junctions.* Proceedings of the National Academy of Sciences of the United States of America, 2010. **107**(22): p. 9944-9949.

88. Uda, Y., Y.C. Poh, F. Chowdhury, et al., *Force via integrins but not E-cadherin decreases Oct3/4 expression in embryonic stem cells.* Biochem Biophys Res Commun, 2011. **415**(2): p. 396-400.

89. Li, D., J. Zhou, L. Wang, et al., *Integrated biochemical and mechanical signals regulate multifaceted human embryonic stem cell functions.* J Cell Biol, 2010. **191**(3): p. 631-44.

90. Walker, A., H. Su, M.A. Conti, et al., *Non-muscle myosin II regulates survival threshold of pluripotent stem cells.* Nat Commun, 2010. **1**: p. 71.

91. Sims, J.R., S. Karp, and D.F. Ingber, *Altering the Cellular Mechanical Force Balance Results in Integrated Changes in Cell, Cytoskeletal and Nuclear Shape.* Journal of Cell Science, 1992. **103**: p. 1215-1222.

92. Hale, C.M., S.X. Sun, and D. Wirtz, *Resolving the Role of Actoymyosin Contractility in Cell Microrheology.* Plos One, 2009. **4**(9).

93. Engler, A.J., M.A. Griffin, S. Sen, et al., *Myotubes differentiate optimally on substrates with tissue-like stiffness: pathological implications for soft or stiff microenvironments.* J Cell Biol, 2004. **166**(6): p. 877-87.

94. Pajerowski, J.D., K.N. Dahl, F.L. Zhong, et al., *Physical plasticity of the nucleus in stem cell differentiation.* Proc Natl Acad Sci U S A, 2007. **104**(40): p. 15619-24.

95. Hughes, C.S., L.M. Postovit, and G.A. Lajoie, *Matrigel: A complex protein mixture required for optimal growth of cell culture.* Proteomics, 2010. **10**(9): p. 1886-1890.

96. Kolind, K., K.W. Leong, F. Besenbacher, et al., *Guidance of stem cell fate on 2D patterned surfaces.* Biomaterials, 2012. **33**(28): p. 6626-33.

97. Stewart, M.H., S.C. Bendall, and M. Bhatia, *Deconstructing human embryonic stem cell cultures: niche regulation of self-renewal and pluripotency.* J Mol Med (Berl), 2008. **86**(8): p. 875-86.

98. Valamehr, B., H. Tsutsui, C.M. Ho, et al., *Developing defined culture systems for human pluripotent stem cells.* Regenerative Medicine, 2011. **6**(5): p. 623-634.

99. Lu, H.F., K. Narayanan, S.X. Lim, et al., *A 3D microfibrous scaffold for long-term human pluripotent stem cell self-renewal under chemically defined conditions.* Biomaterials, 2012. **33**(8): p. 2419-30.

100. Segers, V.F. and R.T. Lee, *Stem-cell therapy for cardiac disease.* Nature, 2008. **451**(7181): p. 937-42.

101. Scadden, D.T., *The stem-cell niche as an entity of action.* Nature, 2006. **441**(7097): p. 1075-9.

102. Serra, M., C. Brito, C. Correia, et al., *Process engineering of human pluripotent stem cells for clinical application.* Trends Biotechnol, 2012. **30**(6): p. 350-9.

103. Burridge, P.W., G. Keller, J.D. Gold, et al., *Production of de novo cardiomyocytes: human pluripotent stem cell differentiation and direct reprogramming.* Cell Stem Cell, 2012. **10**(1): p. 16-28.

104. Jonas, S.J., J.A. Alva, W. Richardson, et al., *A spatially and chemically defined platform for the uniform growth of human pluripotent stem cells.* Materials Science and Engineering: C, 2013. **33**(1): p. 234-241.

105. Irwin, E.F., R. Gupta, D.C. Dashti, et al., *Engineered polymer-media interfaces for the long-term self-renewal of human embryonic stem cells.* Biomaterials, 2011. **32**(29): p. 6912-9.

106. Villa-Diaz, L.G., H. Nandivada, J. Ding, et al., *Synthetic polymer coatings for long-term growth of human embryonic stem cells.* Nat Biotechnol, 2010. **28**(6): p. 581-3.

107. Melkoumian, Z., J.L. Weber, D.M. Weber, et al., *Synthetic peptide-acrylate surfaces for long-term self-renewal and cardiomyocyte differentiation of human embryonic stem cells.* Nature Biotechnology, 2010. **28**(6): p. 606-U95.

108. Saha, K., Y. Mei, C.M. Reisterer, et al., *Surface-engineered substrates for improved human pluripotent stem cell culture under fully defined conditions.* Proceedings of the National Academy of Sciences of the United States of America, 2011. **108**(46): p. 18714-18719.

109. Musah, S., S.A. Morin, P.J. Wrighton, et al., *Glycosaminoglycan-Binding Hydrogels Enable Mechanical Control of Human Pluripotent Stem Cell Self-Renewal.* Acs Nano, 2012. **6**(11): p. 10168-10177.

110. Lee, S., J. Kim, T.J. Park, et al., *The effects of the physical properties of culture substrates on the growth and differentiation of human embryonic stem cells.* Biomaterials, 2011. **32**(34): p. 8816-29.

111. Sun, Y., L.G. Villa-Diaz, R.H. Lam, et al., *Mechanics regulates fate decisions of human embryonic stem cells.* PLoS One, 2012. **7**(5): p. e37178.

112. Chen, W.Q., L.G. Villa-Diaz, Y.B. Sun, et al., *Nanotopography Influences Adhesion, Spreading, and Self-Renewal of Human Embryonic Stem Cells.* Acs Nano, 2012. **6**(5): p. 4094-4103.

113. Keung, A.J., E.M. de Juan-Pardo, D.V. Schaffer, et al., *Rho GTPases mediate the mechanosensitive lineage commitment of neural stem cells.* Stem Cells, 2011. **29**(11): p. 1886-97.

114. Keung, A.J., P. Asuri, S. Kumar, et al., *Soft microenvironments promote the early neurogenic differentiation but not self-renewal of human pluripotent stem cells.* Integr Biol (Camb), 2012. **4**(9): p. 1049-58.

115. Sun, Y., L.G. Villa-Diaz, R.H. Lam, et al., *Micromechanical elastomeric devices for investigations of mechanobiology in human embryonic stem cells.* μTAS, 2012: p. 1714-1716.

116. Zoldan, J., E.D. Karagiannis, C.Y. Lee, et al., *The influence of scaffold elasticity on germ layer specification of human embryonic stem cells.* Biomaterials, 2011. **32**(36): p. 9612-21.

117. Chan, L.Y., W.R. Birch, E.K. Yim, et al., *Temporal application of topography to increase the rate of neural differentiation from human pluripotent stem cells.* Biomaterials, 2013. **34**(2): p. 382-92.

118. Ranga, A. and M.P. Lutolf, *High-throughput approaches for the analysis of extrinsic regulators of stem cell fate.* Curr Opin Cell Biol, 2012. **24**(2): p. 236-44.

119. Ankam, S., M. Suryana, L.Y. Chan, et al., *Substrate topography and size determine the fate of human embryonic stem cells to neuronal or glial lineage.* Acta Biomater, 2013. **9**(1): p. 4535-45.

120. Kong, Y.P., C.H. Tu, P.J. Donovan, et al., *Expression of Oct4 in human embryonic stem cells is dependent on nanotopographical configuration.* Acta Biomater, 2013. **9**(5): p. 6369-80.

121. Ofek, G., V.P. Willard, E.J. Koay, et al., *Mechanical characterization of differentiated human embryonic stem cells.* J Biomech Eng, 2009. **131**(6): p. 061011.

122. Tan, Y., C.W. Kong, S. Chen, et al., *Probing the mechanobiological properties of human embryonic stem cells in cardiac differentiation by optical tweezers.* J Biomech, 2012. **45**(1): p. 123-8.

123. Gossett, D.R., H.T.K. Tse, S.A. Lee, et al., *Hydrodynamic stretching of single cells for large population mechanical phenotyping.* Proceedings of the National Academy of Sciences of the United States of America, 2012. **109**(20): p. 7630-7635.

124. Unadkat, H.V., M. Hulsman, K. Cornelissen, et al., *An algorithm-based topographical biomaterials library to instruct cell fate.* Proceedings of the National Academy of Sciences of the United States of America, 2011. **108**(40): p. 16565-16570.

CHAPTER 3:

INITIAL STUDIES INTO STATIC AND STIRRED SUSPENSION CULTURES AND HOW THE HYDRODYNAMIC ENVIRONMENT CAN AFFECT PLURIPOTENT STEM CELLS IN SUSPENSION

Abstract

An alternative to conventional 2D adherent cultures, 3D suspension cultures are among one of the most promising methods for large-scale production of hESCs and their derivatives. Specifically, 3D suspension as aggregate cultures is advantageous because it allows easy handling of hESC while maintaining native-like 3D cell-cell contact without the need of xenogeneic materials. In this study, we first evaluate the optimal growth medium to use for our subsequent study and found mTeSR1 to be the superior medium for large-scale expansion of hESC in suspension. We then conducted a 2-part study using a conventional stirring vessel to investigate the influence of agitation rates, ranging from 0 rpm (static) to 120 rpm, on the propagation of hESCs in dynamic suspension culture. In part 1, the cells were first grown under static suspension conditions for 2 days, then agitation condition for the next 5. In part 2, agitation was initiated on day 0 after single-cell inoculation. Overall, we found the best agitation condition to improve cell yield is the one that limits production of large-sized aggregates. For this reason, we sought to understand the physical parameters of fluid mixing and its influence on aggregation, viability and other responses that could be exploited to improve and control the culture outcome.

Optimization of basal media in static suspension culture of hESCs

A number of publications describing static and dynamic 3D suspension culture of human pluripotent stem cells have been recently reported. Amit et al. developed a protocol that achieved long-term culture for multiple hPSC lines, plus a 25-fold expansion within 10 days, by producing a medium consisting of DMEM/F12 and KO-serum replacement (KO-SR) as the basal medium, and supplemented with a mix concentrations of bFGF and IL6RIL6 chimera as the main factors to support hPSC's growth in suspension [1]. Similarly, Steiner et al. also developed a protocol that utilized Neurobasal medium with KO-SR and supplemented with growth factors Activin A and bFGF, plus solubilized extracellular matrix (ECM) laminin and fibronectin to support propagation of multiple hESC lines as floating aggregates [2]. However, the medium used in Amit et al. and Steiner et al. may not be cost-effective and efficient to produce and store for industrialization. Further improvements need to be recognized for good manufacturing practice (GMP). Other groups have also had some success in growing hPSC in suspension cultures, but unlike Amit et al. and Steiner et al., a common commercially available medium such as mTeSR or StemPro was implemented for expansion of hPSC in suspension [3-5].

In our preliminary study, we assessed static suspension culture to select an optimal medium to be used for subsequent studies and demonstrate that routine suspension culture and standard cellular and molecular analyses are feasible.

We evaluated four medias, three of which are commercially available media formulations - mTeSR1, StemPro with 40ng/ml of bFGF, and Essential 8 (E8) - plus a modified formulation from Steiner et al. which we call Neurobasal Cocktail [2]. To initiate

our suspension culture, we pre-treated monolayer cultures of hESC that had been stably transfected with an OCT4-eGFP reporter with 10μM of ROCK inhibitor (ROCKi) for at least 1 hr before trypsinization. After trypsinization, single cells were seeded at a concentration of 1×10^5 cells/ml in 4 ml of the respective four media supplemented with 10μM of ROCKi. ROCKi significantly improved the survival of single cells and promoted the formation of aggregates. We discontinued ROCKi treatments on day 4 and allowed the cells to depend on their cell-cell interactions for survival. We measured daily expansion rate up to 7 days and examined the aggregation sizes as well as expression of OCT-4 and SSEA3 pluripotent markers.

At the end of our culture time point (day 7), growth curve revealed an increase in cell number even after the withdrawal of ROCKi on day 4 (Figure 3.1A). The growth curve was assessed by daily cell count of triplicate samples for each condition and in terms of fold increase, which is a function of the cell density output divided by the initial cell density on day 0. Overall, mTeSR1 resulted in the highest cell yield producing up to 19 fold increase, followed by StemPro medium at 12 fold increase, E8 medium at 8 fold increase, and Neurobasal cocktail producing the lowest cell yield (1.5 folds) after 7 days of culture (Figure 3.1A). Upon observing the aggregate culture, the aggregate morphology was observed to be notably different from each growth medium (Figure 3.1B). Aggregates in mTeSR and StemPro were more spherical with sizes ranging from 100 μm to roughly 400 μm. Large sized clusters (> 500 μm) were also apparent and oddly shaped, likely the result of individual aggregates agglomerating to form larger clusters as observed by previous reports [3-5]. In contrast, the other two media produced smaller sized aggregates, but the

E8 generated more spherical shaped aggregates while Neurobasal Cocktail aggregates were less spherical and more cumulus cloud-like morphology. Interestingly, while assessing their OCT4-eGFP reporter by fluorescent microscopy, certain regions of the aggregates showed a decrease in OCT4-eGFP fluorescent (Figure 3.1B). In particular, we observed this to be more abundant in the mTeSR culture and the Neurobasal Cocktail, which suggests a loss of the pluripotent characteristics of the cells. However, single-cell analysis of the OCT4-eGFP expression revealed that only the cells in the Neurobasal Cocktail resulted in a significant decrease in OCT4 pluripotent marker (61.5%), as evidenced by flow cytometry (Figure 3.1C). mTeSR, on the other hand, resulted in the highest OCT4 expression at 88.6%, followed by StemPro (82.8%), then E8 (77.7%) (Figure 3.1C). Results of the SSEA3 analysis further confirmed that both mTeSR and StemPro were superior in supporting the growth and maintenance of hESC, whereas the E8 and neurobasal cocktail was not able to fully support their undifferentiated state. As such, mTeSR was chosen over StemPro to be the media of choice for subsequent scale-up study because of its performance in growth and maintenance of pluripotency after 7 days in static suspension culture. Not to mention that the components to make mTeSR have been fully publicized and is considered to be the ideal system to modify in the future, whereas StemPro is a proprietary medium.

The effects of agitation in stirred suspension culture of hESCs

Because of the limitations in static suspension (e.g. excessive agglomeration), we utilized Corning 125 mL polystyrene disposable spinner flask as the appropriate dynamic culture vessel on suspended cells (Figure 3.2A). In this initial study, we wanted to evaluate how the hydrodynamic condition via agitation rates would impact the propagation of hESCs. Therefore, we tested different agitation rates, ranging from 0 rpm (static) to 120 rpm, on a H9.OCT4-eGFP reporter line suspended in mTeSR and cultured for 7 days in the stirring vessel. We conducted two separate studies, in which the initial condition was different between the two (Figure 3.2B). In part 1, we paused agitation and allowed the cells to grow in static conditions for the first 2 days of culture, and then in agitation conditions for the next 5 days of culture. In part 2, the respective agitation condition was initiated on day 0 after single cell inoculation and continued the culture up to the end of our study (day 7). The starting procedure for both studies was the same and similar to our previous static suspension study where the vessel was seeded at a concentration of $1x10^5$ cells/ml in 50 ml of mTeSR supplemented with 10 μM of ROCKi. As noted in our previous study, cell growth was determined in terms of fold increase, which is a function of the cell density output divided by the initial cell density on day 0.

For the first part of the study, the 0 rpm and 80-120 rpm all produced similar cell yield resulting in ~11 fold increase after 7 days of culture, while 40 and 60 rpm produced 4.5 fold and 7 fold increase, respectively (Figure 3.3A). The 20 rpm condition generated the lowest cell yield among the other conditions with only 2 fold increase. Interestingly,

although differences in growth curve were apparent, flow cytometry analysis showed little variation in pluripotent marker expression between each condition (Figure 3.3B). On the other hand, aggregate morphology and size distribution had varying results (Figure 3.3C). The size distribution at 0 rpm was smaller than at 60-120 rpm where distribution varied greatly, but the majority of sizes were between 400-800 μm. The 20 rpm and 40 rpm condition had a much larger size distribution, and thus, produced the lowest cell yield.

For part 2 of the study, the highest growth curve was observed only in the 100 rpm condition (16.7 fold increase), followed by 0 rpm and 120 rpm condition resulting in 12 fold and 11.5 fold increase, respectively (Figure 3.4A). Again, the lowest growth curve was observed in the 20 rpm and 40 rpm, where both conditions resulted in less than 2 fold increase. Similar to part 1, flow cytometry analysis showed the majority of the cells still retained high levels of pluripotent markers, but the 20 and 40 rpm did have a slight drop in expression (Figure 3.4B). However, apart from the 0 rpm condition, aggregate formation, and size distribution were notably different in part 2, with smaller sized aggregates being more abundant in each condition (Figure 3.4C). Interestingly, similar to part 1 of the study, 20 rpm and 40 rpm produced larger-sized aggregates than any other conditions. This presents an interesting finding in which the condition that produced the lowest cell yield also produced the largest size distribution (20 and 40 rpm). In contrast, the condition that generated the highest cell yield had minimal large-sized aggregates (> 500 μm) and more homogenous size distribution between 200-400 μm.

The difference in part 1 & 2 of our study is the initial growth condition. For this reason, higher agitation rates were more tolerable in part 1 where we observed similar results from 80-120 rpm. The initial aggregate formation improved viability when the cells were exposed to agitation following 2 days in static suspension. As such, we observed higher cell yield at the 20 and 40 rpm for part 1 of the study compared to part 2. In contrast, the overall growth at 80-120 rpm for part 1 was notably less in comparison to the 100 rpm in part 2 of the study. The reason for this result could likely be explained by the differences in aggregate size distribution between the two studies. In particular, part 1 size distribution was more heterogeneous than compared to part 2 where we observed the majority of the aggregates to be less than 500 μm. Collectively, in part 2 of the study, it appears that the mixing condition facilitated the initial aggregate formation and regulated the overall size distribution by the end of the culture time point to improve the cell yield. These results suggest aggregation and regulating the aggregate size is a key parameter that must be controlled in stirred suspension systems. As such, we will discuss some working theories of how the fluid mixing could impact aggregation, viability and other cellular response of hPSCs to rationalize our stirred suspension results.

How the hydrodynamic environment could affect cellular responses of hPSCs

In 2D cultures, hPSCs adhere to ECM-coated surfaces and form colonies for survival and growth. In 3D aggregate suspension culture, there are no surface or microcarriers that hPSCs could adhere to, so they form free-floating aggregate spheroids via binding of the E-cadherin transmembrane proteins that are ubiquitously expressed by pluripotent stem cells [6]. In static suspension (0 rpm), cell aggregate formation is based on the proximity of neighboring cells freely floating in the medium. As such, agglomeration often occurs in a stochastic manner resulting in variation of aggregate sizes and shapes in the culture. In stirred suspension cultures, the initial aggregate formation, whereby single cells come together and assemble via cell-cell adhesion, and the overall aggregate size over the course of culture time point, are controlled by the hydrodynamic mixing condition. With hydrodynamic mixing, convective force enhances the mass transfer of the system that could force more frequent cell-cell interactions bound by the fluidic motion. For this reason, in comparison to static suspension, some have proposed that aggregate sizes could be correlated with the increased in transport parameters in stirred suspension cultures [7, 8]. However, the mass transfer coefficient is known to increase as a power function of the impeller speed with specific parameters given by the fluid and geometrical properties of the culture system [9, 10]. This means that aggregation dynamics is also a function of the fluid properties and design of the culture vessel. As a result, differently designed systems could produce different aggregate sizes under similar agitation rate. Also, the inoculation density is another parameter that could impact aggregation dynamics since the frequency of cell-cell interactions is also dependent on the

cell density in suspension [11]. Nevertheless, the hydrodynamic environment dictates how the cells aggregate for survival, and a fine balance must exist between mixing conditions necessary to control aggregation/size and limiting excessive shear force related cell death. For this reason, understanding the hydrodynamic parameters in a basic stirred suspension system will be useful for future designs of the system to control hPSCs culture.

An important consideration in stirred suspension culture of hPSCs is understanding how shear force can be a critical component in dynamic suspension systems. The current model to calculate the maximum shear stress (τ_{max}) [12] the cells experience in suspension can be estimated from

$$\tau_{max} = 5.33\rho(\varepsilon\nu)^{1/2} \quad (1)$$

where ρ is the medium density, ν is the fluid kinematic viscosity, and ε is the viscous energy dissipation per unit mass. Both ρ and ν are medium properties that could be determined, whereas ε is calculated by

$$\varepsilon = \frac{P}{V_L\rho} \quad (2)$$

V_L represents the working volume of the spinner culture flask, and P is the impeller power input. The power input could be estimated by the following equation

$$P = N_p(N^3)\left(D_i^5\right)\rho \quad (3)$$

where N is the agitation rate and D_i being the impeller diameter. The corresponding N_p is the dimensionless power number that can be calculated as a function of the impeller width (W), impeller diameter (D_i), and vessel diameter (D_t) that was proposed by Nagata [13] for bladed paddle impellers in an unbaffled tank:

$$N_p = {A}/{Re} + B\left(\frac{10^3+1.2Re^{0.66}}{10^3+3.2Re^{0.66}}\right)^p \tag{4}$$

Where coefficient A, B, and p are given by:

$$A = 14 + \left(\frac{W}{D_t}\right)\left[670\left(\frac{D_i}{D_t}\text{-}0.6\right)^2 + 185\right] \tag{5}$$

$$B = 10\text{^}\left\{1.3\text{-}4\left(\frac{W}{D_t}\text{-}0.5\right)^2 \text{-}1.14\left(\frac{D_i}{D_t}\right)\right\} \tag{6}$$

$$p = 1.1 + 4\left(\frac{W}{D_t}\right)\text{-}2.5\left(\frac{D_i}{D_t}\text{-}0.5\right)^2 \text{-}7\left(\frac{W}{D_t}\right)^4 \tag{7}$$

The Reynolds number (Re) in a stirring vessel could be found as a function of the agitation rate, impeller diameter, and kinematic viscosity through

$$Re = \frac{(N)(D_i{}^2)}{\nu} \tag{8}$$

At sufficiently high Reynolds numbers, the kinematic viscosity (ν) and viscous energy dissipation (ε) could also be used to calculate the smallest terminal eddies (η), also known as Kolmogorov eddies [14], given by

$$\eta = (\nu^3/\varepsilon)^{1/4} \tag{9}$$

Agitation results in a transfer of energy from the impeller to the liquid. As the impeller moves through the liquid, primary turbulence is formed and disintegrates to form cascades of small intense turbulence (Kolmogoroff eddies) to dissipates the energy [15, 16]. As agitation increases, the eddy size decreases and creates high localized shear that could be detrimental to the cells [17, 18]. Damage occurs when the size of the eddy is similar to the size of the suspended particle, and thus, the local shear affects the cells residing on the surface of the aggregates in suspension [19, 20]. However, if the aggregate is smaller than the Kolmogorov eddies, the aggregate would be confined within and transported along with the eddy, thereby limiting the cells encounter to the local surface shear [21]. For this reason, single cells in suspension are generally not affected by the eddy since the size a cell are typically much smaller than the size of eddies, unless at impractically intense agitation.

Altogether, previous studies have suggested that Kolmogorov eddies are responsible for controlling aggregate size in suspension [16]. Specifically, if the aggregate size (diameter) is greater than the size of eddies, the cells on the surface could experience enough shear force to dislodge it from the aggregate. Since both aggregate size and eddy size are the result of the hydrodynamic condition, the correlation between maximum mean aggregate size and energy dissipation have been previously investigated using different cell types [7, 8]. It was found that there is some relationship between aggregate size and Kolmogoroff eddy scale governed by the energy dissipation rate. However, Sen et al. report that the Kolmogoroff eddy is only partially responsible for the aggregate size [8]. Reports indicate that a certain ratio of eddy size to aggregate size is necessary for the local shear to have an impact on the surface of the cells [21, 22]. We attempted to understand this

mechanism by correlating our specific parameters, such as fluid viscosity and dimensions of the polystyrene disposable flask, with our observed aggregate size distribution as suggested by Sen et al. [8]. However, our findings were inconclusive since aggregate size were only observed at the end point of our culture (day 7) where we found a number of large aggregates that did not match our calculation (Appendix A).

Certainly, it is the mixing speed that can ultimately change aggregate sizes, with slower rates producing larger size aggregates and faster rates producing smaller size aggregates. However, previous studies suggest that shear stress could modulate the kinetics of E-cadherin interactions [6]. It was found that E-cadherin bonds between cells could readily be broken under mechanical stress [23]. Modulation of adhesion receptors such as E-cadherin can have great implications to downstream signaling pathways that could influence hPSCs fate decisions. Mainly, β-catenin mediates E-cadherin intercellular adhesion, but changes in E-cadherin activity could result to free β-catenin functioning as part of the canonical WNT pathway [24]. This WNT/β-catenin signaling pathways is known to promote lineage-specific differentiation of hPSCs [25]. Therefore, it's possible that aggregation and the process in which agitation-induced shear stress act as a signaling cue via E-cadherin could be inter-related.

Figures

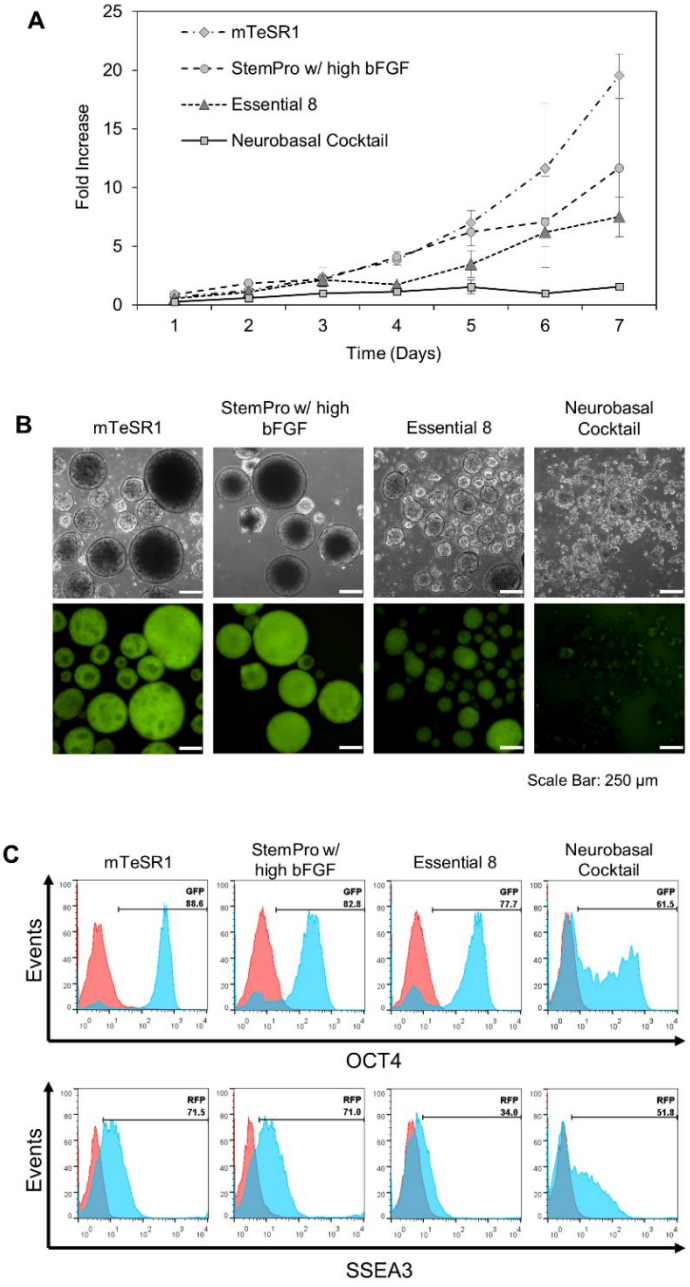

Figure 3.1. Comparison of four growth media on hESCs expansion under static suspension. (A) Daily growth curves in terms of fold increase. (B) Bright field and OCT4-eGFP fluorescent microscopy of cell aggregates after 7 days of culture. Scale bars: 250 µm. (C) Flow cytometry analysis of OCT4 and SSEA3 pluripotency markers.

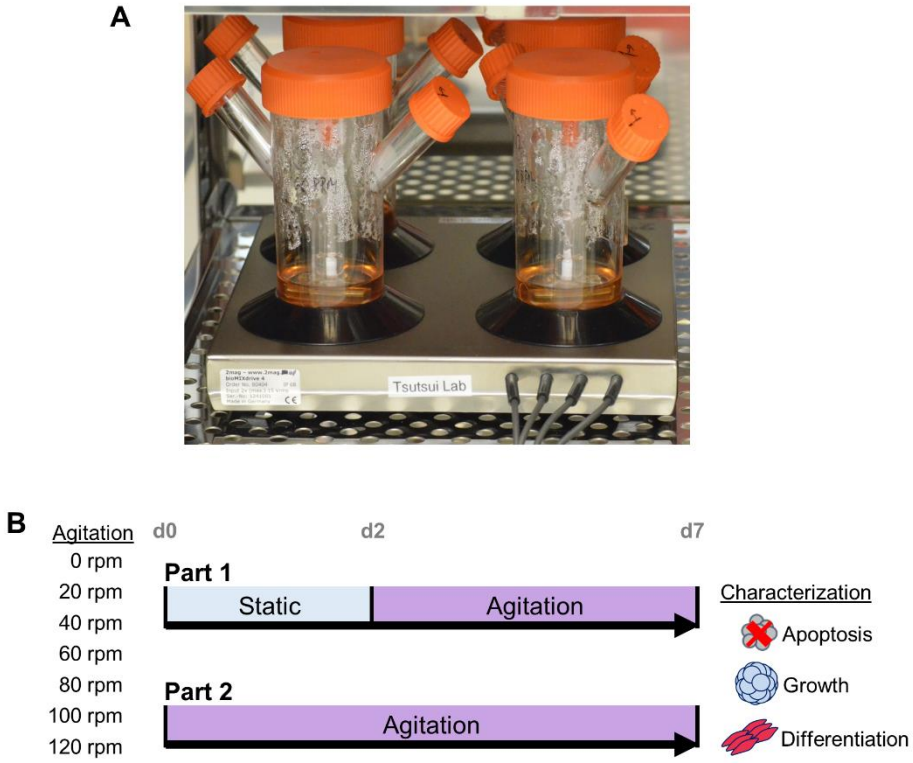

Figure 3.2. Experimental set-up of our initial study into stirred suspension culture. (A) Set-up of the Corning 125 mL polystyrene disposable spinner flask. (B) Schematic of testing varying agitation rates in two separate studies. In part 1, all of the conditions are cultured in static suspension for the first 2 days, then in their agitation condition for the next 5 days. In part 2, agitation was occurred on day 0 to culture end-point, day 7.

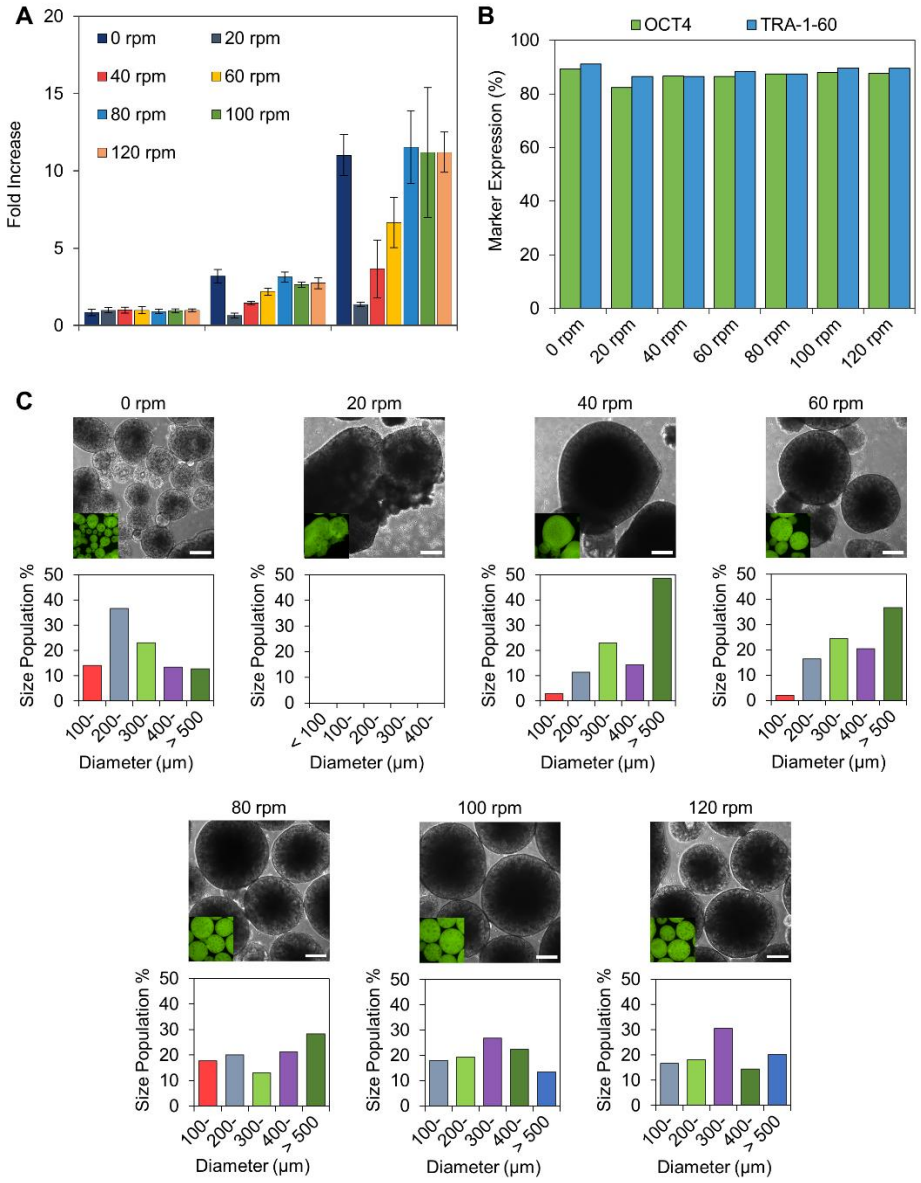

Figure 3.3. Part 1 results of different agitation rates (0-120 rpm) for the propagation of hESC in stirred suspension culture. (A) Growth curve by daily cell counting for each agitation condition. (B) Flow cytometry analysis of OCT4 and TRA-1-60 pluripotency markers. (C) Aggregate formation and quantitative analysis of aggregate size distribution for the different agitation rates. Results at 20 rpm not available due to excessive agglomeration resulting in an insufficient data. Scale bars: 150 µm

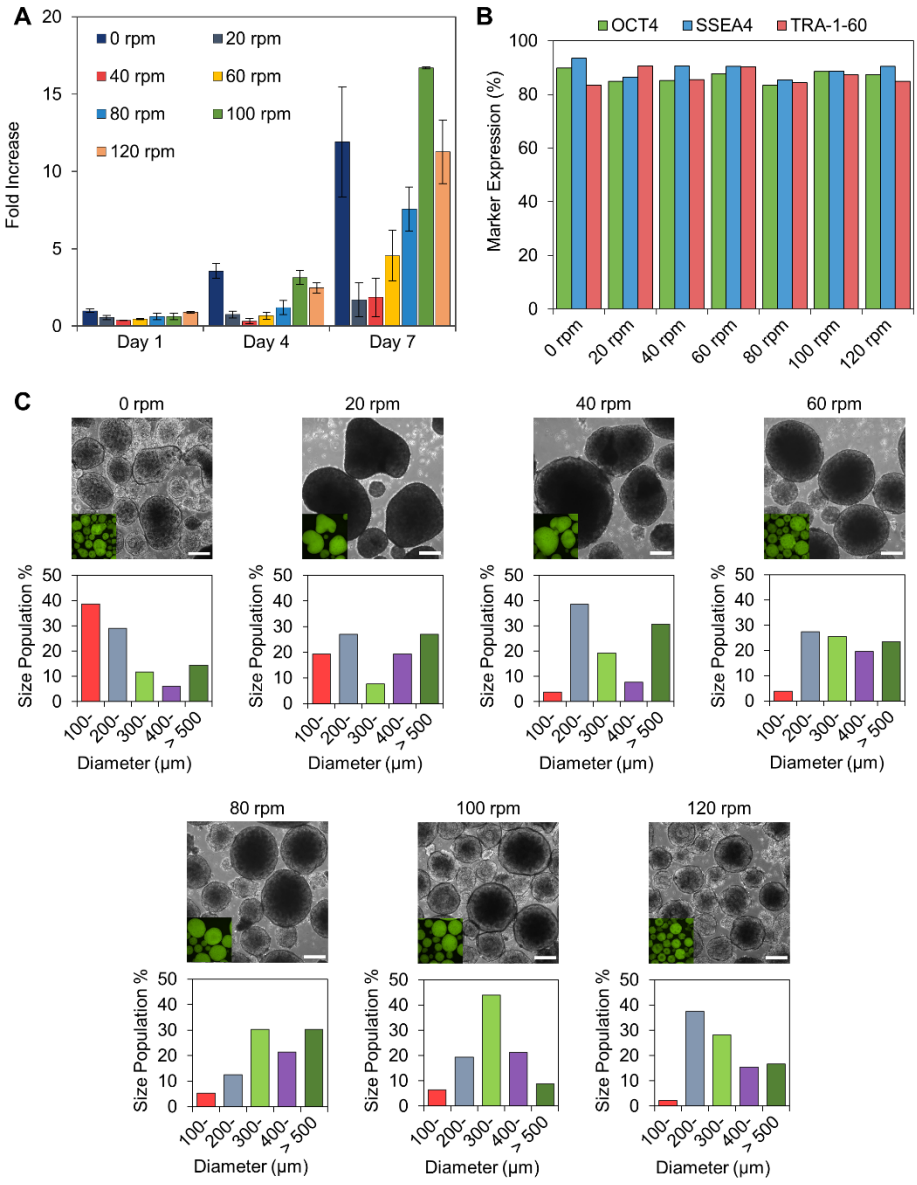

Figure 3.4. Part 2 results of different agitation rates (0-120 rpm) for the propagation of hESC in stirred suspension culture. (A) Growth curve by daily cell counting for each agitation condition. (B) Flow cytometry analysis of OCT4, SSEA4 and TRA-1-60 pluripotency markers. (C) Aggregate formation and quantitative analysis of aggregate size distribution for the different agitation rates. Scale bars: 250 µm

References

1. Amit, M., J. Chebath, V. Margulets, et al., *Suspension culture of undifferentiated human embryonic and induced pluripotent stem cells.* Stem Cell Rev, 2010. **6**(2): p. 248-59.
2. Steiner, D., H. Khaner, M. Cohen, et al., *Derivation, propagation and controlled differentiation of human embryonic stem cells in suspension.* Nat Biotechnol, 2010. **28**(4): p. 361-4.
3. Chen, V.C., S.M. Couture, J. Ye, et al., *Scalable GMP compliant suspension culture system for human ES cells.* Stem Cell Res, 2012. **8**(3): p. 388-402.
4. Singh, H., P. Mok, T. Balakrishnan, et al., *Up-scaling single cell-inoculated suspension culture of human embryonic stem cells.* Stem Cell Res, 2010. **4**(3): p. 165-79.
5. Olmer, R., A. Haase, S. Merkert, et al., *Long term expansion of undifferentiated human iPS and ES cells in suspension culture using a defined medium.* Stem Cell Res, 2010. **5**(1): p. 51-64.
6. Li, L., S.A. Bennett, and L. Wang, *Role of E-cadherin and other cell adhesion molecules in survival and differentiation of human pluripotent stem cells.* Cell Adh Migr, 2012. **6**(1): p. 59-70.
7. Moreira, J.L., P.M. Alves, J.G. Aunins, et al., *Hydrodynamic Effects on Bhk Cells Grown as Suspended Natural Aggregates.* Biotechnology and Bioengineering, 1995. **46**(4): p. 351-360.
8. Sen, A., M.S. Kallos, and L.A. Behie, *Expansion of mammalian neural stem cells in bioreactors: effect of power input and medium viscosity.* Developmental Brain Research, 2002. **134**(1-2): p. 103-113.
9. Curran, S.J. and R.A. Black, *Oxygen transport and cell viability in an annular flow bioreactor: Comparison of Laminar couette and Taylor-Vortex flow regimes.* Biotechnology and Bioengineering, 2005. **89**(7): p. 766-774.
10. Kinney, M.A., C.Y. Sargent, and T.C. McDevitt, *The multiparametric effects of hydrodynamic environments on stem cell culture.* Tissue Eng Part B Rev, 2011. **17**(4): p. 249-62.
11. Hunt, M.M., G. Meng, D.E. Rancourt, et al., *Factorial experimental design for the culture of human embryonic stem cells as aggregates in stirred suspension bioreactors reveals the potential for interaction effects between bioprocess parameters.* Tissue Eng Part C Methods, 2014. **20**(1): p. 76-89.
12. Cherry, R.S. and K.Y. Kwon, *Transient Shear Stresses on a Suspension Cell in Turbulence.* Biotechnology and Bioengineering, 1990. **36**(6): p. 563-571.

13. Nagata, S., *Mixing: Principles and Applications.* New York: John Wiley & Sons, 1975.

14. Papoutsakis, E.T., *Fluid-Mechanical Damage of Animal-Cells in Bioreactors.* Trends in Biotechnology, 1991. **9**(12): p. 427-437.

15. Kehoe, D.E., D.H. Jing, L.T. Lock, et al., *Scalable Stirred-Suspension Bioreactor Culture of Human Pluripotent Stem Cells.* Tissue Engineering Part A, 2010. **16**(2): p. 405-421.

16. Kawase, Y. and M. Mooyoung, *Mathematical-Models for Design of Bioreactors - Applications of Kolmogorov Theory of Isotropic Turbulence.* Chemical Engineering Journal and the Biochemical Engineering Journal, 1990. **43**(1): p. B19-B41.

17. Croughan, M.S., J.F. Hamel, and D.I.C. Wang, *Hydrodynamic Effects on Animal-Cells Grown in Microcarrier Cultures.* Biotechnology and Bioengineering, 1987. **29**(1): p. 130-141.

18. Kunas, K.T. and E.T. Papoutsakis, *Damage Mechanisms of Suspended Animal-Cells in Agitated Bioreactors with and without Bubble Entrainment.* Biotechnology and Bioengineering, 1990. **36**(5): p. 476-483.

19. Cherry, R.S. and E.T. Papoutsakis, *Physical-Mechanisms of Cell-Damage in Microcarrier Cell-Culture Bioreactors.* Biotechnology and Bioengineering, 1988. **32**(8): p. 1001-1014.

20. Cherry, R.S. and E.T. Papoutsakis, *Growth and Death Rates of Bovine Embryonic Kidney-Cells in Turbulent Microcarrier Bioreactors.* Bioprocess Engineering, 1989. **4**(2): p. 81-89.

21. Lakhotia, S. and E.T. Papoutsakis, *Agitation Induced Cell Injury in Microcarrier Cultures - Protective Effect of Viscosity Is Agitation Intensity Dependent - Experiments and Modeling.* Biotechnology and Bioengineering, 1992. **39**(1): p. 95-107.

22. Croughan, M.S., E.S. Sayre, and D.I.C. Wang, *Viscous Reduction of Turbulent Damage in Animal-Cell Culture.* Biotechnology and Bioengineering, 1989. **33**(7): p. 862-872.

23. Perret, E., A.M. Benoliel, P. Nassoy, et al., *Fast dissociation kinetics between individual E-cadherin fragments revealed by flow chamber analysis.* Embo Journal, 2002. **21**(11): p. 2537-2546.

24. Azarin, S.M., X. Lian, E.A. Larson, et al., *Modulation of Wnt/beta-catenin signaling in human embryonic stem cells using a 3-D microwell array.* Biomaterials, 2012. **33**(7): p. 2041-9.

25. Davidson, K.C., A.M. Adams, J.M. Goodson, et al., *Wnt/beta-catenin signaling promotes differentiation, not self-renewal, of human embryonic stem cells and is repressed by Oct4.* Proc Natl Acad Sci U S A, 2012. **109**(12): p. 4485-90.

CHAPTER 4:

IMPACT OF FLUIDIC AGITATION ON HUMAN PLURIPOTENT STEM CELLS IN STIRRED SUSPENSION CULTURE

Abstract

In the current study, we used the 125 mL ProCulture glass spinner flask to systematically investigated various agitation rates and characterize their impact on cell yield, viability, and maintenance of pluripotency. After 7 days of dynamic suspension culture, moderate agitation (60 rpm) was found to produce the highest cell yield (30-40 fold increase) of undifferentiated hPSCs. We then closely examined the distribution of cell aggregates between each condition and evaluated how the observed culture outcomes are attributed to their size distribution. Overall, our results showed that moderate agitation maximized the propagation of hPSCs by limiting cell death caused by excessive fluidic forces and controlling the cell aggregates below the critical size (< 400 μm), beyond which the cells suffer from diffusional limitations. Furthermore, we observed that fluidic agitation could regulate not only cell aggregation, but also expression of some key signaling proteins in hPSCs. This study suggests that fluidic agitation could be a considerable input parameter to facilitate fate determination in dynamic suspension cultures.

Introduction

With their unique ability to expand indefinitely and differentiate into any cell type in the human body, human pluripotent stem cells (hPSCs) – including both human embryonic stem cells (hESCs) [1] and human induced-pluripotent stem cells (hiPSCs) [2, 3] – have emerged as a promising cell source for future cell therapy applications [4]. The prospect of these cells is at a point where researchers can produce quality hPSC-derived products that could be used for pre-clinical and clinical studies [5, 6]. However, progress towards clinical implementation of these hPSC-derived products would be limited by the lack of a robust scalable system that can cost-effectively produce clinically relevant numbers of hPSCs and their derivatives [7]. For instance, treatments for myocardial infarction, type I diabetes, and neurodegenerative diseases have been estimated to require approximately ~10^9 cells per patient [8-10]. Furthermore, given the relatively low efficiency of in vitro directed differentiation, an even larger number of undifferentiated hPSCs are needed to meet the anticipated demand. Producing one billion hPSCs alone by traditional adherent planar culture systems is prohibitively time-consuming and expensive beyond research settings [11, 12].

Over the past decade, researchers have focused on developing alternative strategies to produce large numbers of hPSCs in an economically feasible manner [13]. In particular, stirred suspension culture such as spinner flasks presents an ideal platform for large-scale expansion of hPSCs, where the cells often grow as aggregates. Aggregate suspension cultures eliminate the use of microcarriers because hPSCs adhere together and form free-

floating spheroids for survival and growth, making this system more cost-effective for large-scale expansion [14]. Furthermore, stirring helps minimize heterogeneity in size of cell aggregates that is often observed in static suspension cultures. Reports of the successful demonstrations of stirred suspension culture for the expansion of undifferentiated hPSCs are summarized in Table 4.1. Across these studies, it was found that stirred suspension cultures were more effective in expansion rate and in achieving a high cell yield than static suspension cultures. However, the reported culture outcomes relied on empirically optimized conditions which varied from one system to another [15-17]. This is in part due to the added complexity of hydrodynamic motions present in different designs of the culture vessels. Furthermore, detailed characterizations of different agitation rates and their influence on the propagation of hPSCs were not reported in many studies. Therefore, it is difficult to standardize an optimal protocol for hPSCs in dynamic suspension by drawing a comparison across separate studies.

In this study, we describe how different agitation rates, ranging from 0-100 rpm, impact the survival, growth, maintenance of pluripotency, and protein expression levels of hPSCs in stirred suspension. The investigation of different agitation rates was designed to characterize the efficacy of an optimal agitation rate in comparison to the rates above or below. We further investigated how the cell aggregate size attributed to the culture output. The current study suggests that although higher agitation rates reduce cell viability, the formation of large-sized cell aggregates, typically observed at lower agitation rates, presents a greater limiting factor in hPSCs suspension culture strategies. Another interesting observation in this study is varying expression levels of cell signaling proteins

due to fluidic agitation. This suggests fluidic-agitation-induced mechanotransduction, potentially opening up a new means to control stem cell fate in stirred suspension culture.

Materials and Methods

Maintenance of hPSCs on 2D adherent cultures

The hESC line H9 was obtained from WiCell Research Institute. RIV9-iPSC (from human foreskin fibroblast) lines were derived at the UC Riverside Stem Cell Core facility [18]. hPSCs were maintained in standard culture conditions (37 °C, 5% CO_2, 100% humidity) on Geltrex (LDEV-Free, hESC-qualified, Thermo-Fisher) coated six-well plates (Corning) with complete mTeSR1 medium (StemCell Technologies). Cells were passaged every 5 to 6 days as small clumps via enzymatic treatment with Accutase (Thermo-Fisher) at 37 °C for 5-10 min and washed twice with DMEM (Lonza) before re-plating. Expansion of hPSCs was done the same way as the six-well plate but on T25 (Corning) and T75 (Thermo-Fisher) culture flasks.

Stirred suspension culture

From the 2D adherent culture, hPSCs were treated with 10 μM Y-27632, an inhibitor of Rho-associated protein kinase (ROCKi, Roche), for 1 hr at 37 °C prior to enzymatic dissociation to minimize cell death caused by single-cell dissociation. The cells were then washed three times with 1x PBS (Hyclone), treated with 0.25% Trypsin-EDTA solution (Thermo-Fisher) for 10 min at 37 °C, gently pipetted to break up clumps, and strained through a 40 μm cell strainer (Corning) to obtain single cells. The cells were then diluted (1:10) using 10% fetal bovine serum (FBS, Hyclone) in DMEM (Lonza) to inactivate the trypsin, and spun down at 250×g for 5 min. Cells were resuspended in mTeSR1 medium with 10 μM ROCKi and inoculated at a density of 10^5 cells/mL with a

total volume of 50 mL per flask in Corning 125 mL ProCulture glass spinner flasks that had been siliconized with Sigmacote (Sigma) following the manufacturer's instruction. A custom-made, four-position stirrer (bioMIXdrive4, 2mag-USA) was used to continuously drive the impeller of each flask at its designated agitation rate. The cells grew into and were maintained as aggregate spheroids for seven days. For each flask, a complete medium change was carried out after 24 hrs to remove ROCKi, followed by a 70% medium change with a fresh one on day 3. On day 4, the culture was split in half and replenished with fresh medium, followed by another 70% medium change on day 6.

Daily sampling to determine fold increase

For each condition, three 1 mL samples were taken from the spinner flask for cell counting and replaced with an equal amount of fresh medium. Upon enzymatic digestion, the cells were manually counted by the trypan blue exclusion method. The growth curve was generated based on the daily cell count with an adjustment to the lost volume due to daily sampling and the 50/50 split on day 4.

Quantifying aggregate size distribution

Aggregate samples were taken on day 7 and placed in a 12-mm culture dish (BD falcon) for photomicrographs using a Nikon D5100 camera attached to a Nikon Eclipse TS100 microscope. Three samples for each condition were taken and imaged. Image contrast and brightness were adjusted by ImageJ, and a custom MATLAB script was used to measure and collect the equivalent diameter of each aggregate.

Cell aggregate formation of prescribed sizes

To produce aggregates of prescribed sizes, we first surveyed varying seeding density of single cells to determine estimated numbers of cells needed on day 0 for attaining aggregates of approximately 100, 200, 300, 400, and 500 μm in diameter on day 7. Single cells were obtained as described above. The cells were suspended in mTeSR1 with 10 μM ROCKi and seeded onto an ultra-low-binding 96-microwell plate with a U- or V-shaped bottom (Gel Company, Lipidure-Coat). The plate was centrifuged for 5 min at 400×g to force the initial aggregate formation and incubated in the standard culture condition. After 24 hrs, ROCKi was removed by replacing the medium with fresh mTeSR1, and the aggregates were transferred to a flat bottom ultra-low-attachment microwell plate (Corning) for photomicrographs. Routine medium change was carried out every day by replacing 50% with fresh medium of mTeSR, and multiple images of the cell aggregates were taken every day to observe the progression of size increase. At the culture endpoint, the prescribed aggregates were trypsinized individually for analysis.

Flow cytometry

Cell aggregate samples were trypsinized into single cell as described above. The cells were fixed with 4% paraformaldehyde, washed with 1X PBS, and permeabilized with 0.2% Saponin in wash buffer solution (PBS + 5% FBS) for 15 min on ice. Primary antibodies were then added at suggested dilutions (appendix C) and incubated for 90 min at 4 °C in the dark. Following rinsing, secondary antibodies (appendix C) were added and

incubated for 60 min at 4 °C in the dark. The cells were then washed and suspended in wash buffer and stored at 4 °C in the dark until analyzed.

Apoptosis assay was performed as suggested by manufacturer's instruction with 1X binding buffer, 5 μL of Annexin V-PE (BD Bioscience), and 5 μL of 7-Amino-actinomycin D (7-AAD, Life Technologies).

For cell cycle analysis, single cells were gently vortexed as ice-cold 100% ethanol was added to make a final 70% ethanol solution. The cells were then incubated for 2 hrs at 4 °C in the dark. Ethanol was then removed, and the cells were resuspended in PBS containing 20 μg/mL propidium iodide (Life Technologies) and 10 μg/mL RNase (Sigma) and incubated for 30 min at 37 °C. Flow cytometric analysis was performed with Lab Quanta SC at the UCR Stem Cell Core or BD FACSAria at the UCR Institute for Integrative Genome Biology. Data analysis was done using FlowJo 8.7.

Immunocytochemistry of sectioned aggregates

Cell aggregates from suspension culture were fixed with 4% paraformaldehyde overnight at 4 °C, then treated with PBS-sucrose solution before embedded in an optimal cutting temperature (O.C.T.) compound (Sakura Finetek) and frozen at -80 °C. Samples were sectioned into 10 μm slices using the Microm HM500 OMV Motorized Cryostat at the Institute for Integrative Genome Biology at UC Riverside, then permeabilized with 0.2% Triton-X (Sigma) and blocked with blocking buffer (5% normal serum and 5% FBS in PBS) supplemented with 0.1% Triton X. Primary antibodies were added at the recommended dilution and incubated for overnight at 4 °C. Samples were then washed

with immunocytochemistry (ICC) wash buffer (1% BSA and 5% normal serum) and incubated with an appropriate secondary antibody for 1 hr at room temperature or overnight at 4 °C. After excess antibodies are removed with additional washes, samples were then mounted using Vectashield mounting medium with DAPI (Vector Laboratories) and incubated in the dark for 30 min at room temperature or overnight at 4 °C. Images were taken with the Nikon Eclipse Ti at the UCR Stem Cell Core.

Quantitative Real-Time PCR (qPCR)

Total RNA of cells was extracted using the Qiagen RNA isolation kit (Qiagen RNeasy kit) following the manufacturer's instructions. Purified RNA was then used to synthesize complementary DNA (cDNA) with the iScript cDNA Synthesis Kit (BioRad) following the manufacturer's instructions. Diluted cDNA and specific primers were then added with the Taqman Mastermix Fastmix (Quanta PerfeCTa FastMix) for qPCR. The relative expression of each targeted gene was calculated by the comparative ΔΔCt method normalized by the level of internal housekeeping gene glyceraldehyde-3 phosphate dehydrogenase (GAPDH) and compared to undifferentiated hPSCs from monolayer culture controls [19]. The primer sequences used for qPCR are listed in appendix C.

Protein preparation, SDS-PAGE, and Western blot analysis

In preparation for protein collection, cells were pre-treated with sodium orthovanadate (tyrosine phosphatase inhibitor, 1 mM) for 30 minutes and washed with 1X PBS prior to lysis. To obtain whole cell protein lysates, cells were overlaid with radioimmunoprecipitation assay buffer (10 mM Tris pH 7.2, 10 mM sodium chloride, 0.1%

sodium dodecyl sulfate, 1% Triton X-100, and 1% sodium deoxycholate) supplemented with 10 mM sodium fluoride, 1 mM sodium orthovanadate, 1 mM phenylmethylsulfonyl fluoride, 1x protease inhibitor cocktail (Sigma-Aldrich) and 1x phosphatase inhibitor cocktail (Thermo-Fisher). Protein concentrations were measured with the DC protein assay kit (BioRad) and 30 μg of protein in 1x Laemmli loading buffer with bromophenol blue dye were analyzed using sodium dodecyl sulfate polyacrylamide gel electrophoresis. Gels were run at 160V for 3 hours. Proteins were transferred to a polyvinylidene fluoride membrane (Roche) overnight at 4°C, 30V. After overnight blocking at 4˚C in 5% milk/PBS, membranes were incubated with the corresponding primary antibodies (appendix C). They were washed in 1x PBS and then incubated with the appropriate HRP-conjugated secondary antibody for 2 hours at 25˚C. Antibody binding was detected using SuperSignal West Pico Chemiluminescent Substrate (Thermo Scientific).

Statistical analysis

Data points are presented with a mean value ± standard deviation and were examined with a minimum of triplicate samples. Image analyses were also conducted on triplicate samples per condition. GraphPad InStat 3 software was used to perform analysis of variance (ANOVA) to determine statistical significance between experimental conditions.

Results

Impact of different agitation rates for the propagation of hPSCs

hPSCs are sensitive to a wide range of physical cues [20-23]. In stirred suspension systems, such a physical cue is fluidic force due to stirred agitation. Therefore, we assessed the impact of varied agitation rates on growth, survival, and maintenance of hPSCs [15, 24]. Our strategy is outlined in Figure 4.1A, in which five agitation conditions (0 (static), 40, 60, 80, and 100 rpm) were simultaneously tested on H9s and RIV9-iPSC cell lines. Throughout the culture period, we assessed outputs as daily fold increase in cell number and found that moderate agitation (60 rpm) resulted in the highest fold increase after 7 days of culture (41 and 30 fold increase for H9 and RIV9-iPSC, respectively) (Figure 4.1B). The growth curve demonstrates that the cell yields for static suspension, and low agitation (40 rpm) are far inferior to those for moderate (60 rpm) and high agitation (80-100 rpm) for both cell lines (Figure 4.1B). The growth curve also suggests that moderate agitation is the optimal condition for these cases, and it is likely that excessive agitation attenuates viability and growth. Measuring viability based on the population of cells undergoing apoptosis addresses how varying agitation can impact the survival of hPSCs in suspension. By using an early apoptosis marker, Annexin V (AV), in conjunction with cell death marker 7-AAD, we categorized apoptosis into three stages: early (AV+/7-AAD^{-}), intermediate (AV+/7-AAD+), and late (AV^{-}/7-AAD+). Higher agitation rates were found to compromise the survival of the cells as evidenced by the increase in overall apoptotic cells (Figure 4.1C). Interestingly, although viability percentages in static and low agitation differ slightly from that in moderate agitation, the resulting low cell yield produced under these conditions

(Figure 4.1B) suggest that the self-renewal capacity of the cells is beginning to decline due to a loss in pluripotency.

Flow cytometry analyses showed that for both cell lines, over 90% of the cell population in 60, 80, and 100 rpm expressed pluripotent markers OCT4, TRA-1-60, and SSEA-4 (Figure 4.2A). On the other hand, the cells in static and 40 rpm expressed lower levels of OCT4 (H9: 73.2% and 85%, respectively; RIV9: 85.5% and 73.7%, respectively) and TRA-1-60 (H9: 89.4% and 80.3%, respectively; RIV9: 68.7% and 53.7%, respectively), and a drop in SSEA4 expression was observed in the RIV9-iPSC line (83.4% and 77%, respectively) (Figure 4.2A). Moreover, we carried out qPCR to measure the expression of pluripotency genes OCT4, NANOG, and SOX2. Similar to the flow cytometry data, in both cell lines, agitation rates at 60, 80 and 100 rpm maintained high expression of all three pluripotency genes, whereas static suspension and 40 rpm resulted in a down-regulation of OCT4 gene expression (Figure 4.2C). Interestingly, only the RIV9-iPSC lines experienced a drop in NANOG expression at static and 40 rpm, whereas the H9 lines maintained high expression of NANOG for such conditions. Nevertheless, the results indicate that static suspension and low agitation rates may not be suitable conditions for the expansion of hPSCs. In addition to the low cell yield and the drop in pluripotent markers suggest that hPSCs under these conditions have begun to differentiate spontaneously.

To determine if the drop in pluripotent markers is due to differentiation, we examined gene expression levels associated with the three early germ layers: SOX17 (endoderm), GOOSECOID (GSC, mesoderm), and PAX6 (ectoderm) [25-27]. qPCR

analysis revealed that the decrease in pluripotency for static and 40 rpm was accompanied by an increase in lineage-specific gene expression. In both cell lines, static suspension resulted in the highest level of PAX6, while 40 rpm resulted in the highest levels of SOX17 and GSC (Figure 4.2D). Notably, besides its involvement in undifferentiated hESCs, SOX2 is also known to be expressed in neuroectoderm cells [28]. As such, the observed up-regulation of both SOX2 and PAX6 could indicate that the cells in static suspension were likely differentiating towards a neuroectoderm lineage. Additionally, the data suggest that agitation could influence differentiation towards the mesendoderm lineage, as evidenced by higher expression levels of SOX17 and GSC observed in 40 rpm (Figure 4.2D). Collectively, these experiments show that fluidic agitation could be used to enhance the propagation of undifferentiated hPSCs and could play a role as a potential means of controlling stem cell fate.

Correlation between size of the cell aggregates and the cell yield

Another striking difference observed in this test was the morphology and the size of the cell aggregates at varying agitation rates (Figure 4.3). Given the varied range of sizes, we quantitatively measured the aggregate size distribution and found that static and 40 rpm further separated themselves from moderate and high agitation rates because of the large range of aggregate size distribution. Both static and 40 rpm appear to have multiple aggregates agglomerating together to form large clusters (≥400 μm) (Figure 4.3i). In static suspension, cell aggregate formation is based on the proximity of neighboring cells freely floating in the medium. As such, agglomeration occurs in a stochastic manner, resulting in a wide size distribution. In the case of 40 rpm, it is possible that the low agitation creates

pockets of minimal mixing where cell aggregates may move to and agglomerate into large clusters. In contrast to static and 40 rpm, agitation rates at 60, 80 and 100 rpm produced a more homogeneous size distribution. There is a clear trend that size distribution gradually shifts toward smaller sizes as the agitation rate increases (Figure 4.3ii). Interestingly, though large aggregate sizes (≥400 μm) attribute to less than 10% of the aggregate population, these large aggregates account for a large percent (20-60%) of the total cell population (Figure 4.3iii). Clearly, fluidic mixing caused the observed phenomena, including the significant changes in growth rate and aggregate size distribution. However, it is not clear if agitation directly impacted the cell growth and consequently the overall size, or the flow controlled formation of cell aggregates, which then modulated cell growth.

The effect of aggregate size on expansion rate

In an attempt to decouple the impacts of fluidic agitation and the aggregate size on the observed cell yield, we investigated how aggregates at prescribed sizes could affect growth, viability, and maintenance of pluripotency. A calculated number of single cells were seeded in a V-shaped or U-shaped microwell plate on day 0 to obtain cell aggregate size of approximately 100, 200, 300, 400, and 500 μm in diameter on day 7 (Figure 4.4A & 4.4B). The population growth curve was interpolated based on the aggregate cell density and the progression of aggregate size as a function of time (Figure 4.4C). The highest growth rate was found when starting with approximately 150 cells to obtain an aggregate size of ~300 μm on day 7. This condition had an initial viability of ~70% on day 1, then progressed to 85.7% viability and a 35 fold increase in population by day 7 (Figure 4.4C & 4.4D).

In addition to viability, we wanted to address whether aggregate size could also impact hPSC proliferation kinetics. To evaluate the proliferative capacity of the cells, we performed cell cycle analysis using propidium iodide and flow cytometry to determine the subpopulation of cells that resides in the G0/G1 phase, S phase, or G2/M phase. The cell cycle analysis revealed a bell-shaped distribution for the percentage population of cells in the G2/M phase, where the 300 μm size aggregates were the most proliferative (29.5%) and the 100 μm and 500 μm aggregates were the least proliferative cells (Figure 4.4E). Notably, although the 100 μm and 500 μm size aggregates had similar G2/M percentage (~18.0%), the G0/G1 and S phase percentages displayed their different proliferation kinetics. Furthermore, we observed a clear trend where the subpopulation in the quiescent (G0/G1) phase increased and the subpopulation in the replication (S) phase decreased proportionally to the aggregate size (Figure 4.4E). This result suggests that the cells in the 100 μm sized aggregates entered accelerated growth while anything above 300 μm lead towards the quiescent state. These differences in the cell cycle progressions correlated with the observed cell yield as aggregate size increased (Figure 4.4C & 4.4E).

However, hPSC regulation of the cell cycle is also known to link to its stemness [29]. As such, we examined the influence of aggregate size in the maintenance of pluripotency. Results from flow cytometry demonstrated that only the large aggregates (around 400 μm and above) exhibited a decrease in pluripotency, as shown by the reduction in pluripotency marker OCT4 (Figure 4.5A). Furthermore, qPCR analysis confirmed a drop in OCT4 pluripotent gene expression as aggregates grew larger than 300 μm (Figure 4.5B). This drop in pluripotency and proliferation rate observed in large aggregates suggest that

the cells were beginning to differentiate. Results from qPCR indicate that aggregates greater than 300 μm were beginning to differentiate spontaneously since gene expression for all three early germ layers were significantly up-regulated (Figure 4.5C) [30]. This phenomenon is likely due to diffusion limitation of soluble factors keeping cells located in the aggregate center from receiving adequate factors needed for maintenance of pluripotency (Figure 4.5D) [31].

Western blot analysis

Previous studies have shown that hPSCs can sense and respond to biophysical cues in its microenvironment [32]. Biophysical cues are mechanical stimuli that induce molecular signaling responses (also known as mechanotransduction), thereby modulating regulatory pathways that contribute to the maintenance of pluripotency or initiate early lineage-specific differentiation of hPSCs [33]. Mechanotransduction studies have been extensively explored for 2D adherent cultures over the past decade. However, 2D and 3D methods are disparate culture conditions, and current knowledge of core signaling pathways that are affected in 3D cultures is very limited [34]. In an attempted to shed light on possible mechano-responsive proteins behind 3D suspension cultures, we performed Western blots to identify differences in protein levels in hPSCs cultured under 2D adherent, 3D static suspension (0 rpm), and 3D dynamic suspension (40 – 100 rpm).

First, by comparing 2D adherent and 3D static (0 rpm) conditions, both without fluidic agitation, the data show the level of phosphorylated ERK was noticeably lower in the latter, despite an upregulation of overall ERK levels over the former (Figure 4.6A). A

similar trend, although less prominent, was observed or pJNK1/2 and pan-JNK1/2 (Figure 4.6A). We speculate that these differences arise from the different structural complex and signaling proteins involved between the cell-cell and cell-ECM junctions. In 3D suspension, hPSCs have no rigid surface to adhere to, thus leading towards cell-cell adhesion and forming free-floating aggregate spheroids. In 3D stirred suspension (40 – 100 rpm), as seen in levels of JNK1/2 phosphorylation, protein levels were further modulated as agitation increases. While simple aggregation without stirring (0 rpm) did not seem to change β-catenin (CTNNB1) levels, a rpm-dependent CTNNB1 regulation was observed, with 40 rpm resulting in the lowest amount of CTNNB1 (Figure 4.6A). Increasing the rotation speed had cell line-dependent effects: In RIV9-iPSCs, CTNNB1 increased with higher rpm, but always remained below 2D adherent levels, while in H9 cells CTNNB1 recovered almost to 2D static levels. In addition, there was consistent activation of the 75kDa CTNNB1 form, which is supposedly the transcriptionally active form at all rpms in H9 cells [35], but not the RIV9-hiPSCs.

We speculate that these differences arise from the different structural complex and signaling proteins involved between the cell-cell and cell-ECM junctions. In 3D suspension, hPSCs have no rigid surface to adhere to, thus leading towards cell-cell adhesion and forming free-floating aggregate spheroids. In 3D dynamic suspension, these protein levels are further modulated as agitation increases.

The most interesting modulation pattern we identified was from levels of AKT and pAKT at different agitation rates. As shown in Figure 4.6A, the pan-AKT level increased

steadily with the increase in agitation, yet levels of phosphorylated activated AKT remained consistently low. This pattern demonstrates that the ratio of pAKT to pan-AKT was much lower in dynamic suspension than in static suspension and 2D adherent culture, which suggests that fluidic agitation may directly or indirectly inhibit AKT phosphorylation.

Altogether, the western data have two important implications: (1) cells in 3D culture conditions have different protein expression levels than those in 2D adherent conditions; and (2) fluidic agitation further modulates these protein expression levels of hPSCs in suspension. It is important to note that the western blot analyses do not take into account differences in protein levels due to aggregate size. However, the wide variation of sizes and differences in protein levels between static and 40 rpm suggest that aggregate size had little effect on the western data. Furthermore, the trend in protein expression levels from 40 to 100 rpm strongly indicates the influence of various agitation rates in modulating expression levels regardless of size (Figure 4.6).

Discussion

The advantage of stirred suspension culture is that it enables the efficient expansion and large-scale production of undifferentiated hPSCs without the use of costly substrates or microcarriers. For instance, our optimal agitation condition resulted in a 30-40 fold increase in cell yield after 7 days of culture. Other studies have shown similar or lower fold increases with their reported optimal agitation condition (Table 4.1). However, in many of these studies, detailed information regarding how other agitation rates in their system would affect viability, maintenance of pluripotency, and aggregate size was limited. In this study, we present a detailed analysis of various agitation rates and their impacts on the expansion of hPSCs in suspension culture. Besides growth, viability, and maintenance of hPSCs, we assessed how cell aggregate size played a role in the culture output and uncovered molecular changes at the different agitation rates to identify possible mechanosensitive signaling proteins at work in dynamic suspension of hPSCs.

In this study, we used the 125 mL ProCulture glass spinner flask with 50 mL working volume and found 60 rpm to be the optimal condition that consistently produced the highest cell yield and expansion rate of hPSCs. We observed a pattern with all of the tested cell lines that showed a strong relationship between the cell yield and the size of the cell aggregates produced at the different agitation rates. Specifically, agitation rates that produced cell aggregates greater than 400 μm (static and 40 rpm) yielded a much lower fold increase than agitation rates that produced cell aggregates below 400 μm (60-100 rpm). It is interesting to note that we observed a similar pattern in our preliminary study of

different agitation rates (0-120 rpm) using the Corning 125 mL polystyrene disposable spinner flask. In this disposable spinner flask, the best agitation rate for the expansion of hPSCs was found in the condition that produced the majority of cell aggregates sizes under 400 μm (100 rpm, Chapter 3). The biggest difference between the ProCulture and the disposable polystyrene flasks was that the latter is more primitive in its design while the former has added side baffles to enhance aeration and agitation of flask contents. This change in design would explain the differences in results between the two systems. Nevertheless, data from both systems suggest a common denominator; though higher agitation rates attenuate viability, overall, the agitation conditions that produced a more homogeneous cell aggregate sizes between 100-300 μm resulted in a higher cell yield and improved maintenance of pluripotency compared to conditions that generated larger-sized aggregates.

Optimizing the inoculation density is also considered an important culture parameter that can affect expansion rates and cell yield, which we did not explore. However, Hunt et al. reported that the effects of varying inoculation densities were insignificant for conditions outside the optimal agitation rate [36]. In fact, they found that the optimal agitation condition resulted in the greatest growth kinetics regardless of inoculation density. Interestingly, they observed that at higher inoculation density, growth was initially faster, and speculated that the overall drop in growth rate was due to limitations upon reaching a critical aggregate size [36]. We thus investigated this critical size using fixed sized aggregates, and our data indicate that this critical size starts around 400 μm where the population percentage of proliferating cells, as well as pluripotent

markers, were reduced (Figure 4.4 & 4.5). Wu et al. demonstrated that if the radii of aggregates become greater than the diffusion limitation of essential factors (~150 μm, that is ~300 μm in diameter), cells located more than 150 μm from the aggregate surface could suffer from the insufficient transport of oxygen and necessary nutrients required for maintenance of pluripotency [31]. As such, the reduction in pluripotent markers for aggregate size around 400 μm and above was found to be prominent at the center of the cell aggregate (Figure 4.5D), and as evidenced by the up-regulation of early germ layer gene expressions, this decrease in pluripotency was followed by spontaneous differentiation. Additionally, Ungrin et al., through an investigation of suspended cell aggregates in microwells, showed similar consequences of large aggregate sizes in both maintenance of undifferentiated hPSCs and subsequent direct differentiation toward definitive endoderm [37]. Taken together, it appears that an appropriate seeding density would aid in the initial aggregate formation to improve viability, but the mixing condition controls the aggregate size over the course of culture and the conditions that generate cell aggregate sizes greater than 300 μm could impose challenges in expansion and downstream process of hPSCs in suspension culture systems.

Another aspect of this study was to uncover possible mechanosensitive signaling proteins at work in our dynamic suspension cultures. Since the discovery of hPSCs, understanding of signaling mechanisms has provided practical implications for controlling hPSC culture to sustain growth and maintenance of pluripotency, as well as directing lineage-specific differentiation [32]. However, signaling mechanisms in suspension cultures are often overlooked because little is known about the molecular changes that

occur from 2D adherent culture to 3D suspension. Recently, Konze et al. have provided some insight into this gap in knowledge by finding that a truncated form of β-catenin is present in free-floating hPSC aggregates and describing a model where calpain cleaves β-catenin to aid in stabilizing pluripotency of hPSCs in suspension [38]. Data presented in this study also reveal this truncated form of β-catenin, as well as other changes in protein expression levels between 2D adherent culture and 3D static suspension counterpart, albeit only in H9 cells.

More importantly, we suggested regulation of AKT to be a prominent mechanosensitive effector in dynamic suspension culture of hPSCs. Interestingly, cross-talks among AKT and β-catenin pathways have been recently suggested as the master regulator in balancing between self-renewal and differentiation in 2D adherent cultures [39, 40]. Though it is unclear how the two pathways coordinate together to influence self-renewal or differentiation in our system, we speculate that pAKT activity may not be crucial for self-renewal in dynamic suspension since low expression levels of pAKT was found at 60-100 rpm, where pluripotent markers were still apparent. To explain the drop in pluripotency at static and 40 rpm, it is plausible that a relative basal level of β-catenin, serving as an essential E-cadherin and β-catenin-mediated intercellular adhesion, is more critical for self-renewal given that both low and high levels have been shown to promote the initial stages of differentiation [41-43]. Nevertheless, the molecular mechanism for this remains unclear, and a more thorough investigation is needed to understand interactions between fluidic forces and core biochemical signals in 3D culture systems.

In summary, we have described that the optimal agitation condition to enhance expansion of hPSCs in dynamic suspension requires a balance between producing uniform cell aggregates below the critical size and limiting excessive force-related cell death. This balance is expected to be an important parameter for scalable production of hPSCs in 3D suspension systems. Furthermore, this study suggests fluidic agitation being a critical input parameter to potentially alter molecular mechanisms, thereby affecting hPSC fate determination in dynamic suspension. This means that fluidic agitation could be a considerable physical cue, along with or in place of chemical cues, to facilitate differentiation of hPSCs.

Table & Figures

III Table 4.1. Summary of published protocols for the expansion of hPSCs in stirred suspension culture system. *Aggregate size was estimated based on the reported number of cells per average cluster size. bFGF = basic fibroblast growth factor. CM = conditioned medium. FI = fold increase. IL6RIL6 = interleukin-6 receptor fused to interleukin-6. KOSR = Knockout-serum replacement. NA = data not available.

References	*Cell Types*	*Stirrer Type*	*Medium*	*Inoculation Density (cells/mL)*	*Agitation (rpm) – Culture time point*	*Fold Increase (FI) – Aggregate Size*
Singh et al. 2010	hESCs	100 ml flask (Integra)	mTeSR1	1 x 10^5	40 rpm – 7 days	10 FI – 350-500* µm
Krawetz et al. 2010	hESCs	125 mL flask (NDS)	mTeSR1	1.8 x 10^4	100 rpm – 6 days	12 FI – NA
Zweigerdt et al. 2011	hESCs and hiPSCs	100 mL flask (Integra)	mTeSR1	1 x 10^6	40 rpm – 7 days	3 FI – 350-550 µm
Amit et al. 2011	hESCs and hiPSCs	100 ml flask (Integra)	DMEM/F12 + KOSR, IL6RIL6, and bFGF	1 x 10^5	60-90 rpm – 6 days	17.7 FI – NA (unpublished data)
Chen et al. 2012	hESCs	125 mL flask (Cimarec Biosystem)	StemPro + bFGF	2.5 x 10^5	70 rpm – 4 days	4.3 FI – NA
Abbasalizadeh et al. 2012	hESCs and hiPSCs	100 mL flask (Integra)	DMEM/F12-CM + GlutaMAX and bFGF	3 x 10^5	40 rpm – 8 days	6.5 FI – 190-215 µm
Olmer et al. 2012	hiPSCs	100 mL flask (DasGip Cellferm Pro)	mTeSR1	5 x 10^5	60 rpm – 7 days	5.5 FI – 100-150 µm
Wang et al. 2013	hiPSCs	100 ml flask (Integra)	Essential 8	5 x 10^5	60 rpm – 5 days	3 FI – 150-250 µm
Hunt et al. 2014	hESCs	125 mL flask (NDS)	mTeSR1	2 x 10^4	100 rpm – 6 days	12 FI – 150-350 µm
Current Study	hESCs and hiPSCs	125 mL flask (ProCulture)	mTeSR1	1 x 10^5	60 rpm – 7 days	40 FI – 100-300 µm

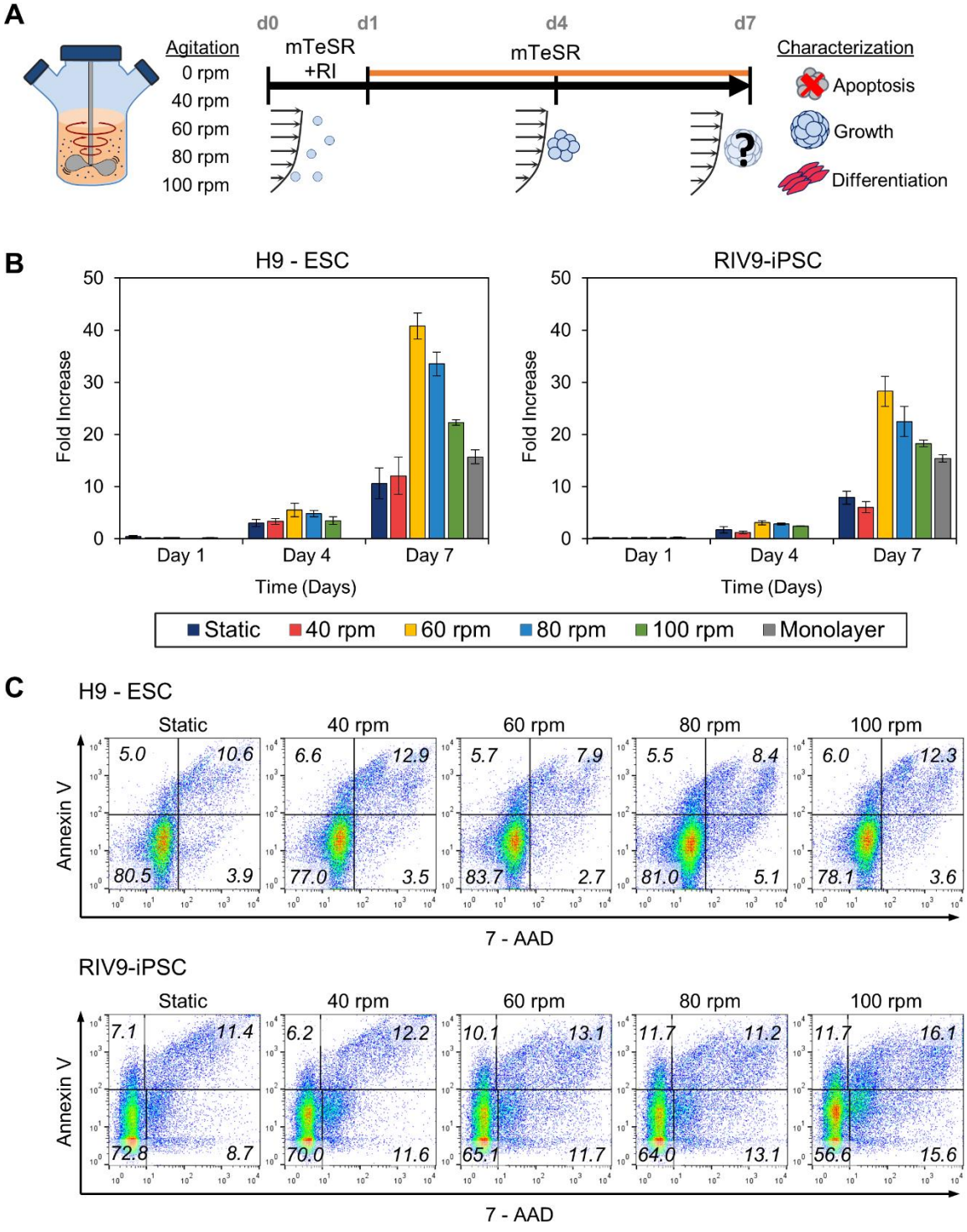
A
Agitation
0 rpm
40 rpm
60 rpm
80 rpm
100 rpm
d0
d1
d4
d7
mTeSR
+RI
mTeSR
Characterization
Apoptosis
Growth
Differentiation
B
H9 - ESC
RIV9-iPSC
Fold Increase
Day 1
Day 4
Day 7
Time (Days)
Static
40 rpm
60 rpm
80 rpm
100 rpm
Monolayer
C
H9 - ESC
RIV9-iPSC
Static
40 rpm
60 rpm
80 rpm
100 rpm
Annexin V
7 - AAD
5.0
10.6
80.5
3.9
6.6
12.9
77.0
3.5
5.7
7.9
83.7
2.7
5.5
8.4
81.0
5.1
6.0
12.3
78.1
3.6
7.1
11.4
72.8
8.7
6.2
12.2
70.0
11.6
10.1
13.1
65.1
11.7
11.7
11.2
64.0
13.1
11.7
16.1
56.6
15.6

Figure 4.1. The impact of different agitation rates for the propagation of hPSCs in dynamic suspension. (A) Illustration outlining our culture scheme to assess the influence of varying agitation rates on day 0, spinner flasks for the varying agitation rates were seeded with 10^5 cells/mL hPSCs each. The daily growth rate was determined, and the cells were characterized on day 7. (B) Growth curve of H9-ESC and RIV9-iPSCs over 7 days. (C) The viability of H9-ESC and RIV9-iPSCs measured via flow cytometry using Annexin V and 7-AAD on day 7. Data points shown as mean ± SD (N=3).

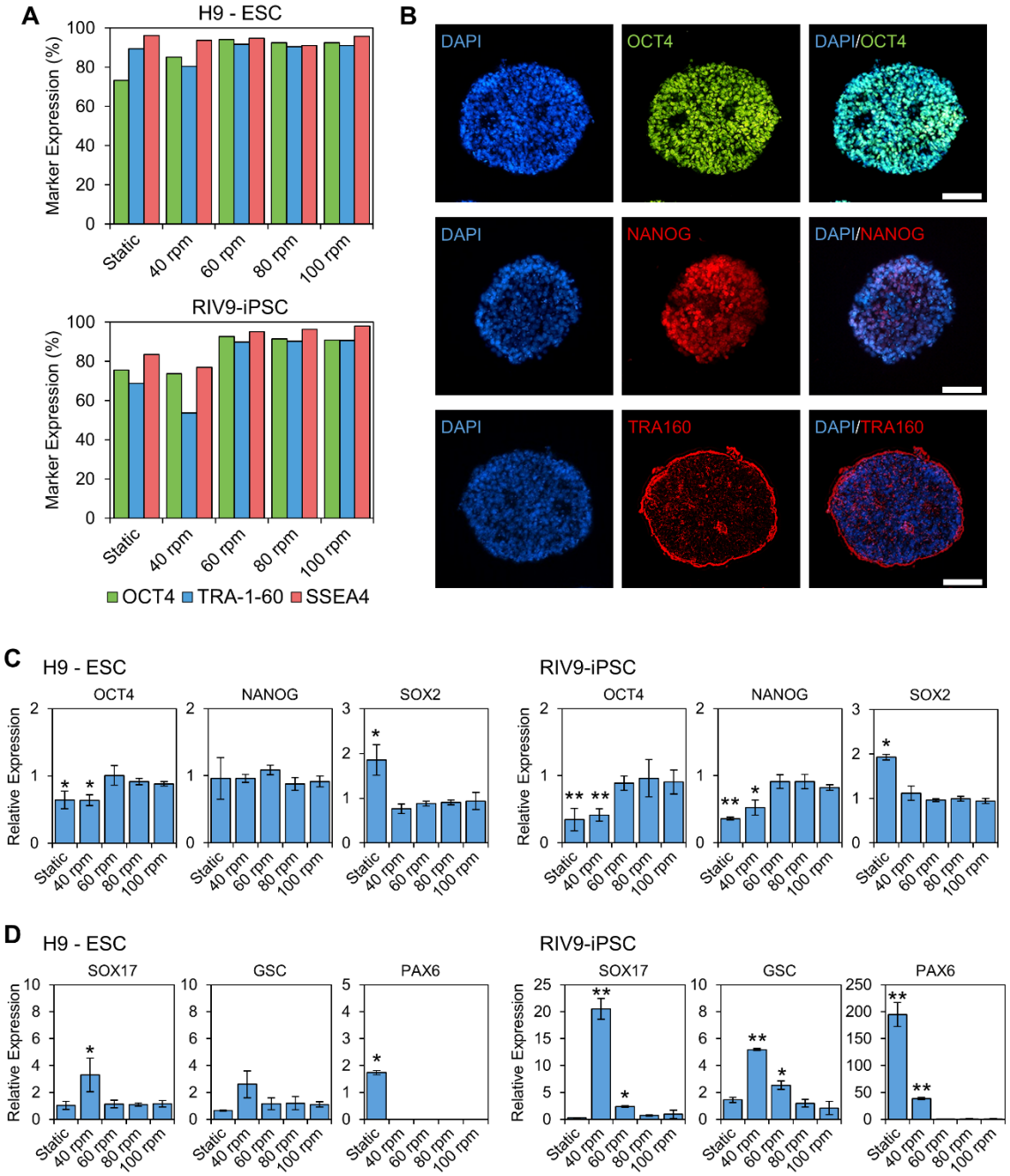
A
H9 - ESC
Marker Expression (%)
100
80
60
40
20
0
Static
40 rpm
60 rpm
80 rpm
100 rpm
RIV9-iPSC
OCT4
TRA-1-60
SSEA4
B
DAPI
OCT4
DAPI/OCT4
NANOG
DAPI/NANOG
TRA160
DAPI/TRA160
C
H9 - ESC
RIV9-iPSC
OCT4
NANOG
SOX2
Relative Expression
D
SOX17
GSC
PAX6

Figure 4.2. Influence of agitation rates in maintenance of pluripotency and differentiation after 7 days in dynamic suspension. (A) Flow cytometry quantified the subpopulation of cells expressing OCT4, TRA-1-60 & SSEA4 pluripotent markers. (B) Sectioned H9 aggregates from 60 rpm, immunofluorescently stained for OCT4, NANOG, and TRA-1-60. (C) Gene expression analysis by qPCR for *OCT4*, *NANOG*, and *SOX2* pluripotent genes. (D) qPCR also quantified early germ layer genes for *SOX17* (endoderm), *GOOSECOID* (*GSC* – mesoderm), and *PAX6* (ectoderm). Scale bars: 100 µm. Data points shown as mean ± SD (N=3). *, $p \leq 0.05$; **, $p \leq 0.01$.

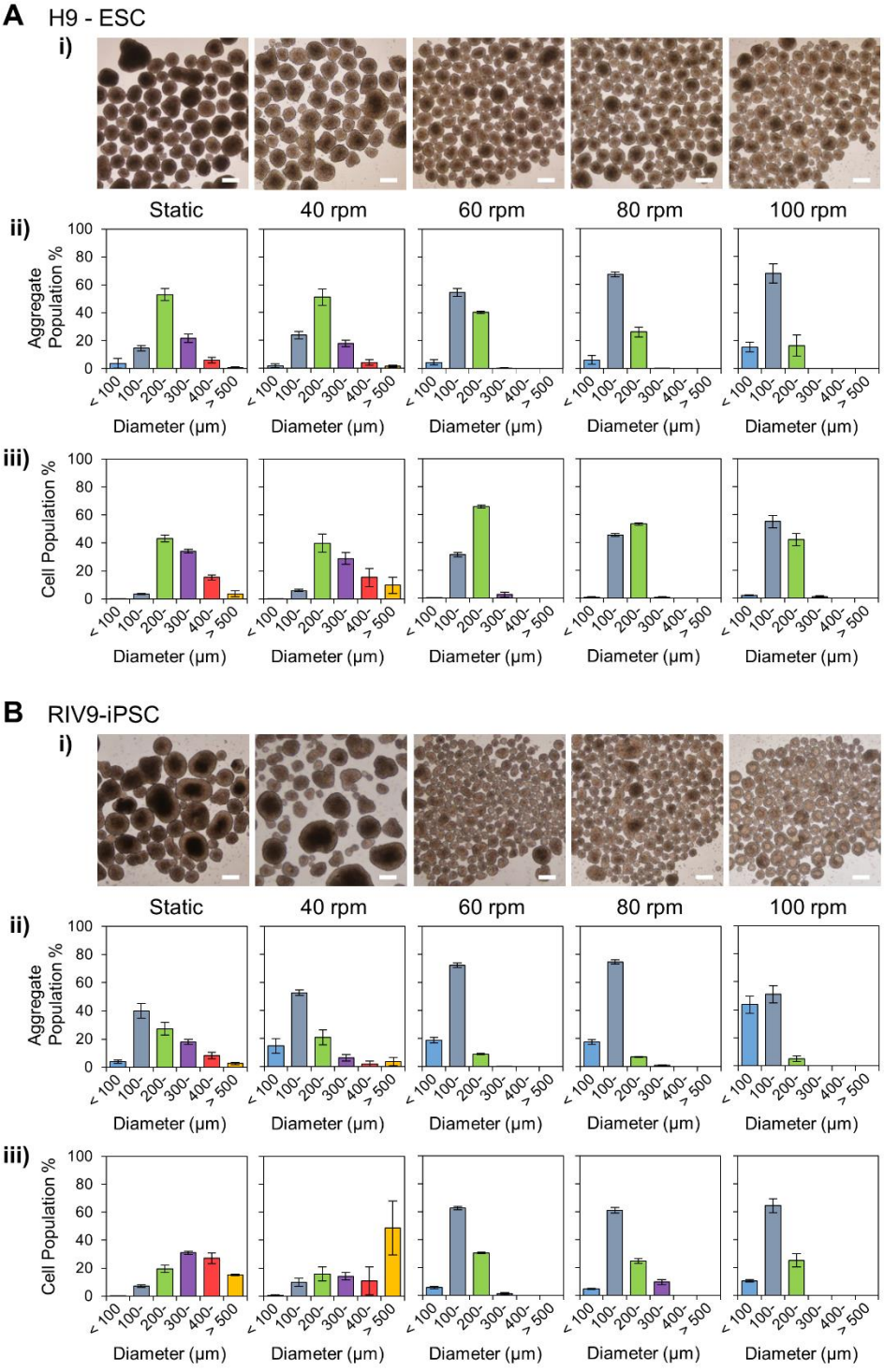
A
H9 - ESC
i)
Static
40 rpm
60 rpm
80 rpm
100 rpm
ii)
Aggregate Population %
iii)
Cell Population %
< 100
100-
200-
300-
400-
> 500
Diameter (µm)
B
RIV9-iPSC

Figure 4.3. Cell aggregate population at varying agitation rates. (A) H9-ESCs and (B) RIV9-iPSCs cell aggregate assessment for each agitation rate on day 7. (i) Photomicrographs of cell aggregate morphology. (ii) Distribution of aggregate population by aggregate size. (iii) Distribution of cell population by aggregate size. Scale bars: 250 μm. Data points shown as mean ± SD (N=3).

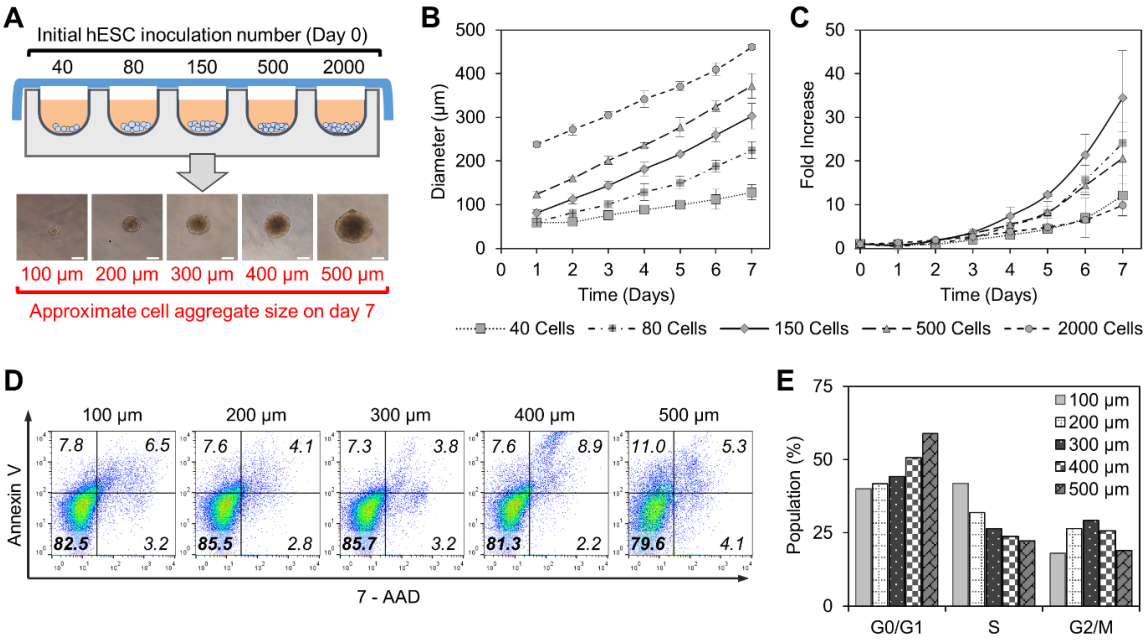

Figure 4.4. Controlled size study to assess the influence of aggregate size. (A) Schematic diagram showing initial inoculation number of hESC and resulting aggregates on day 7. (B) Daily growth of aggregate size. (C) Population growth curves over 7 days. (D) Cell viability of prescribed aggregate sizes on day 7. (E) Cell cycle analysis for prescribed aggregate sizes on day 7. Scale bars: 200 µm. Data points shown as mean ± SD (N≥5).

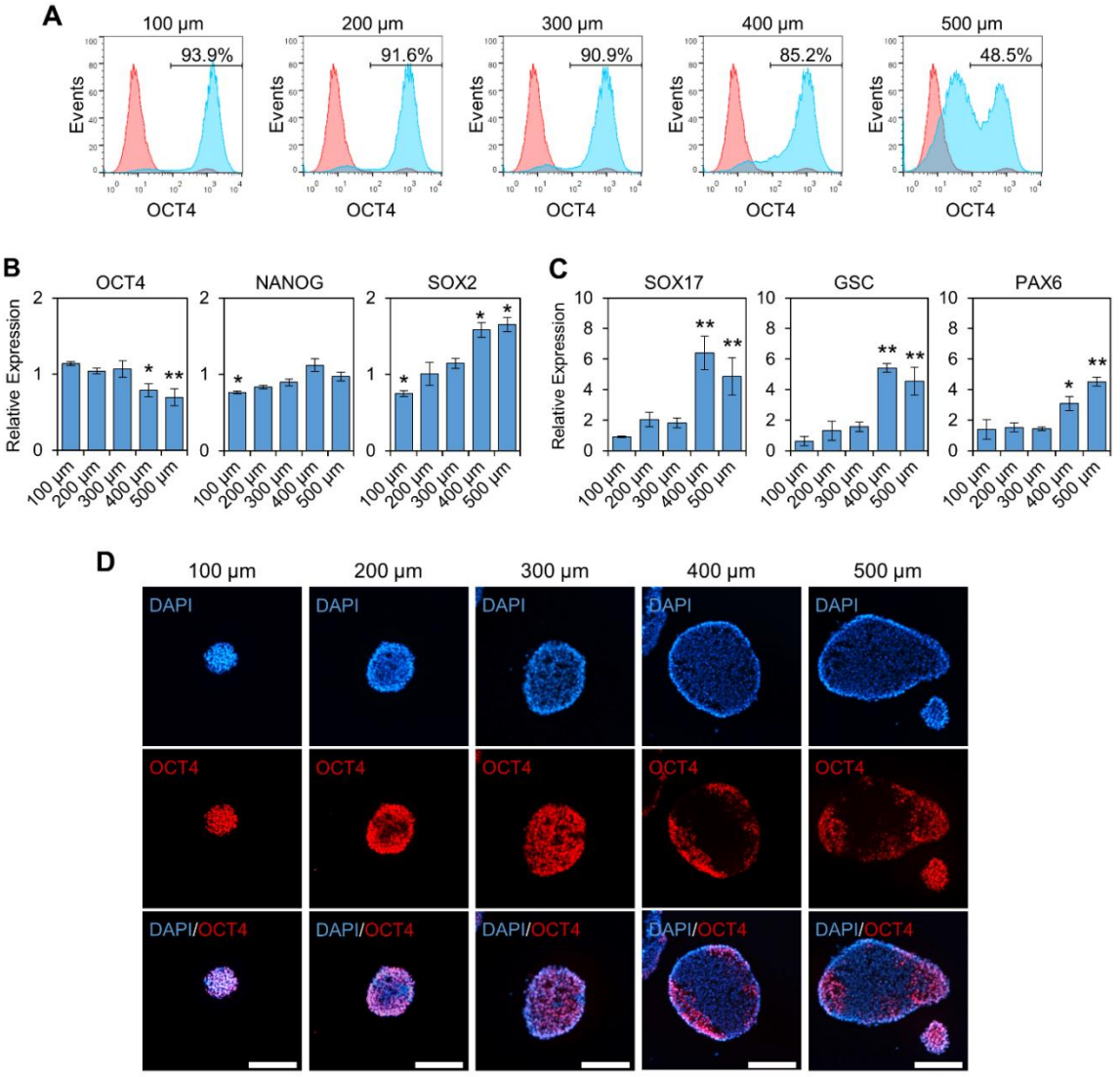

Figure 4.5. Reduction in the maintenance of pluripotency as aggregate size grows greater than 300 µm. (A) Expression of OCT4 pluripotency marker from the prescribed aggregate sizes by flow cytometry. (B) Gene expression analysis by qPCR for *OCT4*, *NANOG*, and *SOX2* pluripotent genes. (C) Gene expression analysis for *SOX17*, *GSC*, and *PAX6* genes. (D) Immunostaining of OCT4 pluripotency marker in sectioned aggregate samples. Scale bars: 200 µm. Data points shown as mean ± SD (N=3). *, $p \leq 0.05$; **, $p \leq 0.01$.

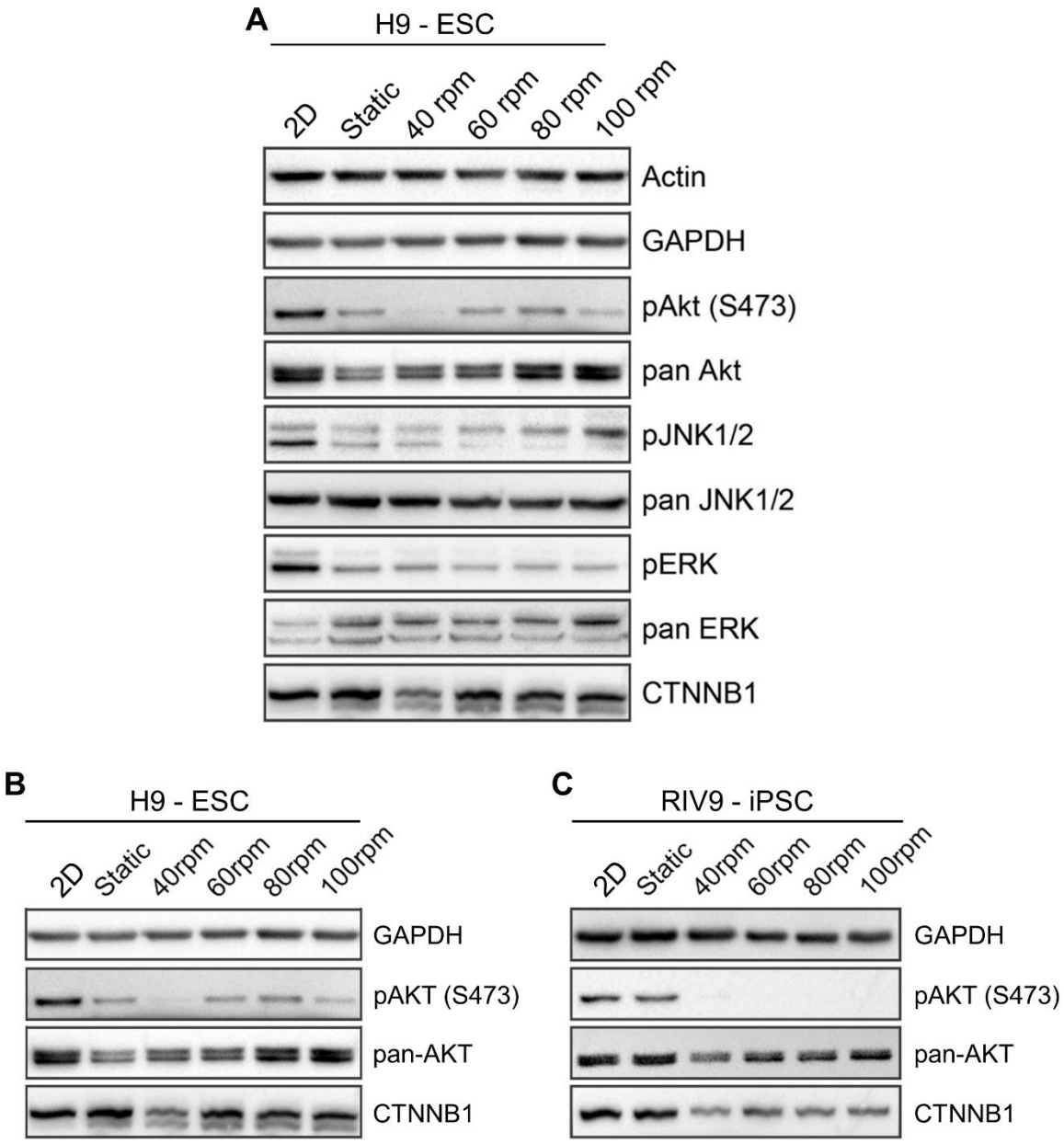

Figure 4.6. Western blot analysis of selected protein expressions on day 7 samples. (A) H9-ESC full western analysis. (B) Truncated form of H9-ESC western to compare with (C) RIV9-iPSC.

References

1. Thomson, J.A., *Embryonic Stem Cell Lines Derived from Human Blastocysts.* Science, 1998. **282**(5391): p. 1145-1147.
2. Takahashi, K., K. Tanabe, M. Ohnuki, et al., *Induction of pluripotent stem cells from adult human fibroblasts by defined factors.* Cell, 2007. **131**(5): p. 861-72.
3. Yu, J., M.A. Vodyanik, K. Smuga-Otto, et al., *Induced pluripotent stem cell lines derived from human somatic cells.* Science, 2007. **318**(5858): p. 1917-20.
4. Robinton, D.A. and G.Q. Daley, *The promise of induced pluripotent stem cells in research and therapy.* Nature, 2012. **481**(7381): p. 295-305.
5. Kiskinis, E. and K. Eggan, *Progress toward the clinical application of patient-specific pluripotent stem cells.* Journal of Clinical Investigation, 2010. **120**(1): p. 51-59.
6. Murry, C.E. and G. Keller, *Differentiation of embryonic stem cells to clinically relevant populations: Lessons from embryonic development.* Cell, 2008. **132**(4): p. 661-680.
7. Serra, M., C. Brito, C. Correia, et al., *Process engineering of human pluripotent stem cells for clinical application.* Trends Biotechnol, 2012. **30**(6): p. 350-9.
8. Burridge, P.W., G. Keller, J.D. Gold, et al., *Production of de novo cardiomyocytes: human pluripotent stem cell differentiation and direct reprogramming.* Cell Stem Cell, 2012. **10**(1): p. 16-28.
9. Lindvall, O. and Z. Kokaia, *Stem cells for the treatment of neurological disorders.* Nature, 2006. **441**(7097): p. 1094-6.
10. Lock, L.T. and E.S. Tzanakakis, *Stem/Progenitor cell sources of insulin-producing cells for the treatment of diabetes.* Tissue Eng, 2007. **13**(7): p. 1399-412.
11. Celiz, A.D., J.G.W. Smith, R. Langer, et al., *Materials for stem cell factories of the future.* Nature Materials, 2014. **13**(6): p. 570-579.
12. Valamehr, B., H. Tsutsui, C.M. Ho, et al., *Developing defined culture systems for human pluripotent stem cells.* Regenerative Medicine, 2011. **6**(5): p. 623-634.
13. Chen, K.G., B.S. Mallon, R.D. McKay, et al., *Human pluripotent stem cell culture: considerations for maintenance, expansion, and therapeutics.* Cell Stem Cell, 2014. **14**(1): p. 13-26.
14. Steiner, D., H. Khaner, M. Cohen, et al., *Derivation, propagation and controlled differentiation of human embryonic stem cells in suspension.* Nat Biotechnol, 2010. **28**(4): p. 361-4.

15. Sargent, C.Y., G.Y. Berguig, M.A. Kinney, et al., *Hydrodynamic modulation of embryonic stem cell differentiation by rotary orbital suspension culture.* Biotechnol Bioeng, 2010. **105**(3): p. 611-26.

16. Wang, Y., B.K. Chou, S. Dowey, et al., *Scalable expansion of human induced pluripotent stem cells in the defined xeno-free E8 medium under adherent and suspension culture conditions.* Stem Cell Research, 2013. **11**(3): p. 1103-1116.

17. Abbasalizadeh, S., M.R. Larijani, A. Samadian, et al., *Bioprocess development for mass production of size-controlled human pluripotent stem cell aggregates in stirred suspension bioreactor.* Tissue Eng Part C Methods, 2012. **18**(11): p. 831-51.

18. Chatterjee, P., Y. Cheung, and C. Liew, *Transfecting and Nucleofecting Human Induced Pluripotent Stem Cells.* Jove-Journal of Visualized Experiments, 2011(56).

19. Schmittgen, T.D. and K.J. Livak, *Analyzing real-time PCR data by the comparative C-T method.* Nature Protocols, 2008. **3**(6): p. 1101-1108.

20. Nampe, D. and H. Tsutsui, *Engineered Micromechanical Cues Affecting Human Pluripotent Stem Cell Regulations and Fate.* Jala, 2013. **18**(6): p. 482-493.

21. Sun, Y. and J. Fu, *Mechanobiology: a new frontier for human pluripotent stem cells.* Integr Biol (Camb), 2013. **5**(3): p. 450-7.

22. Mammoto, A., T. Mammoto, and D.E. Ingber, *Mechanosensitive mechanisms in transcriptional regulation.* J Cell Sci, 2012. **125**(Pt 13): p. 3061-73.

23. Keller, K.C., B. Rodrigues, and N.I. zur Nieden, *Suspension Culture of Pluripotent Stem Cells: Effect of Shear on Stem Cell Fate.* Critical Reviews in Eukaryotic Gene Expression, 2014. **24**(1): p. 1-13.

24. Titmarsh, D., A. Hidalgo, J. Turner, et al., *Optimization of flowrate for expansion of human embryonic stem cells in perfusion microbioreactors.* Biotechnol Bioeng, 2011. **108**(12): p. 2894-904.

25. Irie, N., L. Weinberger, W.W.C. Tang, et al., *SOX17 Is a Critical Specifier of Human Primordial Germ Cell Fate.* Cell, 2015. **160**(1-2): p. 253-268.

26. Tada, S., T. Era, C. Furusawa, et al., *Characterization of mesendoderm: a diverging point of the definitive endoderm and mesoderm in embryonic stem cell differentiation culture.* Development, 2005. **132**(19): p. 4363-4374.

27. Zhang, X.Q., C.T. Huang, J. Chen, et al., *Pax6 Is a Human Neuroectoderm Cell Fate Determinant.* Cell Stem Cell, 2010. **7**(1): p. 90-100.

28. Brafman, D.A., N. Moya, S. Allen-Soltero, et al., *Analysis of SOX2-expressing cell populations derived from human pluripotent stem cells.* Stem Cell Reports, 2013. **1**(5): p. 464-78.

29. Wu, J., Y. Fan, and E.S. Tzanakakis, *Increased culture density is linked to decelerated proliferation, prolonged G1 phase, and enhanced propensity for*

differentiation of self-renewing human pluripotent stem cells. Stem Cells Dev, 2015. **24**(7): p. 892-903.

30. Itskovitz-Eldor, J., M. Schuldiner, D. Karsenti, et al., *Differentiation of human embryonic stem cells into embryoid bodies compromising the three embryonic germ layers.* Mol Med, 2000. **6**(2): p. 88-95.

31. Wu, J., M.R. Rostami, D.P. Cadavid Olaya, et al., *Oxygen transport and stem cell aggregation in stirred-suspension bioreactor cultures.* PLoS One, 2014. **9**(7): p. e102486.

32. Sun, Y., C.S. Chen, and J. Fu, *Forcing stem cells to behave: a biophysical perspective of the cellular microenvironment.* Annu Rev Biophys, 2012. **41**: p. 519-42.

33. Ding, S., P. Kingshott, H. Thissen, et al., *Modulation of human mesenchymal and pluripotent stem cell behavior using biophysical and biochemical cues: A review.* Biotechnol Bioeng, 2016.

34. Jenkins, M.J. and S.S. Farid, *Human pluripotent stem cell-derived products: Advances towards robust, scalable and cost-effective manufacturing strategies.* Biotechnology Journal, 2015. **10**(1): p. 83-95.

35. Abe, K. and M. Takeichi, *NMDA-receptor activation induces calpain-mediated beta-catenin cleavages for triggering gene expression.* Neuron, 2007. **53**(3): p. 387-397.

36. Hunt, M.M., G. Meng, D.E. Rancourt, et al., *Factorial experimental design for the culture of human embryonic stem cells as aggregates in stirred suspension bioreactors reveals the potential for interaction effects between bioprocess parameters.* Tissue Eng Part C Methods, 2014. **20**(1): p. 76-89.

37. Ungrin, M.D., G. Clarke, T. Yin, et al., *Rational bioprocess design for human pluripotent stem cell expansion and endoderm differentiation based on cellular dynamics.* Biotechnol Bioeng, 2012. **109**(4): p. 853-66.

38. Konze, S.A., L. van Diepen, A. Schroder, et al., *Cleavage of E-cadherin and beta-catenin by calpain affects Wnt signaling and spheroid formation in suspension cultures of human pluripotent stem cells.* Mol Cell Proteomics, 2014. **13**(4): p. 990-1007.

39. Huang, T.S., L. Li, L. Moalim-Nour, et al., *A Regulatory Network Involving beta-Catenin, E-Cadherin, PI3K/Akt, and Slug Balances Self-Renewal and Differentiation of Human Pluripotent Stem Cells in Response to Wnt Signaling.* Stem Cells, 2015. **33**(5): p. 1419-1433.

40. Singh, A.M., D. Reynolds, T. Cliff, et al., *Signaling Network Crosstalk in Human Pluripotent Cells: A Smad2/3-Regulated Switch that Controls the Balance between Self-Renewal and Differentiation.* Cell Stem Cell, 2012. **10**(3): p. 312-326.

41. Azarin, S.M., X. Lian, E.A. Larson, et al., *Modulation of Wnt/beta-catenin signaling in human embryonic stem cells using a 3-D microwell array.* Biomaterials, 2012. **33**(7): p. 2041-9.

42. Blauwkamp, T.A., S. Nigam, R. Ardehali, et al., *Endogenous Wnt signalling in human embryonic stem cells generates an equilibrium of distinct lineage-specified progenitors.* Nature Communications, 2012. **3**.

43. Davidson, K.C., A.M. Adams, J.M. Goodson, et al., *Wnt/beta-catenin signaling promotes differentiation, not self-renewal, of human embryonic stem cells and is repressed by Oct4.* Proc Natl Acad Sci U S A, 2012. **109**(12): p. 4485-90.

44. Singh, H., P. Mok, T. Balakrishnan, et al., *Up-scaling single cell-inoculated suspension culture of human embryonic stem cells.* Stem Cell Res, 2010. **4**(3): p. 165-79.

45. Krawetz, R., J.T. Taiani, S.Y. Liu, et al., *Large-Scale Expansion of Pluripotent Human Embryonic Stem Cells in Stirred-Suspension Bioreactors.* Tissue Engineering Part C-Methods, 2010. **16**(4): p. 573-582.

46. Zweigerdt, R., R. Olmer, H. Singh, et al., *Scalable expansion of human pluripotent stem cells in suspension culture.* Nat Protoc, 2011. **6**(5): p. 689-700.

47. Amit, M., I. Laevsky, Y. Miropolsky, et al., *Dynamic suspension culture for scalable expansion of undifferentiated human pluripotent stem cells.* Nature Protocols, 2011. **6**(5): p. 572-579.

48. Chen, V.C., S.M. Couture, J. Ye, et al., *Scalable GMP compliant suspension culture system for human ES cells.* Stem Cell Res, 2012. **8**(3): p. 388-402.

49. Olmer, R., A. Lange, S. Selzer, et al., *Suspension culture of human pluripotent stem cells in controlled, stirred bioreactors.* Tissue Eng Part C Methods, 2012. **18**(10): p. 772-84.

CHAPTER 5:

CONTROLLING AGITATION TO IMPROVE CARDIAC DIFFERENTIATION OF HUMAN PLURIPOTENT STEM CELLS IN STIRRED SUSPENSION CULTURE

Abstract

Cardiac differentiation of human pluripotent stem cells (hPSCs) has progressed to a point where their use in cell therapy appears conceivable. Although hESCs may serve as an unlimited source for generating functional cardiomyocytes, current methods of production towards clinically relevant numbers of cells are still inefficient. In addition, the inconsistency in outcomes from cardiac differentiation protocols presents a limiting step to both the research and therapeutic use of hPSCs. In this study, we demonstrate that pausing agitation during a critical induction step improved cardiac differentiation efficiency and generated over 90% cTnT-positive cells. Our approach was formulated based on our previous study where AKT activity was highly regulated by fluidic agitation (Chapter 4). We speculated that pausing agitation could be beneficial for AKT activity, and in turn, improve cardiac differentiation. Overall, pausing agitation during stage-2 of differentiation (WNT inhibition) improved not only differentiation efficiency but also the maturation of cardiomyocytes, as indicated by the highly organized sarcomere structure.

Introduction

Despite advances in biotechnology and medicine, cardiovascular disorders are still a leading cause of death worldwide. There are different forms of cardiovascular diseases, but the common feature in heart failure is a severe loss of cardiomyocytes, the muscle cells that make up the contractile heart tissue [1]. The heart is known to be one of the least regenerative organs in the body, and a myocardial infarction can damage 25% of the 2-4 billion cardiomyocytes that reside in the left ventricle [2]. This means that approximately 1 billion cardiomyocytes need to be replaced to repair the damage. Otherwise, a progressive loss would most likely lead to complete heart failure. For this reason, hPSCs have emerged as a promising tool for heart regeneration because of their potential to provide an inexhaustible supply of human cardiomyocytes [3]. The challenge now is developing a scalable production process that could readily provide large quantities of hPSC-derived cardiomyocytes at a reasonable cost.

Progress in cardiac differentiation is at a point where multiple protocols could provide a large population of cardiac troponin T (cTnT) positive cells with relative ease [4]. For instance, protocols for the scalable production of cardiomyocytes starting from embryoid bodies (EBs) could provide over 60% cTnT-positive cells by temporally modulating signaling pathways using appropriate soluble factors [5]. However, the efficacy of this method may require timing and concentration of growth factors to be individually optimized for each hPSC lines, which could be a tedious process for large-scale production. On the other hand, the most efficient approach to date only requires temporal modulation

of WNT signaling pathway by small molecules to generate over 80% cardiomyocytes [6]. This approach, however, lacks scalability because it relies on confluent monolayer cultures that may not readily provide large numbers of hPSC-derived cardiomyocytes. Nonetheless, the commonality among various established protocols is the importance of timing to regulate specific pathways for an effective differentiation process.

In this study, we aimed to translate this WNT modulation by a small molecules protocol to an integrated process for hESC expansion and cardiac differentiation in stirred suspension culture. Although similar approaches have been recently reported by other groups [7, 8], we present a novel strategy where the agitation condition was leveraged to promote cardiac specification and enhance differentiation efficiency. This approach was derived from our previous study in which we observed that stirred-agitation reduced AKT phosphorylation in suspension cultures of hPSCs. We demonstrate that pausing agitation during a critical induction step improved cardiac differentiation efficiency to produce over 90% cTnT-positive cells. Furthermore, immunofluorescence suggests that this process also increases maturation of cardiomyocytes, as evidenced by the highly organized sarcomere structure. Overall, this study provides a promising approach for harnessing the hydrodynamic conditions for the scalable mass production of cardiomyocytes in stirred suspension culture.

Materials and Methods

Cardiac differentiation in 2D adherent cultures

H9 hESC line maintained on geltrex in mTeSR1 were treated with 10 μM Y-27632 (ROCK inhibitor, ROCKi) for 1 hr at 37 °C prior to enzymatic dissociation to minimize cell death caused by single-cell dissociation. The cells were then washed three times with 1x PBS (Hyclone), treated with 0.25% Trypsin-EDTA solution (Thermo-Fisher) for 10 min at 37 °C, gently pipetted to break up clumps, and strained through a 40 μm cell strainer (Corning) to obtain single cells. The cells were then diluted (1:10) using 10% fetal bovine serum (FBS, Hyclone) in DMEM (Lonza) to inactivate the trypsin, and spun down at 250×g for 5 min. Cells were then seeded onto a geltrex-coated cell culture dish at 10^5 cells/mL in mTeSR1 medium supplemented with 10 μM ROCKi (day -4) for 24 hrs. The cells were cultured in mTeSR1 during the expansion phase (day -4 to day 0).

To initiate cardiac differentiation (day 0), cells were treated with 7.5 μM CHIR (CHIR99021, GSK3 inhibitor) in RPMI/B27-insulin for 24 hrs, after which the CHIR was removed by medium change. At day 3, cells were treated with 5 μM IWP2 (Tocris) for 48 hrs and were removed during medium change on day 5. Cells were cultured in RPMI/B27-insulin from day 0 to day 7. Starting day 7, the medium was then changed to RPMI/B27 (complete) and cultured to day 15, with fresh medium changed every 3 days.

Expansion and cardiac differentiation in 3D suspension cultures

To initiate the expansion phase in 3D suspension, the cells were treated as described above, with 10 ROCKi 1 hr before trypsin dissociation. The enzymatically isolated single

cells were resuspended in mTeSR1 medium with 10 μM ROCKi and inoculated at a density of 10^5 cells/mL with a total volume of 50 mL per spinner flask (Corning 125 mL ProCulture glass spinner flasks) that had been siliconized with Sigmacote (Sigma) following the manufacturer's instruction. ROCKi was removed by complete medium change after 24 hrs. The cells grew into and were maintained in mTeSR1 as aggregate spheroids during the expansion phase (day -4 to day 0). At day 0, three 1 mL samples were taken from the spinner flask to determine the cell concentration. The cells were kept as aggregate spheroids for cardiac differentiation, but the starting cell concentration was normalized to an even baseline across each spinner flask on day 0.

Protocol for cardiac differentiation in 3D suspension was as described in 2D adherent culture. For the stage-specific static condition, agitation was paused, and the cells were maintained in static suspension under standard culture conditions (37 °C, 5% CO2, 100% humidity). For the inhibitor study, cells were treated with 10 μM ROCKi (with or without 5 μM IWP2) for 48 hrs and were removed during medium change on day 5.

Daily sampling to determine fold increase

For each condition, three 1 mL samples were taken from the spinner flask for cell counting and replaced with an equal amount of fresh medium. Upon enzymatic digestion, the cells were manually counted, and viability was determined by the trypan blue exclusion method. The growth curve was generated based on cell count with an adjustment to the lost volume due to sampling.

Aggregate morphology and quantifying size distribution

Aggregate samples were taken on specific time points and placed in a 12-mm culture dish (BD falcon) for photomicrographs using a Nikon D5100 camera attached to a Nikon Eclipse TS100 microscope. For quantifying aggregate size distribution at day 0, three samples for each condition were taken and imaged. Image contrast and brightness were adjusted by ImageJ, and a custom MATLAB script was used to measure and collect the equivalent diameter of each aggregate.

Flow cytometry

Cell aggregate samples were trypsinized into single cell as described above. The cells were fixed with 4% paraformaldehyde, washed with 1X PBS, and permeabilized with 0.2% Saponin in wash buffer solution (PBS + 5% FBS) for 15 min on ice. Primary antibodies were then added at suggested dilutions (appendix C) and incubated for 90 min at 4 °C in the dark. Following rinsing, secondary antibodies (appendix C) were added and incubated for 60 min at 4 °C in the dark. The cells were then washed and suspended in wash buffer and stored at 4 °C in the dark until analyzed. Flow cytometric analysis was performed with ACEA Biosciences NovoCyte flow cytometer at the UCR Stem Cell Core or BD FACSAria at the UCR Institute for Integrative Genome Biology. Data analysis was done using FlowJo 10.

Quantitative Real-Time PCR (qPCR)

Total RNA of cells was extracted using the Qiagen RNA isolation kit (Qiagen RNeasy kit) following the manufacturer's instructions. Purified RNA was then used to

synthesize complementary DNA (cDNA) with the iScript cDNA Synthesis Kit (BioRad) following the manufacturer's instructions. Diluted cDNA and specific primers were then added with the Taqman Mastermix Fastmix (Quanta PerfeCTa FastMix) for qPCR. The relative expression of each targeted gene was calculated by the comparative ΔΔCt method normalized by the level of internal housekeeping gene glyceraldehyde-3 phosphate dehydrogenase (GAPDH) and compared to undifferentiated hPSCs from monolayer culture controls [29]. The primer sequences used for qPCR are listed in appendix C.

Immunocytochemistry

Cell aggregate samples were trypsinized into single cell as described above. The cells were resuspended in RPMI20 solution (20% FBS in RPMI) supplemented with 5 μM ROCKi and plated onto a 0.1% (wt/vol) gelatin-coated coverslip at a concentration of 10^5 cells/mL. The cells were incubated for 2 days without medium change, after which the medium in replaced with RPMI/B-27 medium and maintained for additional 2-5 days. After the desired time is reached, the cells were washed with 1X PBS and fixed with 4% paraformaldehyde for 30 min at room temperature (RT). The cells were then washed with 1X PBS and permeabilized with 0.1% Triton-X (Sigma) and blocked with blocking buffer (5% normal serum and 5% FBS in PBS) supplemented with 0.1% Triton X. Primary antibodies were added at the recommended dilution and incubated for 3 hrs at RT. Samples were then washed with immunocytochemistry (ICC) wash buffer (1% BSA and 5% normal serum) and incubated with an appropriate secondary antibody for 1 hr at RT. Samples were then mounted using Vectashield mounting medium with DAPI. Images were taken with the Nikon Eclipse Ti at the UCR Stem Cell Core and analysis was done using ImageJ.

Results

Optimization of Cardiomyocyte Differentiation in Stirred Suspension Culture

For cardiac differentiation, the timing of activated regulatory signals at different stages of differentiation is crucial for improving efficiency. For this reason, the most efficient protocols require step-wise modulation of key regulatory signals for cardiac specification. Therefore, we sought to determine if temporally regulating the agitation conditions at different stages of differentiation would improve cardiac differentiation efficiency. The principle hypothesis of this study is that agitation could play a critical mechanotransduction signaling role to impact the culture outcome. Specifically, the role of AKT has been implicated as an important signaling factor in lineage determination and cardiac specification following early differentiation [9-13]. Since we observed AKT to be heavily regulated by fluidic agitation, it is plausible that pausing agitation would rescue AKT activity during a specific stage of differentiation to generate pure hESC-derived cardiomyocytes. Our strategy is outlined in Figure 5.1, where a four-step process was conducted, in which we test the effects of pausing agitation during Stage-1 (S1, WNT activation) or Stage-2 (S2, WNT inactivation) of differentiation. We also added a constant static (CS) and constant agitation (CA) condition to compare their performances against the paused-agitation conditions. Before initiating cardiac differentiation, the cells were first expanded in mTeSR for 4 days to obtain large numbers of hESCs aggregates that were directly used for differentiation.

Since differentiation efficiency also depends on the quality of the starting material, the growth, pluripotency, and aggregate morphology from each condition were examined at the end of the expansion phase (day 0). In terms of growth, the three conditions that were cultured at 60 rpm during the expansion phase resulted in a 4.5 fold increase, while the CS condition only produced a 3 fold increase (Figure 5.2A). This result is in accordance with our previous study where we found 60 rpm to be more effective in the expansion of hPSCs than static suspension conditions. Also from our previous study, we found both that the aggregate size and loss of pluripotency could affect the overall cell yield. When we quantitatively measured the aggregate size distribution (Figure 5.2B), the 3 conditions under 60 rpm produced a more homogeneous size distribution (~100-200 μm) than the wider size distribution in the CS condition. The lower cell yield and larger-sized aggregates in the CS condition suggest the quality of hESCs had been compromised. However, flow cytometry analysis revealed that maintenance of pluripotency was still apparent in every condition (Figure 5.2C). Therefore, the lower cell yield is likely the product of a reduced proliferation from the larger-sized aggregates, whereas the baseline quality of the cells seemed to be similar across all four conditions.

The effects of stage-specific intermittent agitation

Following expansion, mTeSR growth medium was replaced with RPMI1640/B27 (minus insulin) basal medium supplemented with 7.5 μM of CHIR for 24 hrs to initiate WNT activation for stage-1 of differentiation. Since the CS condition could only produce a 3 fold increase during the expansion phase, the starting concentration for all four conditions was adjusted to approximately 0.3×10^5 cells/mL to ensure a standard baseline.

At this point, we paused agitation for the S1 condition, rendering the cells to be cultured under static suspension until day 3. Similarly, following stage-1 of differentiation, the cells are then treated with 5 μM of IWP2 for 48 hrs to inhibit the WNT pathway and initiate stage-2 of differentiation, at which time the S1 condition was cultured at 60 rpm, and the S2 condition was cultured under static conditions up to day 7.

Interestingly, a reduction in growth and viability was observed in the S1 and S2 condition when the cells were temporarily cultured under static suspension (data not shown). By day 15, it was clear that agitated conditions resulted in a higher cell yield compared to static conditions (Figure 5.3A). Specifically, the CA condition produced a 6 fold increase after 15 days of differentiation, followed by the S1 and S2 condition that resulted in a 3.8 and 3.4 fold increase, respectively. The CS condition produced the lowest cell yield after 15 days at 1.7 fold increase (Figure 5.3A). This result corroborated our observation that static suspension mitigates cell proliferation in the S1 and S2 condition. Interestingly, though the CA condition resulted in the highest cell yield, flow cytometry analysis revealed that this condition was the least efficient in producing cardiac cells, as evidenced by the low expression of α-actinin and cTnT cardiac markers (56.7% and 60.1%, respectively). The CS condition, on the other hand, performed better than the CA condition to produce 73.1% α-actinin and 75.4% cTnT-positive population (Figure 5.2C & D). Next to that is the S1 condition which resulted in 85.4% α-actinin and 81.9% cTnT-positive population. Importantly, the S2 condition was the most efficient of all the group in generating over 90% positive for both α-actinin and cTnT markers after 15 days of differentiation (Figure 5.2C & D).

RT-PCR analysis was then performed to examine gene expression levels during the differentiation process. At the start of differentiation (day 0), we observed that all of the conditions expressed relatively high levels of OCT4 and NANOG pluripotency genes (Figure 5.4A). After stage-1 of differentiation (day 3), both OCT4 and NANOG expression levels significantly dropped while gene expression for mesendoderm markers SOX17 and T increased (Figure 5.4A & B). Interestingly, the CS condition maintained a high OCT4 expression level and a lower NANOG expression level than the S1 or S2 condition. In contrast, the S1 condition expressed the lowest OCT4 expression level, but the S2 condition showed the highest NANOG expression levels after 3 days of differentiation. This result had an interesting correlation with the mesendoderm markers because the S1 condition resulted in the lowest SOX17, but the highest T expression levels when compared to the other conditions (Figure 5.4B). This suggests that the condition to which the cells are exposed before differentiation could also affect the induction process, as indicated by the differences in gene expression levels among the 3 best conditions. After day 3, cardiac genes for MYH6 and MYH7 were up-regulated by day 7. Notably, MYH6 expression was highest on day 7 and progressively dropped, whereas MYH7 showed steady up-regulation to the end-point of our study (Figure 5.4C). Remarkably, although both α-actinin and cTnT levels were lower in comparison, we found the CS condition to exhibit higher MYH6 and MYH7 expression than the S1 and S2 condition. One possible explanation for this result is that the CS condition resulted in a heterogeneous mixture of non-cardiac and cardiac cells, as well as their different stage of maturation.

Nevertheless, these results indicate that stopping agitation during stage-2 of differentiation was beneficial in generating over 90% pure cardiomyocytes. This means that the S2 condition was able to produce 0.94 x 10^6 cardiomyocytes per mL, totaling to approximately 47 million cardiomyocytes after 15 days of differentiation.

Inhibiting the possible effects of agitation on AKT activity via Rho/ROCK pathway

Since it appears that pausing agitation benefitted AKT activity, and in turn enhanced cardiac differentiation, it would be interesting to examine if the regulatory effect of agitation is mediated by another mechanosensitive effector, inhibition of which may also improve cardiac differentiation. A recent study showed that mechanically stimulated induced-pluripotent stem cells (iPSCs) promote activation of the Rho/ROCK pathway, and subsequently reduction of AKT phosphorylation [9]. Importantly, when the Rho-associated kinase ROCK was inhibited by ROCK inhibitor (ROCKi), AKT phosphorylation was rescued in human iPSCs under mechanical stimulation. This study then suggests that the effects of fluidic agitation could potentially be mediated by Rho/ROCK signaling, and the use of ROCKi presents a way to negate this effect on AKT activity for cardiac differentiation. Therefore, we utilized ROCKi during stage-2 of differentiation (+RI) to determine if its effects would improve cardiac differentiation similar to pausing agitation (Figure 5.5). Moreover, another condition was added in which the cells were treated with ROCKi and agitation, but minus IWP2 (+RI/-IW) as outlined in Figure 5.5. This third condition will assess if the fluidic motion and ROCKi are sufficient to promote cardiac differentiation without the chemical cue for WNT inhibition.

Similar to our previous study, the characteristics of the pluripotent stem cells were first evaluated to determine the quality of the starting material before differentiation. After the expansion phase, characteristics of the cells from all three conditions were similar in their cell aggregate size distribution, cell yield (~5 fold increase), and maintenance of pluripotency as evidenced by the high expression of both SSEA4 and OCT4 pluripotent markers (over 95%) (Figure 5.6A-C).

On day 0, the seeding density was readjusted to 0.35 x 10^5 cells/mL. By day 3, aggregate size grew to ~200 μm, and cell number increased to 5 fold (~1.5 x 10^6 cells/mL). Flow cytometry analysis on day 3 reveals that 95% of the cells were positive for Brachyury in all of the conditions, indicating their successful induction to Mesendoderm cells (Figure 5.6D). From the expansion phase to stage-1 of differentiation (day -4 to day 3), the results were as expected since the parameters were the same for all three spinners flasks. However, after stage-2 of differentiation (day 7), aggregate morphology and cell yield differ between the conditions (Figure 5.7). In particular, cell yield from the S2 condition significantly dropped from day 3 to day 7 (5.3 to 4.1 fold increase, respectively), but leveled off on day 10 to 15 (~3.4 FI) (Figure 5.7A). This initial drop in cell yield occurred when agitation was paused during stage-2 of differentiation. Viability was further compromised when agitation was resumed, with the percentage of viable cells dropping from 85.4% on day 7 to 75% on day 10 (Figure 5.7B). Notably, the +RI and the +RI/-IWP2 conditions sustained approximately similar cell number from day 3 to day 10 with a slight dropped on day 15 (ranging from 5.0 to 5.5 fold increase), but viability was consistently around 90%.

On day 10 and 15, flow cytometry was used to quantify the population of cells expressing α-actinin, troponin I (cTnI) and troponin T (cTnT) cardiac markers. In addition, we performed the same cardiac differentiation protocol in 2D monolayer culture as a comparison measurement for the stirred suspension cultures. Interestingly, flow cytometry analysis revealed that in most of the tested conditions, the highest expression for α-actinin and/or cTnI was observed on day 10, and later expression decreased on day 15 (Figure 5.8A & B). For instance, the +RI/-IWP2 was the only condition that observed a slight increase in α-actinin expression from 89% on day 10 to 90.9% on day 15 (Figure 5.8A). Similarly, the monolayer was the only condition that resulted in an increase in cTnI expression from 75.2 % on day 10 to 92.7% on day 15 (Figure 5.8B). This result was unexpected because all of the tested conditions displayed an increasing expression for α-actinin (from day 10 to day 15) in our previous study. However, cTnT more accurately reflects the efficacy of the protocol, and analysis for cTnT-positive cells did show this increasing trend (Figure 5.8C). Overall, the monolayer and the constant agitation condition produced the lowest cTnT-positive cells by day 15 (~79.0%). The highest cTnT-positive cells were found in the S2 condition at 91.4%. Remarkably, the addition of ROCK inhibitor, with or without IWP2, resulted in over 80% cTnT-positive cells (86.4% with and 82.1% without IWP2) (Figure 5.8C). This result suggests that the Rho/ROCK pathway could play a significant role in lineage determination of hPSCs. However, when the cells were stained for cTnT, α-actinin, and MLC2a on day 22, the cells generated from constant agitation and +ROCKi (with or without IWP2) displayed structural features that suggest such conditions may not be sufficient to enhance cardiomyocyte commitment. In

particular, the cardiomyocytes produced under constant agitation and +ROCKi condition were small in their morphology and showed irregular subcellular organization and low myofibril density, which are the characteristics consistent with fetal and immature hPSC-derived cardiomyocytes (Figure 5.9). As human cardiomyocytes mature, they increase in size with a more elongated morphology due to physiological hypertrophy. In particular, adult cardiomyocytes have a rod-shaped morphology and a highly organized sarcomere structure, the contractile unit of cardiomyocytes. The cells in the stage-2 static condition displayed such mature features with visibly clear striated patterns, indicating a dramatic maturation in their morphology (Figure 5.10). Motivated by this initial observation, we further examined the structural features of the stage-2 static cells to characterize their stage of maturation on day 22.

Characterizing the Structural Maturation of hESC-derived Cardiomyocytes

In addition to providing a scalable method for mass production of hPSC-derived cardiomyocytes, their functional characteristic is an important criterion for translation into clinical applications. For this reason, we plated the cells on day 18 and fixed/stained on day 22 to evaluate the structural maturation via immunofluorescence. The cells were double-stained for cTnT or α-actinin with myosin light chain two atrial isoforms (MLC2a) to determine the assembly of myofilament proteins in sarcomeres. In particular, overlapping MLC2a with α-actinin marks the A-bands and the Z-disks sarcomere border, respectively, to show if the different functional units of the sarcomere are aligned and highly organized similarly to that of adult cardiomyocytes [10].

Immunocytochemistry (ICC) showed that the S2 cells have a lot of characteristics that are typically observed in mature cardiomyocytes. Specifically, the high degree of myofilament protein density and the altering pattern of A-bands and Z-disks labeling is in accordance with previously published reports on the structural maturation of cardiomyocytes [11] (Figure 5.11). Among its morphological features, the cell's perimeter, area, and circularity could be used to distinguish the cardiomyocyte stage of maturation. The cardiomyocytes with a more mature phenotype have a larger perimeter and area, and a decrease in circularity index compared to the immature phenotypes. But one of the biggest indicators of cardiomyocyte maturation could be observed through the sarcomere length, which is the distance between two Z-disks of the sarcomeres [12]. Adult cardiomyocytes are more elongated and have longer sarcomere length than fetal or immature hPSC-derived cardiomyocytes [13]. Specifically, cardiomyocytes in the early-

stage of maturation have a sarcomere length of ~1.6 μm, in late-stage maturation the length grows to ~1.8 μm, and adult cardiomyocytes have a sarcomere length of ~2.2 μm [10, 14]. Typically, improving maturation would require longer culture time, in which features of late-stage maturation could be observed if the hPSC-derived cardiomyocyte was kept for 50-100 days in culture. However, quantitative ICC analysis of the S2 cells shows a dramatic increase in maturation was observed after ~20 days in stirred suspension culture (Figure 5.10 & 5.11). Based on the sarcomere length, cardiomyocytes from stage-2 static condition displayed structural characteristics similar to late-stage maturation (Figure 5.11A). But the most surprising are those that resulted in a sarcomere length similar to adult-like cardiomyocyte phenotypes (~2.2 μm) (Figure 5.11B & C). However, further study of their maturation will require electrophysiological characterization to determine if the functional performance of the S2 cells are similar to published reports for adult cardiomyocytes. Nevertheless, we were captivated to observe such unprecedented degree of structural organization within less than 25 days in culture. This result suggests that mechanical stimulation through fluidic agitation could not only improve cardiac differentiation efficiency but also rapidly enhance its maturation.

Discussion

Guiding hPSCs' fate requires a process to finely tune signaling mechanisms that either support growth and self-renewal, or direct lineage-specific differentiation. For cardiac differentiation, use of two small molecules to modulate the WNT pathway sequentially has enabled efficient production of hPSC-derived cardiomyocytes with relative ease [6]. Recently, Kempf et al. adapted this method to develop an integrated strategy for hPSCs expansion and cardiac differentiation in stirred suspension culture [7]. Although the authors were able to generate up to 85% cardiomyocytes, reproducibility was an issue as their results varied between batches with its efficiency ranging from 53.9% to 84.1%, as indicated by cTnT-positive cells [7]. From our previous study, we identified regulation of AKT to be a prominent mechanosensitive effector and suggested that such signaling mechanisms in dynamic suspension culture of hPSCS should not be overlooked. We speculated that regulation of AKT could be a critical signaling mechanism when directing hPSCs fate in stirred suspension culture. Although it is still unclear how the down-regulation of AKT was beneficial for the expansion of hPSCs, we presume that its role could be associated with lineage-specific determination.

Here, we explored the possibility of harnessing this agitation-induced regulation to improve expansion and cardiac differentiation of hPSCs in stirred suspension culture. Our first approach was to determine if pausing agitation would increase AKT activity, and in turn, improves cardiac differentiation. From this initial study, we found that the WNT inhibition process (stage-2 of differentiation – S2 condition) is the critical time point at

which AKT activity is likely necessary for cardiac specification. As such, we were able to consistently generate over 90% cTnT and α-actinin positive cells by simply allowing the cells to be cultured under static suspension during stage-2 of differentiation (day 3 – 7). In comparison to pausing agitation during WNT activation (stage-1 of differentiation – S1 condition), an S2 condition also displayed higher mesendoderm gene (day 3) and cardiac-specific gene expressions (day 7 – 15) at their respective time point.

AKT is a protein kinase that is activated by the phosphoinositide 3-kinase (PI3K). AKT is well-known for its role in cellular proliferation and protection from apoptosis, but compelling evidence now suggests that AKT activity plays a bigger part in cellular function and embryonic development [15-17]. Recently, PI3K/AKT activity has been considered to be one of the master regulators for self-renewal of hPSCs in 2D adherent cultures, whereas the other being the canonical WNT pathway [18, 19]. For lineage-specific differentiation, Freund et al. reported that PI3K/AKT activity, via downstream of insulin-like growth factor-1 receptor (IGF-1R), mediates the negative effects of insulin for early cell fate decisions towards cardiac lineages [10]. In fact, they reported that insulin strongly enhanced phosphorylation of AKT, thereby block mesendoderm induction and promote neuroectoderm differentiation. However, Klinz et al. found that PI3K/AKT signaling is an important process for cardiac specification. Inhibiting this pathway following hESC early differentiation would result in a decrease in cardiomyocyte phenotype [11]. This result seems to be in accordance with another report where PI3K/AKT signaling was reported to be essential in stimulating proliferation of immature hESC-derived cardiomyocyte [12]. Together, these findings suggest a biphasic role for AKT signaling in embryonic

cardiogenesis; where the initial inhibition of AKT would favor mesendoderm induction [10], but activation of AKT following mesendoderm development is necessary for cardiac specification [11] and proliferation of immature cardiomyocyte [12] (Figure 5.12). This process is likely the reason that the S2 condition resulted in the highest cTnT-positive cells. It is presumed that agitation was beneficial for mesendoderm induction during stage-1 of differentiation, and subsequently, a static condition triggered AKT activity to specify the S2 cells towards cardiac development during stage-2 of differentiation. This process highlights the notion of how mechanosensitive mechanisms, governed by fluidic agitation, could be timely leveraged to enhance hPSCs differentiation in stirred suspension culture.

In our next set of study, similar to pausing agitation, we utilized ROCK inhibitor to counteract the antagonistic effects of agitation on AKT phosphorylation. The Rho/ROCK pathway is a molecular feedback mechanism also known to be a primary effector of mechanical stimulation. Previous reports have indicated that RhoA/ROCK involvement in mechanotransduction signaling is attributed to their downstream cascade interactions with pathways such as AKT, ERK, p38 MAP kinases, and JNK signaling [23, 24]. A study by Teramura et al. demonstrates this interaction where mechanical stimulation of cyclic strain to hPSCs resulted in an up-regulation of RhoA/ROCK pathway and subsequent decrease of AKT phosphorylation. But when the Rho-associated kinase ROCK was inhibited with ROCK inhibitor, phosphorylation of AKT was recovered under mechanical stress [9]. Results from this study are similar to what we observed in our previous study, which suggested that the RhoA/ROCK pathway mediates the effect of fluidic agitation on AKT signaling activity. Therefore, instead of pausing agitation during stage-2 of differentiation,

we added the ROCK inhibitor to rescue AKT phosphorylation and found some improvement in producing cTnT-positive cells compared to a continuous agitation condition. Interestingly, when we tested a similar condition, but without IWP2, we found that both cases of ROCKi treatment (with or without IWP2) resulted in over 80% positive expression for three different cardiac markers. This result could suggest an important mechanism for Rho/ROCK signaling to promote cardiac differentiation. But this data is still inconclusive, and we will need to accumulate more careful evidence to elucidate the molecular mechanisms in future studies. Nevertheless, our findings demonstrate a connection between fluidic agitation and critical signaling pathways, such as AKT, to promote uniform differentiation of hPSCs in stirred suspension culture.

In addition to producing the highest cTnT positive cells, immunofluorescence analysis also suggests that the S2 condition could enhance maturation of hESC-derived cardiomyocytes. We were intrigued to find a number of these cells to possess elongated morphology with clear striations along the long axis of the cells. Within 22 days of differentiation, the cells displayed highly organized sarcomere structure with the visible distance between each Z-disks that would extend to neighboring myofibrils. Assessment of their sarcomere length suggests some expedited maturation that is similar to those previously reported for adult human cardiomyocytes. At this point, the mechanism behind this phenomenon remains unknown, but we speculate that the transition between static and agitation following stage-2 of differentiation could be the start to myofibrillogenesis. Interestingly, Fischer et al. show that overexpression of nuclear AKT actually hindered lineage commitment of cardiac progenitor cells [13]. As such, it is plausible that the

transition from static to agitation attenuated AKT activity, just as the authors found that inhibition of AKT kinase significantly improved lineage commitment in their cardiac progenitor cells. Nonetheless, it is difficult to validate this speculation since our findings are only initial results to demonstrate how signaling mechanism from both mechanical and chemical cues could be tailored to enhance hPSCs differentiation in stirred suspension culture. Future studies using qPCR and western blot would provide more insight into this mechanism from early hPSCs differentiation to cardiomyocyte development and maturation.

In summary, we presented an interesting study on how fluidic agitation could be leveraged to promote cardiac differentiation in stirred suspension culture of hPSCs. Although the actual mechanism is still unclear, we provide a proof-of-concept result that supports agitation to be a critical parameter in altering molecular mechanism, thereby effecting hPSC fate determination in dynamic suspension.

Figures

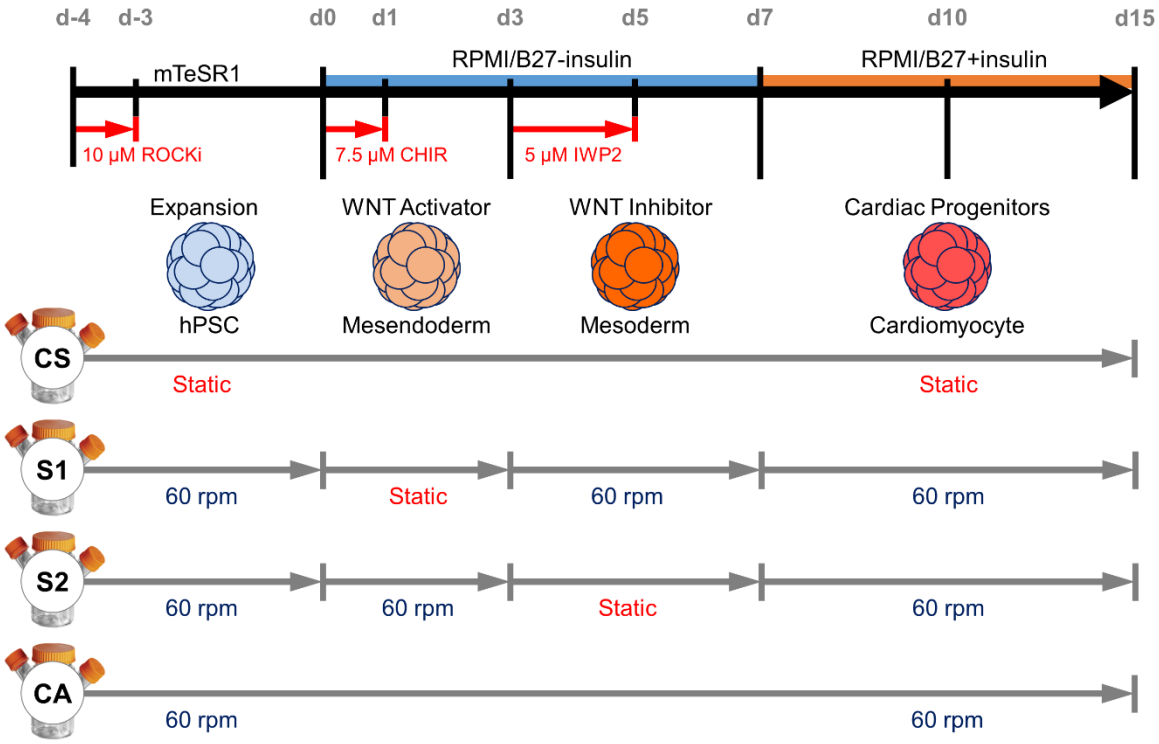

Figure 5.1. Optimization of hESCs cardiac differentiation in stirred suspension culture. Scheme for constant static (CS), stage-1 static (S1), stage-2 static (S2), and constant agitation (CA) condition towards cardiomyocyte differentiation via expansion phase, Stage-1 differentiation (WNT activation), Stage-2 differentiation (WNT Inhibition), and Cardiomyocyte commitment.

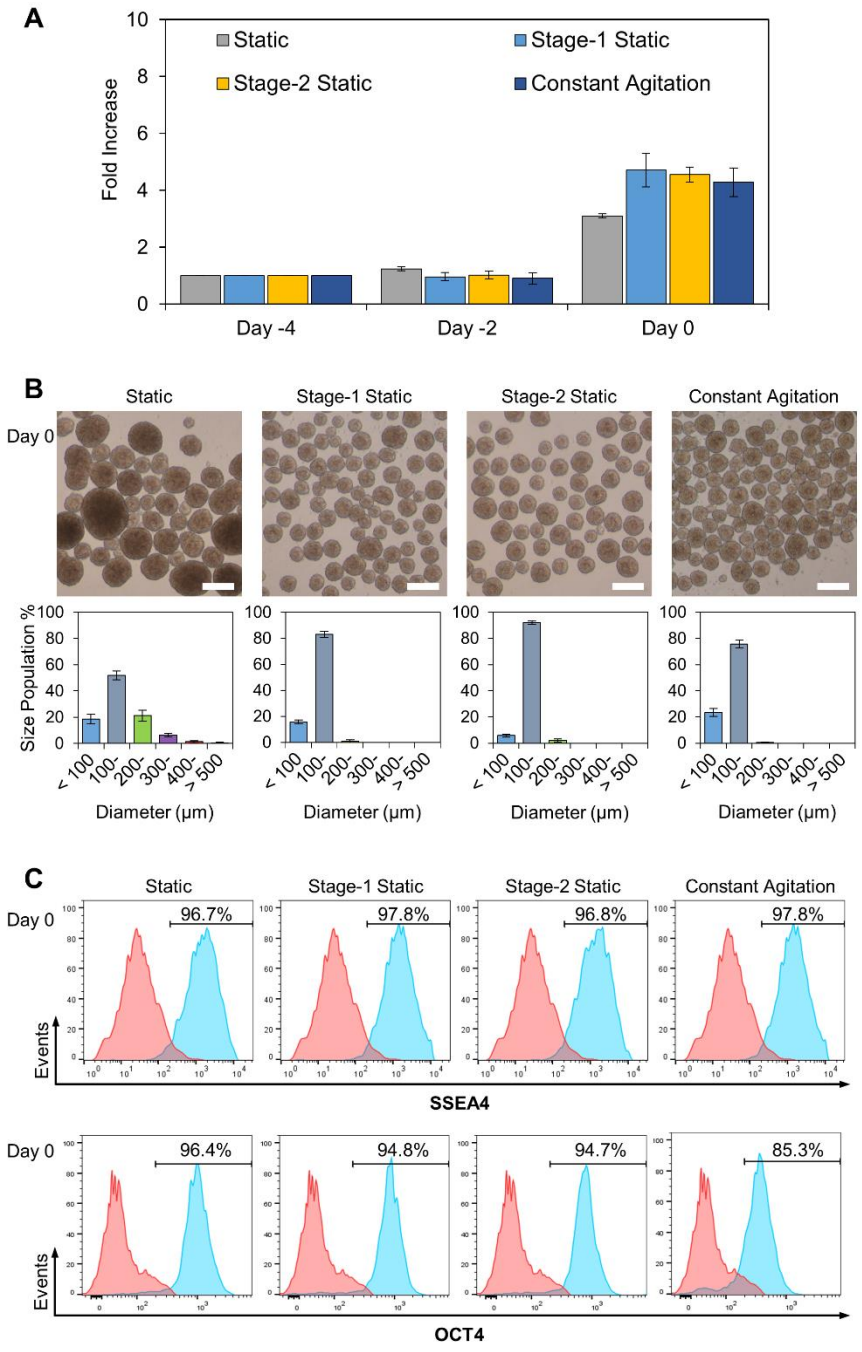

Figure 5.2. Day 0 analysis before proceeding to cardiac differentiation. (A) Growth curves during the expansion phase. (B) Cell aggregate morphology and size distribution. Scale bar: 250 µm. (C) pluripotent markers for SSEA4 and OCT4 were quantified by flow cytometry.

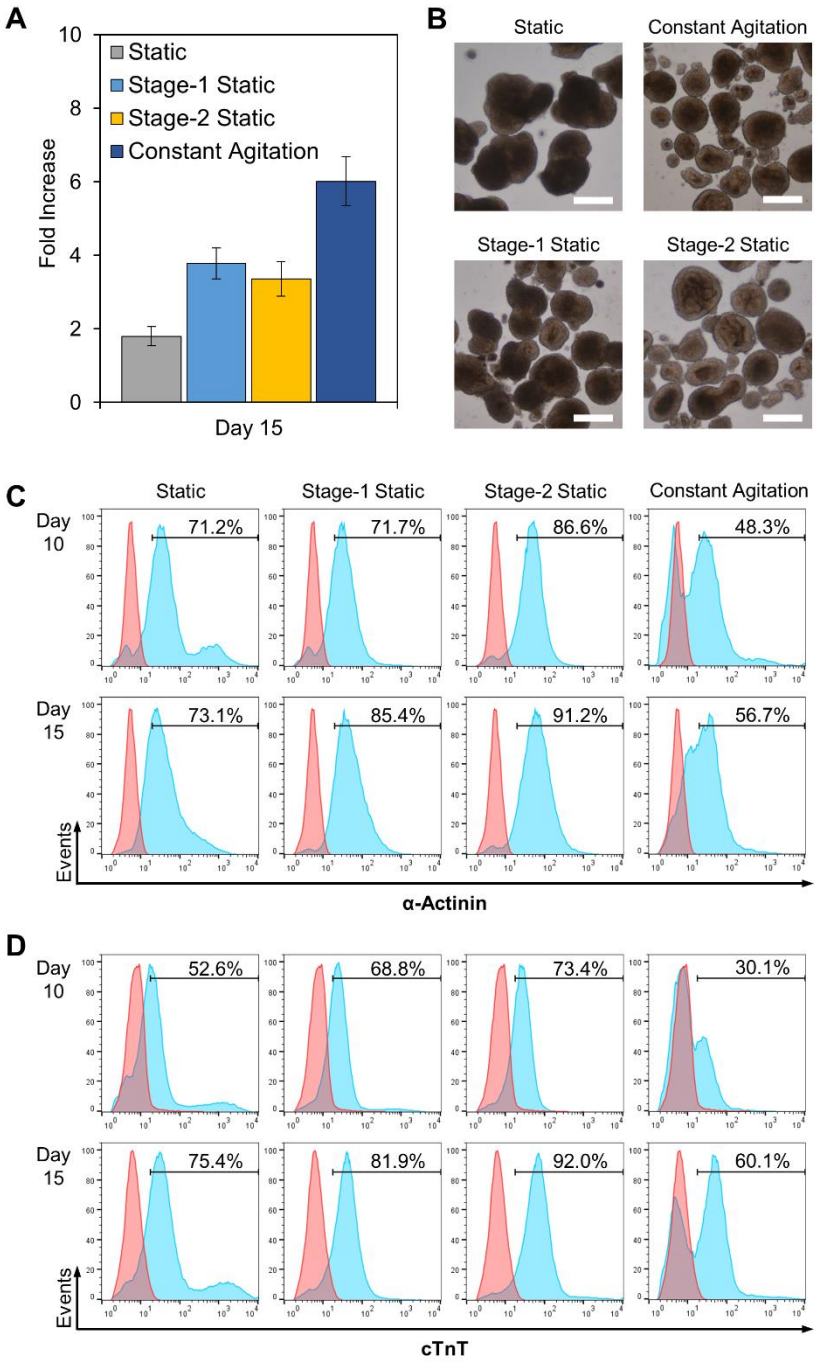

Figure 5.3. Cell yield and differentiation efficiency over the course of the culture. (A) Production of cells and (B) photomicrograph of the aggregate morphology after 15 days of differentiation. Scale bars: 250 µm. (C) Flow cytometry analysis of day 10 and day 15 expression of α-actinin and cTnT cardiac markers.

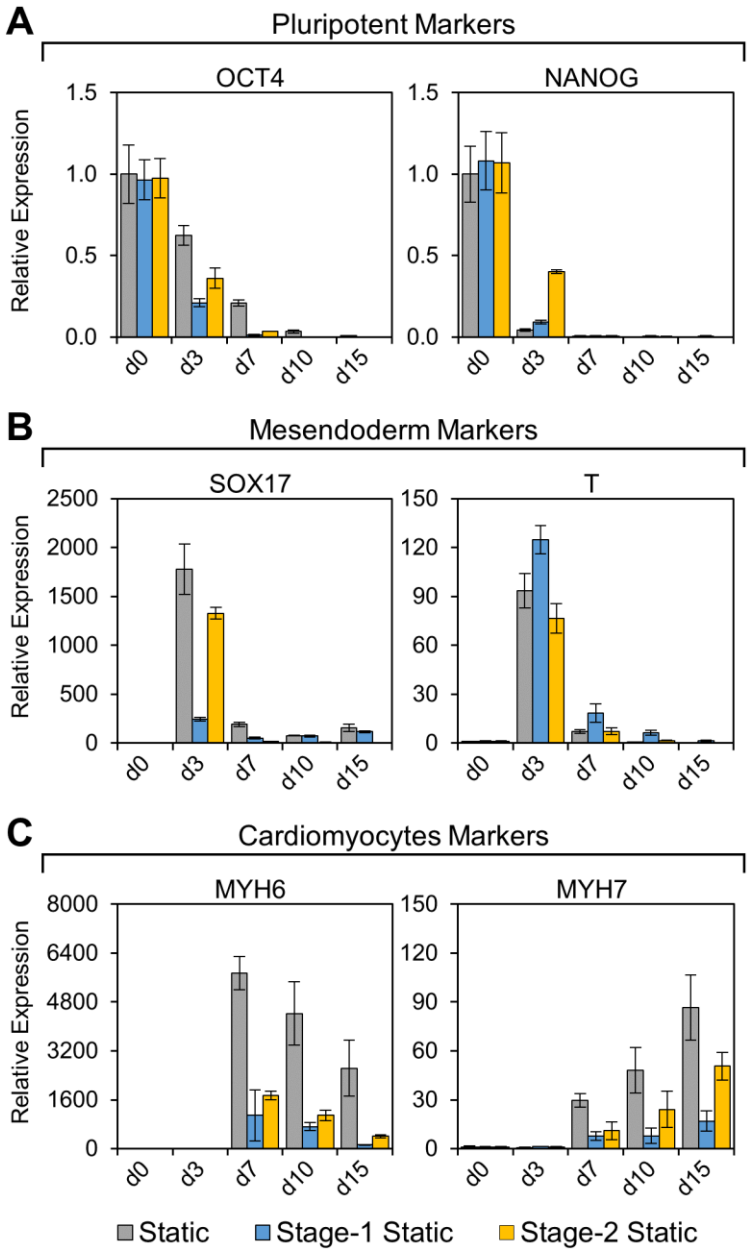

Figure 5.4. Marker gene expression over the course of differentiation. Markers for (A) pluripotency, (B) mesendoderm and (C) cardiac genes were examined after specific process time-point.

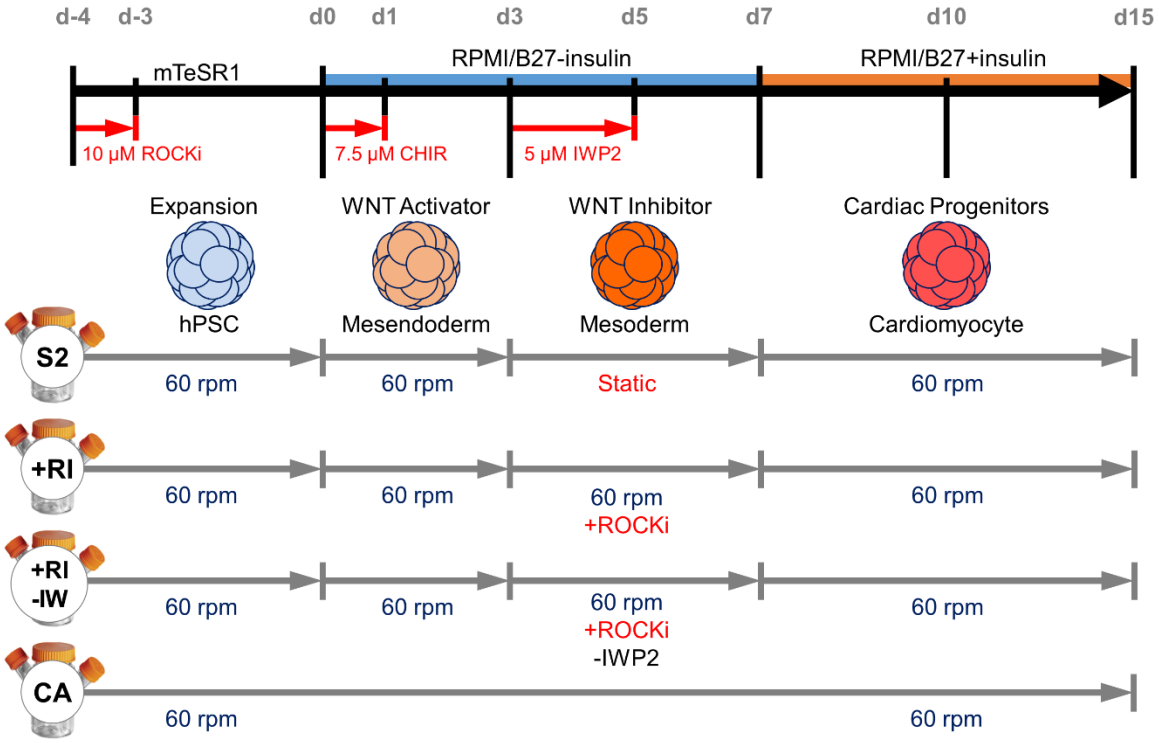

Figure 5.5. Inhibitor study with ROCK inhibitor to counteract the adverse effect of agitation on cardiac differentiation. Scheme for stage-2 static (S2), +ROCKi (+RI), +ROCKi and –IWP2 (+RI/-IW), and constant agitation (CA) condition towards cardiomyocyte differentiation.

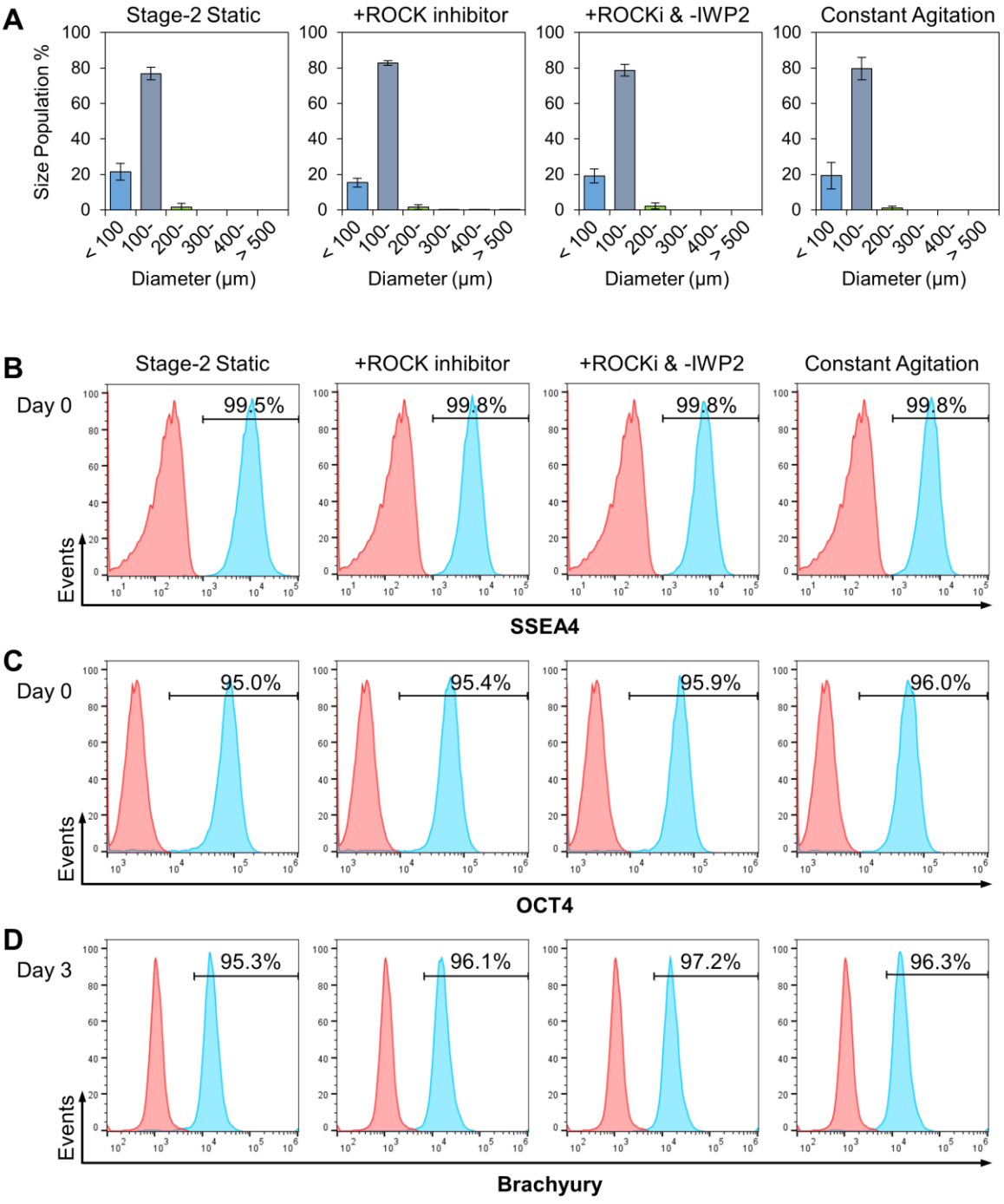

Figure 5.6. Baseline quality assessment of the starting material and intermediate product before cardiac specification. (A) Aggregate size distribution, (B) SSEA4 pluripotent marker, and (C) OCT4 pluripotent marker were examined on day 0. (D) Quality of intermediate product was also examined by expression of Brachyury mesendoderm marker on day 3.

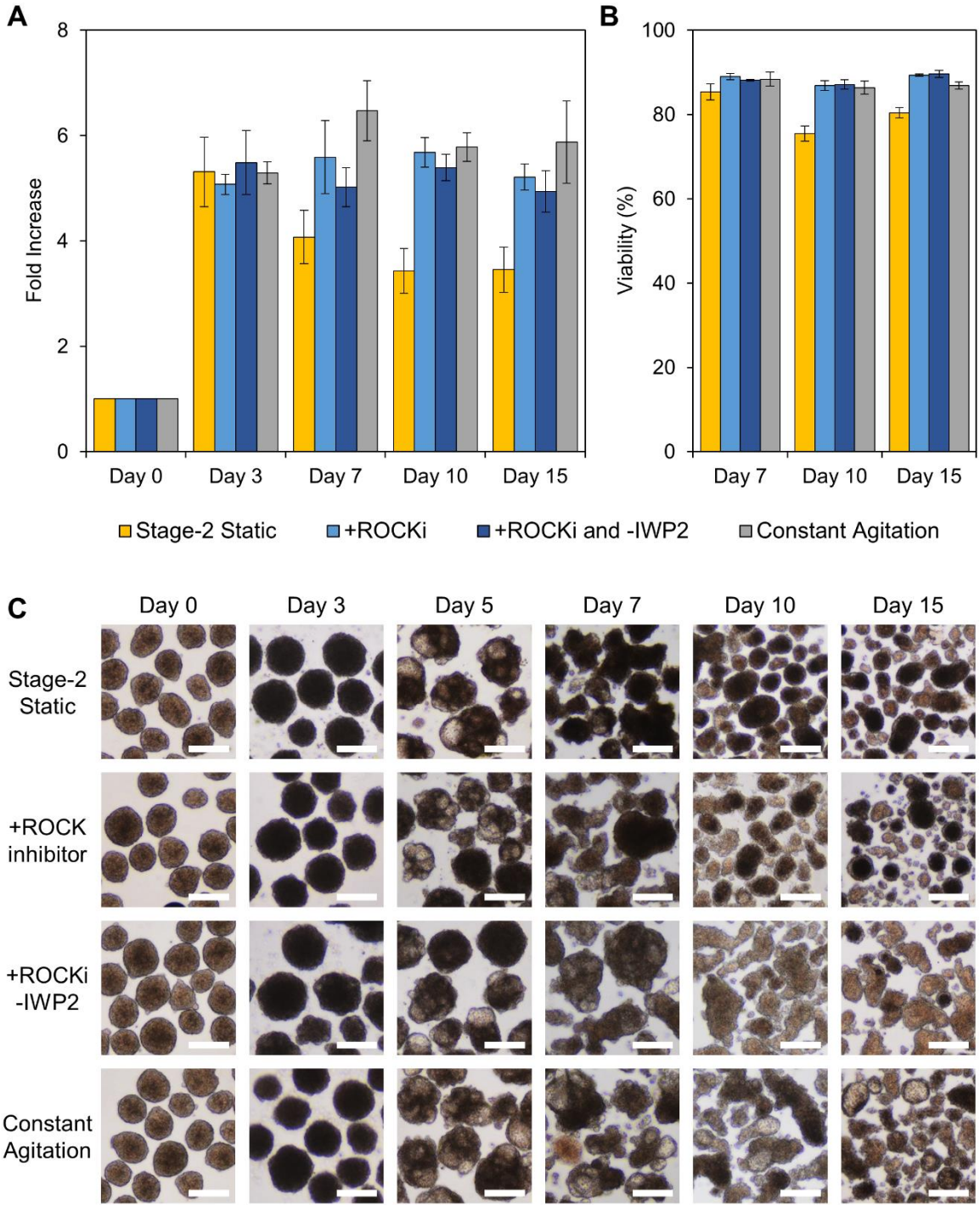

Figure 5.7. Static conditions mitigate overall cell production and viability when agitation in resumed. (A) Cell yield over the course of culture. (B) Cell viability. (C) Aggregate morphology over the course of culture. Scale bars: 200 µm.

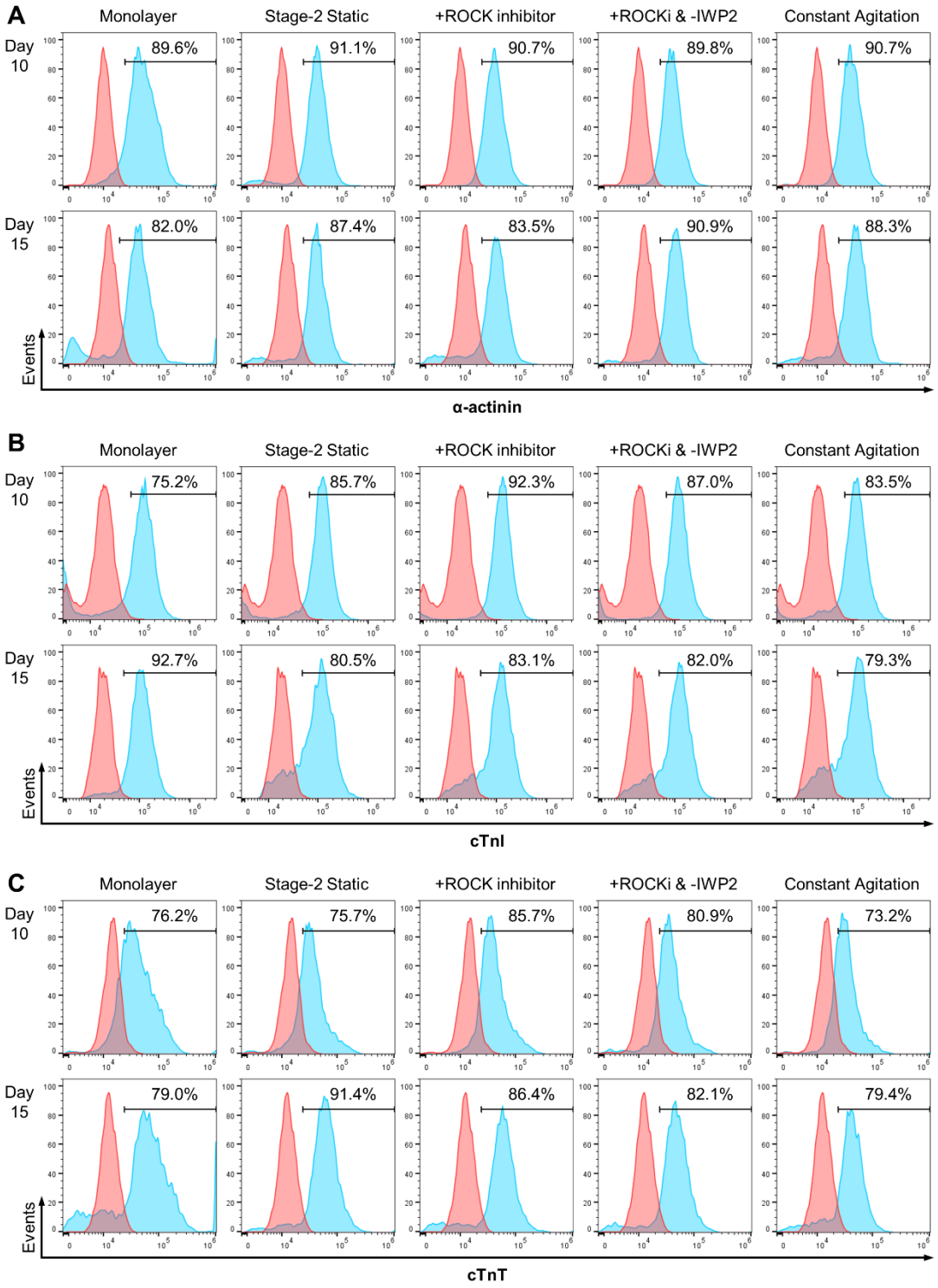

Figure 5.8. Evaluating differentiation efficiency with a monolayer-based method included as a comparison. Expression of (A) α-actinin, (B) cTnI and (C) cTnT were examined on day 10 and 15 by flow cytometry.

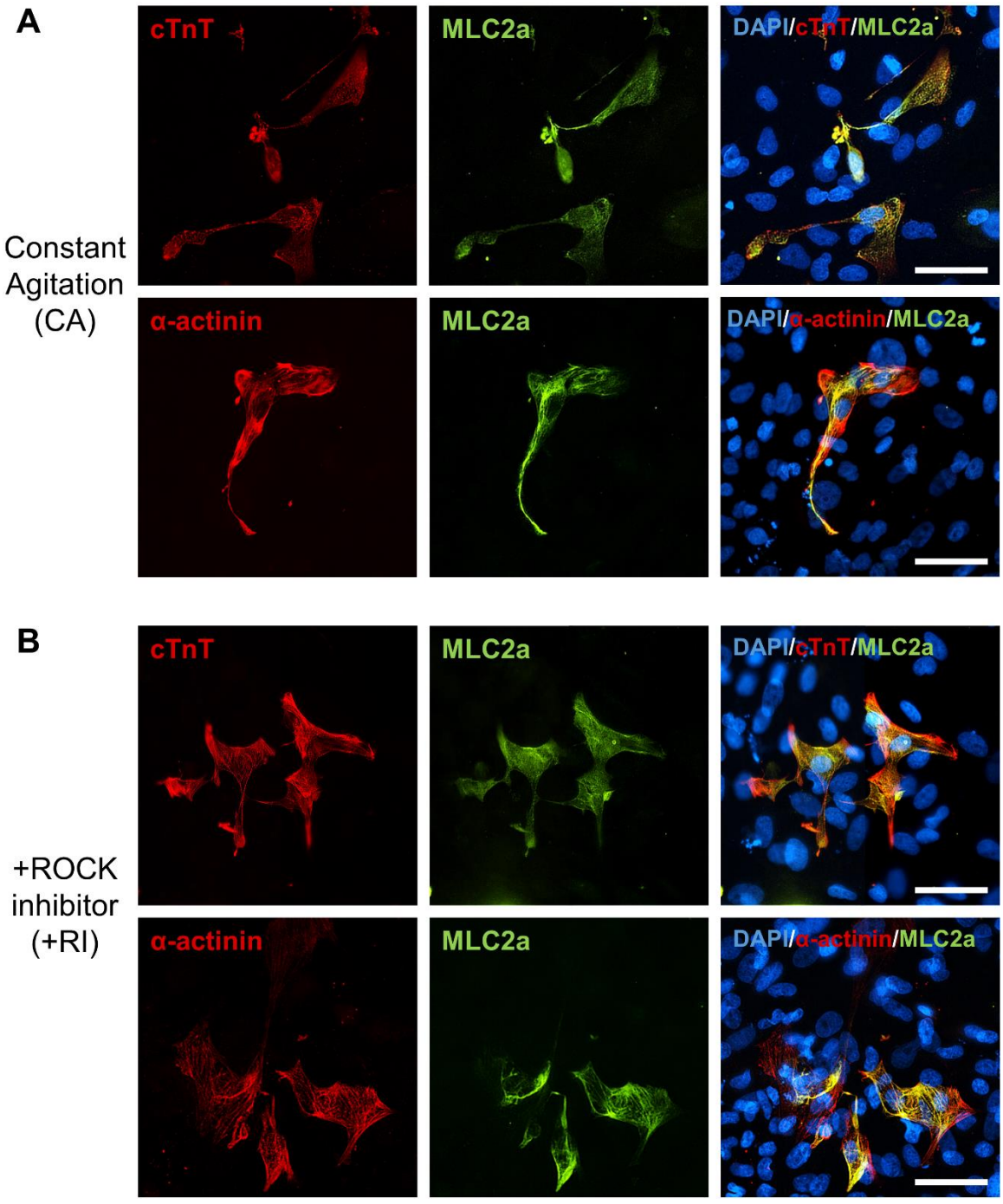

Figure 5.9. Structural characterization of cardiomyocytes generated from different stirred suspension conditions. Cells from (A) CA and (B) +RI condition were immunostained for cTnT, α-actinin, and MLC2a to show expression of myofilament proteins and sarcomeric organization. Immunofluorescent staining for +RI/-IWP2 condition not shown due to the low fluorescence intensity at the set exposure time. Scale bars: 50 μm.

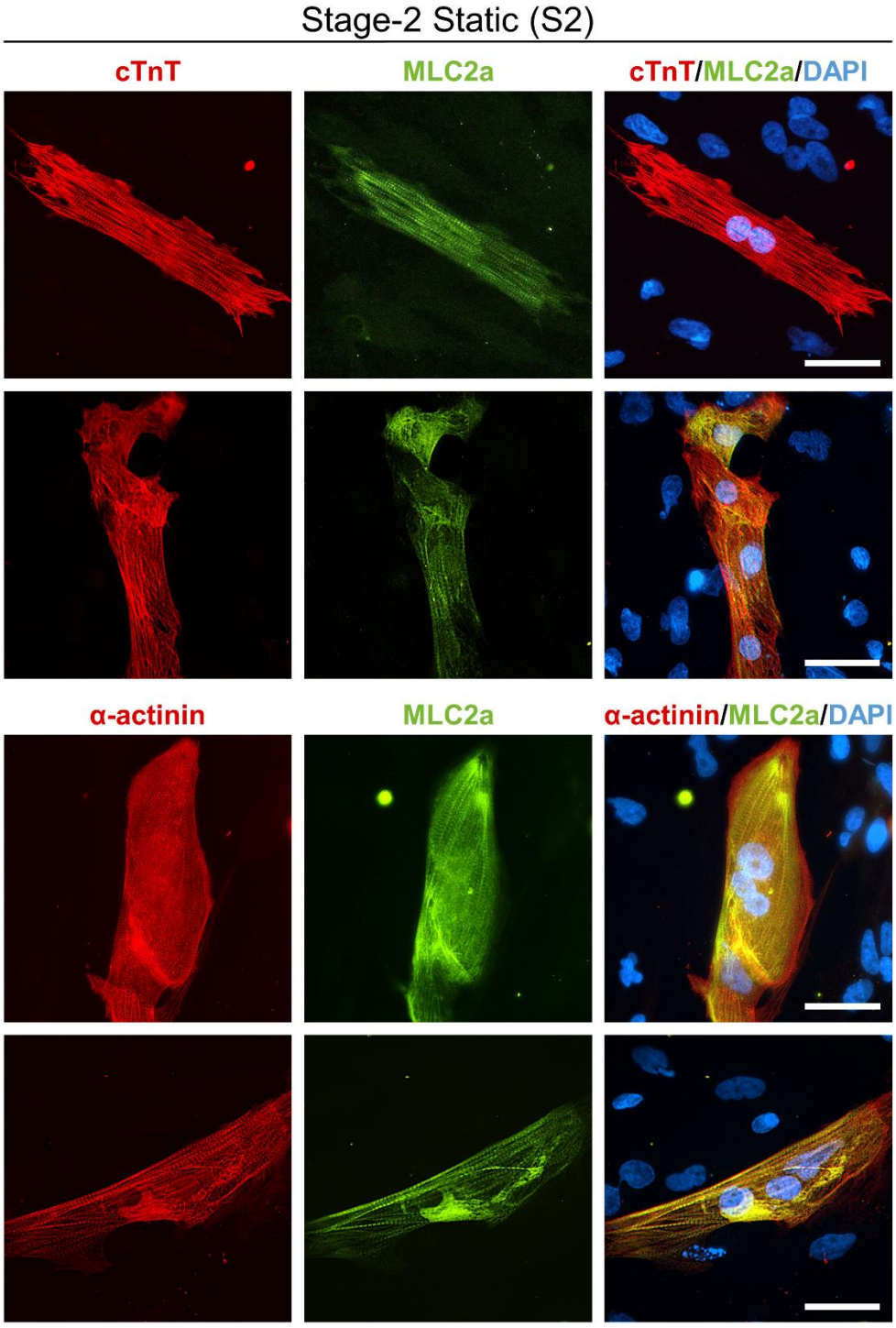

Figure 5.10. Structural characterization of cardiomyocytes generated from Stage-2 static condition. Immunostaining for cTnT, α-actinin, and MLC2a shows cells from the S2 condition to have a large morphology and highly organized sarcomere structure, indicating their increase in maturation compared to the other conditions. Scale bars: 50 μm.

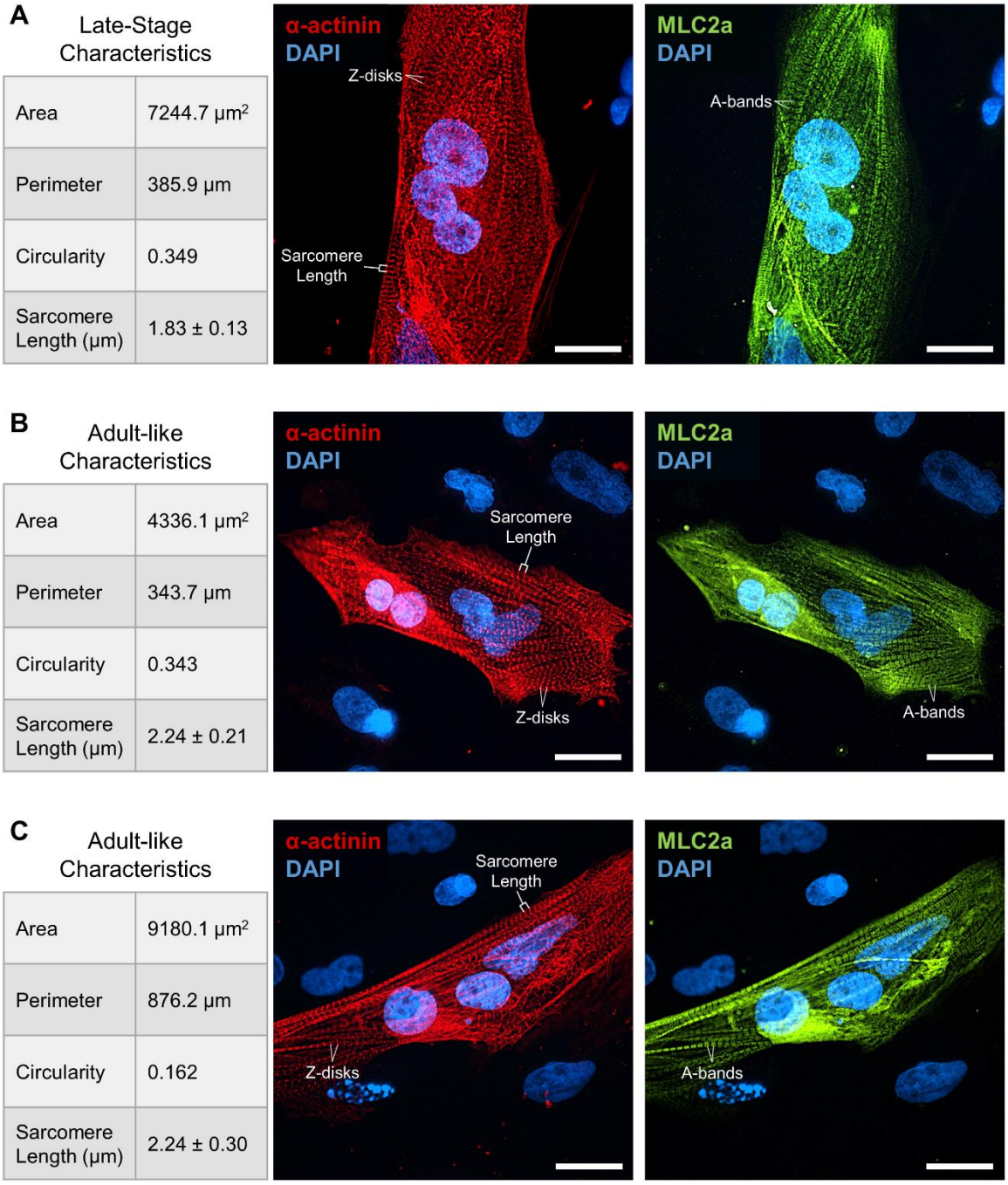

Figure 5.11. Structural maturation analysis of cardiomyocytes generated from Stage-2 static condition. Immunolabeling of α-actinin and MLC2a displays the alternating striated patterns between the Z-disk and A-bands of the sarcomere structure. Quantitative analysis of their morphology and structural organization reveals an unprecedented increase in maturation similar to published reports that demonstrate (A) late-stage maturation and (B & C) adult cardiomyocyte phenotype in less than 25 days of culture. Scale bars: 25 μm.

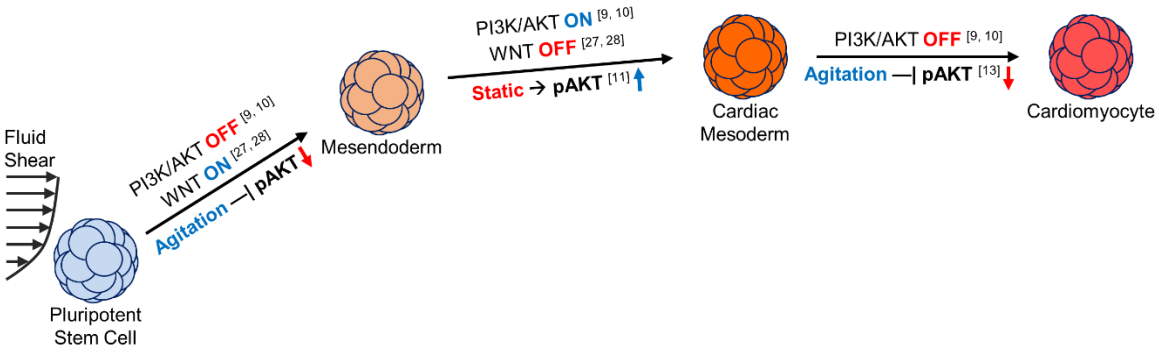

Figure 5.12. A possible mechanism of how AKT activity governed by fluid agitation was used to promote cardiac differentiation of hESC. Mechanism based on our previous data and reports of AKT activity in cardiac lineages [9-13, 27, 28].

References

1. Segers, V.F. and R.T. Lee, *Stem-cell therapy for cardiac disease.* Nature, 2008. **451**(7181): p. 937-42.
2. Laflamme, M.A. and C.E. Murry, *Heart regeneration.* Nature, 2011. **473**(7347): p. 326-35.
3. Burridge, P.W., G. Keller, J.D. Gold, et al., *Production of de novo cardiomyocytes: human pluripotent stem cell differentiation and direct reprogramming.* Cell Stem Cell, 2012. **10**(1): p. 16-28.
4. Burridge, P.W., E. Matsa, P. Shukla, et al., *Chemically defined generation of human cardiomyocytes.* Nat Methods, 2014. **11**(8): p. 855-60.
5. Kattman, S.J., A.D. Witty, M. Gagliardi, et al., *Stage-specific optimization of activin/nodal and BMP signaling promotes cardiac differentiation of mouse and human pluripotent stem cell lines.* Cell Stem Cell, 2011. **8**(2): p. 228-40.
6. Lian, X.J., C. Hsiao, G. Wilson, et al., *Robust cardiomyocyte differentiation from human pluripotent stem cells via temporal modulation of canonical Wnt signaling.* Proceedings of the National Academy of Sciences of the United States of America, 2012. **109**(27): p. E1848-E1857.
7. Kempf, H., R. Olmer, C. Kropp, et al., *Controlling expansion and cardiomyogenic differentiation of human pluripotent stem cells in scalable suspension culture.* Stem Cell Reports, 2014. **3**(6): p. 1132-46.
8. Chen, V.C., J.J. Ye, P. Shukla, et al., *Development of a scalable suspension culture for cardiac differentiation from human pluripotent stem cells.* Stem Cell Research, 2015. **15**(2): p. 365-375.
9. Vallier, L., T. Touboul, S. Brown, et al., *Signaling Pathways Controlling Pluripotency and Early Cell Fate Decisions of Human Induced Pluripotent Stem Cells.* Stem Cells, 2009. **27**(11): p. 2655-2666.
10. Freund, C., D. Ward-van Oostwaard, J. Monshouwer-Kloots, et al., *Insulin redirects differentiation from cardiogenic mesoderm and endoderm to neuroectoderm in differentiating human embryonic stem cells.* Stem Cells, 2008. **26**(3): p. 724-33.
11. Klinz, F.J., W. Bloch, K. Addicks, et al., *Inhibition of phosphatidylinositol-3-kinase blocks development of functional embryonic cardiomyocytes.* Experimental Cell Research, 1999. **247**(1): p. 79-83.
12. McDevitt, T.C., M.A. Laflamme, and C.E. Murry, *Proliferation of cardiomyocytes derived from human embryonic stem cells is mediated via the IGF/PI 3-kinase/Akt signaling pathway.* J Mol Cell Cardiol, 2005. **39**(6): p. 865-73.

13. Fischer, K.M., S. Din, N. Gude, et al., *Cardiac progenitor cell commitment is inhibited by nuclear Akt expression.* Circ Res, 2011. **108**(8): p. 960-70.

14. Teramura, T., T. Takehara, Y. Onodera, et al., *Mechanical stimulation of cyclic tensile strain induces reduction of pluripotent related gene expressions via activation of Rho/ROCK and subsequent decreasing of AKT phosphorylation in human induced pluripotent stem cells.* Biochem Biophys Res Commun, 2012. **417**(2): p. 836-41.

15. Yang, X.L., L. Pabon, and C.E. Murry, *Engineering Adolescence Maturation of Human Pluripotent Stem Cell-Derived Cardiomyocytes.* Circulation Research, 2014. **114**(3): p. 511-523.

16. Zhang, J.H., G.F. Wilson, A.G. Soerens, et al., *Functional Cardiomyocytes Derived From Human Induced Pluripotent Stem Cells.* Circulation Research, 2009. **104**(4): p. E30-E41.

17. Lundy, S.D., W.Z. Zhu, M. Regnier, et al., *Structural and Functional Maturation of Cardiomyocytes Derived from Human Pluripotent Stem Cells.* Stem Cells and Development, 2013. **22**(14): p. 1991-2002.

18. Veerman, C.C., G. Kosmidis, C.L. Mummery, et al., *Immaturity of human stem-cell-derived cardiomyocytes in culture: fatal flaw or soluble problem?* Stem Cells Dev, 2015. **24**(9): p. 1035-52.

19. Bird, S.D., P.A. Doevendans, M.A. van Rooijen, et al., *The human adult cardiomyocyte phenotype.* Cardiovascular Research, 2003. **58**(2): p. 423-434.

20. Sussman, M.A., M. Volkers, K. Fischer, et al., *Myocardial Akt: The Omnipresent Nexus.* Physiological Reviews, 2011. **91**(3): p. 1023-1070.

21. Aly, H., N. Rohatgi, C.A. Marshall, et al., *A Novel Strategy to Increase the Proliferative Potential of Adult Human beta-Cells While Maintaining Their Differentiated Phenotype.* Plos One, 2013. **8**(6).

22. Keung, A.J., E.M. de Juan-Pardo, D.V. Schaffer, et al., *Rho GTPases mediate the mechanosensitive lineage commitment of neural stem cells.* Stem Cells, 2011. **29**(11): p. 1886-97.

23. Singh, A.M., D. Reynolds, T. Cliff, et al., *Signaling Network Crosstalk in Human Pluripotent Cells: A Smad2/3-Regulated Switch that Controls the Balance between Self-Renewal and Differentiation.* Cell Stem Cell, 2012. **10**(3): p. 312-326.

24. Huang, T.S., L. Li, L. Moalim-Nour, et al., *A Regulatory Network Involving beta-Catenin, e-Cadherin, PI3k/Akt, and Slug Balances Self-Renewal and Differentiation of Human Pluripotent Stem Cells In Response to Wnt Signaling.* Stem Cells, 2015. **33**(5): p. 1419-33.

25. Sun, Y., C.S. Chen, and J. Fu, *Forcing stem cells to behave: a biophysical perspective of the cellular microenvironment.* Annu Rev Biophys, 2012. **41**: p. 519-42.

26. Mammoto, A., T. Mammoto, and D.E. Ingber, *Mechanosensitive mechanisms in transcriptional regulation.* J Cell Sci, 2012. **125**(Pt 13): p. 3061-73.

27. Menendez, L., T.A. Yatskievych, P.B. Antin, et al., *Wnt signaling and a Smad pathway blockade direct the differentiation of human pluripotent stem cells to multipotent neural crest cells (vol 108, pg 19240, 2011).* Proceedings of the National Academy of Sciences of the United States of America, 2012. **109**(23): p. 9220-9220.

28. Blauwkamp, T.A., S. Nigam, R. Ardehali, et al., *Endogenous Wnt signalling in human embryonic stem cells generates an equilibrium of distinct lineage-specified progenitors.* Nature Communications, 2012. **3**.

29. Schmittgen, T.D. and K.J. Livak, *Analyzing real-time PCR data by the comparative C-T method.* Nature Protocols, 2008. **3**(6): p. 1101-1108.

CHAPTER 6:

CONCLUSION AND FUTURE DIRECTIONS

In this work, 3D suspension cultures were explored as an alternative culture platform for the large-scale production of hPSCs and their derivatives. Although various forms of 3D systems are available, a matrix/carrier-free cell aggregate approach was found to be the simplest and cost-effective method for the production of hPSCs. Also, from chapter 3, utilizing a conventional spinner flask (Corning polystyrene disposable spinner flask) was found to be more effective in the expansion of hPSCs than static suspension culture. However, stirred-agitation was mainly beneficial if the mixing condition prevents large aggregate formation over the course of the culture. As such, when we utilized the ProCulture glass spinner flask in chapter 4, production of hPSCs at moderate or high agitation rate was far superior to any of the agitation rate in conventional spinner flask system. The added side baffles in the ProCulture glass spinner flask enabled the production of a more uniformed sized aggregate to which resulted in an increase in cell yield. This result demonstrates that aggregate size has more influence on propagation than the reduction in viability due to higher agitation rates, albeit higher shear stress could be more detrimental downstream of hPSCs processes. Additional studies found that the critical size where the proliferation kinetics and even pluripotent markers start to decrease in around 400 μm and above. Taken together, the agitation conditions that produced a more homogeneous cell aggregate within 100-300 μm, where optimal growth and maintenance

of pluripotency was sustained, are expected to be an important parameter for scalable production of hPSCs in 3D suspension systems.

Another aspect of this work was to uncover possible mechanotransduction signaling proteins at work in dynamic suspension cultures. Since stem cells are capable of detecting and processing various physical forces in their microenvironment, it is expected that fluidic agitation would have some influence in altering signaling pathways of hPSCs. In this study, AKT activity was found to be a prominent mechanosensitive effector that was modulated in stirred suspension culture of hPSCs. Upon discovering this mechanosensitive effector, protocols for expansion and cardiomyocyte differentiation with respect to AKT activity was further optimized to produce over 90% hPSC-derived cardiomyocytes consistently. Structural characterization of these cardiomyocytes also suggests that the timing of induction cues and fluidic agitation could enhance maturation of hESC-derived cardiomyocyte. It is anticipated that our set of studies could provide useful implications for other culture designs and lead to more investigations of hPSCs mechanobiology in dynamic suspension cultures.

Future Directions

This research explores the possibility of harnessing the fluidic microenvironment to promote survival, self-renewal and direct differentiation of hPSCs. This research is potentially transformative because its success will enable new methods to tightly control downstream differentiation process of hPSCs and maximize cell yield while minimizing

cost. However, many issues still remains that need to be addressed to further the development of stirred suspension culture towards clinical applications.

Uncovering the shear distributions and flow properties could facilitate the scaling up of our suspension system to larger volumes. The spinner flask used in this study has a small working volume of 50 ml (125 mL max). If the culture was scaled up, more challenges would arise given the uncertainty in the flow regime for differently designed systems. This means that the optimal agitation rate for 50 ml may not transfer to the 100 ml or the 500 ml system. This aspect is crucial because as shown earlier, a slight change in agitation condition (e.g. 40 rpm and 60 rpm) could yield a significantly different result. As such, detailed characterization of the mixing properties in association with the culture outcomes of this study would help elucidate key parameters that must be controlled when scaling up.

As noted earlier, the optimal agitation condition for expansion of hPSCs in stirred suspension requires a balance between producing uniform cell aggregates below the critical size and limiting excessive force-related cell death. The balance is crucial because the transport parameters that control the aggregation dynamics also bestow shear stress that the cells experience. The total shear stress includes the local shear given by eddy viscosity, which is a function of the flow properties of the vessel. Therefore, to address the issue in scaling up, mathematical modeling of the flow properties in 50 mL volume at the optimal agitation rate would offer significant insight into determining this balance for larger spinner flask systems. In collaboration with Dr. Marko Princevac group in the Department of

Mechanical Engineering at UCR, we have begun this phase of development by combining the use of Particle Image Velocimetry (PIV) with computational fluid dynamics (CFD) modeling through ANSYS CFX program. However, this development is still in an early phase with many issues that need to be resolved. In particular, a more accurate analysis from the PIV is needed to enact a more accurate turbulence model (e.g., k-ω, k-ε, baseline Reynolds stress model) in the CFD. Once these issues are resolved, our effort in this direction should provide outstanding contributions to rationalize designs of larger bioreactors systems.

Another issue that must be addressed in the future development is in regards to mechanotransduction signaling mechanisms that promotes pluripotency or lineage-specific differentiation of hPSCs in 3D stirred suspension cultures. This study has only scratched the surface of how fluid agitation impact signaling pathways of hPSCs in suspension, but many more studies are needed given that signaling mechanisms may differ greatly between 3D suspension and 2D cultures. For instance, as mentioned earlier, pAKT is known to be essential for self-renewal in 2D methodologies, yet our data indicates that it may not be critical in 3D stirred suspension cultures. Reasons for why shear supports pluripotency without the need of pAKT should be further investigated. It could be possible that other mechanosensitive signaling pathways that mediate the effects of fluidic agitation on AKT activity are also responsible for supporting self-renewal.

Finally, our method of pausing agitation for cardiac differentiation showed promising results in improving efficiency and maturation, but more studies are needed to

fully understand the efficacy of this process. Such studies include 1) a detailed qPCR analysis to provide an extensive comparison of activated genes at different time points in each condition, 2) electrophysiology measurements to determine the functional characteristics of these hPSC-derived cardiomyocytes and 3) using iPSCs and other ESCs lines to address the interline variability of this method. A more crucial need of investigation now is understanding the signaling mechanisms behind this process. Clearly, pausing agitation at a specific time point is the key factor that allowed signaling pathways to take its course for differentiation. Although the overall mechanism is unclear, it is presumed that AKT activity governed by fluidic agitation attributed to this result. Ultimately, with more evidence of mechanotransduction mechanisms, this method could be further refined to enhance cardiomyocyte maturation, and even tailor protocols for differentiation towards other lineages including, but not limited to, pancreatic cells and motor neurons (Figures 6.1).

Overall, results presented in this work provide strong implications for an innovative approach for controlling expansion and differentiation of hPSCs in stirred suspension cultures.

Figure

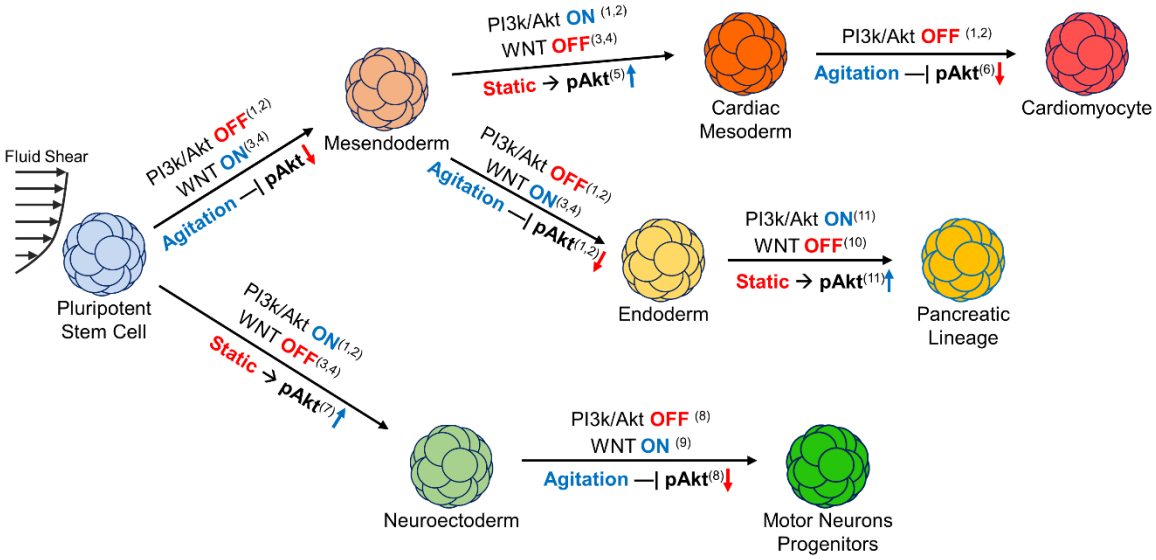

Figure 6.1. Possible mechanism of how shear-induced pathways could assist differentiation and lineage specification. Developed based on reported findings in [1-11].

References

1. Freund, C., D. Ward-van Oostwaard, J. Monshouwer-Kloots, et al., *Insulin redirects differentiation from cardiogenic mesoderm and endoderm to neuroectoderm in differentiating human embryonic stem cells.* Stem Cells, 2008. **26**(3): p. 724-33.
2. Vallier, L., T. Touboul, S. Brown, et al., *Signaling Pathways Controlling Pluripotency and Early Cell Fate Decisions of Human Induced Pluripotent Stem Cells.* Stem Cells, 2009. **27**(11): p. 2655-2666.
3. Menendez, L., T.A. Yatskievych, P.B. Antin, et al., *Wnt signaling and a Smad pathway blockade direct the differentiation of human pluripotent stem cells to multipotent neural crest cells (vol 108, pg 19240, 2011).* Proceedings of the National Academy of Sciences of the United States of America, 2012. **109**(23): p. 9220-9220.
4. Blauwkamp, T.A., S. Nigam, R. Ardehali, et al., *Endogenous Wnt signalling in human embryonic stem cells generates an equilibrium of distinct lineage-specified progenitors.* Nature Communications, 2012. **3**.
5. Klinz, F.J., W. Bloch, K. Addicks, et al., *Inhibition of phosphatidylinositol-3-kinase blocks development of functional embryonic cardiomyocytes.* Experimental Cell Research, 1999. **247**(1): p. 79-83.
6. Fischer, K.M., S. Din, N. Gude, et al., *Cardiac progenitor cell commitment is inhibited by nuclear Akt expression.* Circ Res, 2011. **108**(8): p. 960-70.
7. Keung, A.J., E.M. de Juan-Pardo, D.V. Schaffer, et al., *Rho GTPases mediate the mechanosensitive lineage commitment of neural stem cells.* Stem Cells, 2011. **29**(11): p. 1886-97.
8. Ojeda, L., J.L. Gao, K.G. Hooten, et al., *Critical Role of PI3K/Akt/GSK3 beta in Motoneuron Specification from Human Neural Stem Cells in Response to FGF2 and EGF.* Plos One, 2011. **6**(8).
9. Maury, Y., J. Come, R.A. Piskorowski, et al., *Combinatorial analysis of developmental cues efficiently converts human pluripotent stem cells into multiple neuronal subtypes.* Nat Biotechnol, 2015. **33**(1): p. 89-96.
10. Nostro, M.C., F. Sarangi, S. Ogawa, et al., *Stage-specific signaling through TGF beta family members and WNT regulates patterning and pancreatic specification of human pluripotent stem cells.* Development, 2011. **138**(5): p. 861-871.
11. Pezzolla, D., J. Lopez-Beas, C.C. Lachaud, et al., *Resveratrol Ameliorates the Maturation Process of beta- Cell-Like Cells Obtained from an Optimized Differentiation Protocol of Human Embryonic Stem Cells.* Plos One, 2015. **10**(3).

Appendix A

Power dissipation study in the 125 mL polystyrene disposable spinner flask based on Sen et al., 2002.

We attempt to replicate Sen et al. study so that we could translate the calculation to our stirred suspension culture and correlate our observed aggregate size with the power dissipated per unit mass.

Reported parameters for 125 mL Spinner Flask with PPRF-m4 Medium			
Volume Height	*H*	2.674	cm
Vessel Diameter	*D or* D_t	6.9	cm
Impeller Diameter	*d or* D_i	5.3	cm
Impeller Width (up to top of magnet)	*b or W*	1.8	cm
Kinematic Viscosity (@ 37C)	ν	8.60E-03	cm^2/s
Dynamic Viscosity (@ 37C)	μ	8.50E-01	cP
Density of Fluid	ρ	1.006	g/mL
Working Volume	*V*	100	mL or cm^3

Power Number (N_p) is given by:

$$Np = \frac{A}{Re} + B(Z)^p$$

Where:

$$Re = \frac{(N)(d^2)}{\nu}$$

$$A = 14 + \left(\frac{b}{D}\right)\left\{670\left(\frac{d}{D} - 0.6\right)^2 + 185\right\}$$

$$B = 10\text{^}\left\{1.3 - 4\left(\frac{b}{D} - 0.5\right)^2 - 1.14\left(\frac{d}{D}\right)\right\}$$

$$p = 1.1 + 4\left(\frac{b}{D}\right) - 2.5\left(\frac{d}{D} - 0.5\right)^2 - 7\left(\frac{b}{D}\right)^4$$

$$z = \left(\frac{10^3 + 1.2Re^{0.66}}{10^3 + 3.2Re^{0.66}}\right)$$

So from the specified parameters: H/D = 0.388
b/D = 0.261
d/D = 0.768

And therefore: *Coefficient A* = 67.20
Coefficient B = 1.57
Coefficient p = 1.93

Altogether,

Agitation Rate	*Rev/min (rpm)*	60	80	100	120
	Rev/sec (rps)	1	1.333	1.667	2
Reynolds number	*Re*	3.27E+03	4.36E+03	5.44E+03	6.53E+03
ln(Reynolds Number)	*ln(Re)*	8.091	8.379	8.602	8.785
$Re^{0.66}$		208.58	252.19	292.21	329.58
$z = \left(\frac{10^3 + 1.2Re^{0.66}}{10^3 + 3.2Re^{0.66}}\right)$		0.750	0.721	0.698	0.679
Power Number	*Np*	0.920	0.849	0.796	0.754
ln(Power Number)	*ln(Np)*	-0.083	-0.163	-0.228	-0.283

Power Consumed $P = (NP)(N^3)(d^5)(\rho)$		$P\ (cm^2g/s^3)$	3871.79	8469.30	15500.32	25361.09
Power Dissipated per unit Mass	$\varepsilon = \frac{(P)}{(V)(\rho)}$	$\varepsilon\ (cm^2/s^3)$	38.49	84.19	154.08	252.10
ln(ϵ)			3.628	4.485	5.151	5.696

These results showed similarities to Sen et al. report. In particular, the plot that demonstrates the relationship between Reynolds number and power number were close to their report and our result using their specific parameters. In addition, they report a power dissipation per unit mass value of 158.9 cm^2/s^3 for 100 rpm, and our replicated calculation resulted in 154.08 cm^2/s^3 for 100 rpm, further indicating the similarities. As such, we then apply our specific parameters to this calculation.

Parameters for our 125 mL polystyrene disposable spinner flask and mTeSR			
Volume Height	*H*	1.579	cm
Vessel Diameter	*D or* D_t	6.35	cm
Impeller Diameter	*d or* D_i	4.0	cm
Impeller Width (up to top of magnet)	*b or W*	1.5	cm
Kinematic Viscosity (@ 37C) (appendix B)	*v*	7.40E-03	cm2/s
Dynamic Viscosity (@ 37C) (appendix B)	*μ*	7.39E-04	Pa·s
Density of Fluid	ρ	0.9985	g/mL
Working Volume	*V*	50	mL or cm^3

And

H/D =	0.2486	*Coefficient A* =	57.842
b/D =	0.2362	*Coefficient B* =	2.012
d/D =	0.6299	*Coefficient p* =	1.981

Altogether,

Agitation Rate	*Rev/min (rpm)*	60	80	100	120
	Rev/sec (rps)	1	1.333	1.667	2
Reynolds number	*Re*	2.16E+03	2.88E+03	3.61E+03	4.33E+03
ln(Reynolds Number)	*ln(Re)*	7.679	7.967	8.190	8.372
$Re^{0.66}$		1.59E+02	1.92E+02	2.23E+02	2.51E+02
$z = \left(\frac{10^3 + 1.2Re^{0.66}}{10^3 + 3.2Re^{0.66}}\right)$		0.789	0.762	0.740	0.722
Power Number	*Np*	1.286	1.194	1.124	1.067
ln(Power Number)	*ln(Np)*	0.251	0.178	0.117	0.065

Power Consumed $P = (NP)(N^3)(d^5)(\rho)$	*P (cm^2g/s^3)*	1314.67	2894.68	5320.59	8730.33
Power Dissipated per unit Mass $\varepsilon = \frac{(P)}{(V)(\rho)}$	*ε (cm^2/s^3)*	26.33	57.98	106.57	174.87
ln(ϵ)		3.27	4.06	4.67	5.16

Appendix B

Kinematic viscosity Study

Density of MilliQ water at room temperature

	Volume (mL)	Mass (g)		Density (g/mL)
Trial 1:	10	9.97		0.997
Trial 2:	10	9.92		0.992
Trial 3:	5	4.96		0.992
			Average:	0.9937
			STDev.:	0.00289

Kinematic Viscosity of MilliQ water at 37°C Volume: 15 mL

Viscometer Constant @ 37°C: 0.00392763 mm^2/s^2, (cSt/s)

Efflux T:	min:sec	seconds	Kinematic Vis.	Viscosity (Pa·s)
Trial 1:	3:20	200	0.78553	0.000780551
Trial 2:	3:20	200	0.78553	0.000780551
Trial 3:	3:21	201	0.78945	0.000784454
		Average:	0.7868	7.82E-04
		STDev.:	0.00227	2.25E-06

Kinematic Viscosity of MilliQ water at 37°C Volume: 7 mL

Viscometer Constant @ 37°C: 0.00392763 mm^2/s^2, (cSt/s)

Efflux T:	Temp. (°C)	seconds	Kinematic Vis.	Viscosity (Pa·s)
Trial 1:	36.7	179	0.70305	0.000698594
Trial 2:	37.1	177	0.69519	0.000690788
Trial 3:	37.2	178	0.69912	0.000694691
Average:	37.00	178.00	0.6991	6.95E-04
STDev.:	0.26	1.00	0.00393	3.90E-06

Density of mTeSR at room temperature

	Volume (mL)	Mass (g)		Density (g/mL)
Trial 1:	10	10.065		1.0065
Trial 2:	10	9.99		0.999
Trial 3:	5	4.95		0.9900
			Average:	0.9985
			STDev.:	0.00826

Kinematic Viscosity of mTeSR at 37°C Volume: 15 mL

Viscometer Constant @ 37°C: 0.00392763 mm^2/s^2, (cSt/s)

Efflux T:	min:sec	seconds	Kinematic Vis.	Viscosity (Pa·s)
Trial 1:	3:33	213	0.83659	0.000835331
Trial 2:	3:34	214	0.84051	0.000839252
Trial 3:	3:34	214	0.84051	0.000839252
		Average:	0.8392	8.38E-04
		STDev.:	0.00227	2.26E-06

Kinematic Viscosity of mTeSR at 37°C Volume: 7 mL

Viscometer Constant @ 37°C: 0.00392763 mm^2/s^2, (cSt/s)

Efflux T:	Temp. (°C)	seconds	Kinematic Vis.	Viscosity (Pa·s)
Trial 1:	36.9	189	0.74232	0.000741209
Trial 2:	37.5	188	0.73839	0.000737287
Trial 3:	37.7	188	0.73839	0.000737287
Average:	37.37	188.33	0.7397	7.39E-04
STDev.:	0.42	0.58	0.00227	2.26E-06

Dynamic viscosity data obtained with help from Professor Tak-Sing Wong's Group at Penn State University.

Shear rate 1/s	Viscosity (Pa.s)					
	Milli-Q Water		mTeSR		DMEM + 10% FBS	
	Average	Stand. Dev.	Average	Stand. Dev.	Average	Stand. Dev.
0	7.84E-04	6.76E-06	8.31E-04	6.79E-06		
50	7.68E-04	6.6E-05	7.62E-04	9.7E-06	2.11E-03	7.4E-04
150	7.16E-04	2.5E-05	7.54E-04	9.5E-06	1.37E-03	2.9E-04
250	7.06E-04	1.7E-05	7.53E-04	9.6E-06	1.16E-03	1.7E-04
350	6.99E-04	1.4E-05	7.51E-04	9.6E-06	1.05E-03	1.1E-04
450	6.96E-04	1.4E-05	7.50E-04	8.9E-06	9.90E-04	8.1E-05
550	6.95E-04	1.5E-05	7.50E-04	8.6E-06	9.47E-04	6.3E-05
650	6.95E-04	1.6E-05	7.50E-04	8.5E-06	9.18E-04	5.2E-05
750	6.95E-04	1.7E-05	7.50E-04	8.0E-06	8.97E-04	4.5E-05
850	6.95E-04	1.8E-05	7.50E-04	8.1E-06	8.80E-04	3.9E-05
950	6.95E-04	1.8E-05	7.50E-04	9.0E-06	8.67E-04	3.5E-05
1050	6.95E-04	1.8E-05	7.50E-04	8.8E-06	8.56E-04	3.2E-05

Shear rate 1/s	Viscosity (Pa.s)					
	DMEM/F12 + 20% KOSR		Osteo Media		Osteo-Control	
	Average	Stand. Dev.	Average	Stand. Dev.	Average	Stand. Dev.
0						
50	2.14E-03	4.9E-04	2.88E-03	5.3E-04	2.67E-03	5.3E-04
150	1.38E-03	1.9E-04	1.65E-03	1.6E-04	1.57E-03	1.9E-04
250	1.19E-03	1.2E-04	1.34E-03	9.3E-05	1.29E-03	1.1E-04
350	1.09E-03	8.5E-05	1.20E-03	6.7E-05	1.15E-03	7.7E-05
450	1.04E-03	6.6E-05	1.12E-03	5.2E-05	1.08E-03	6.0E-05
550	9.97E-04	5.3E-05	1.06E-03	4.2E-05	1.03E-03	4.8E-05
650	9.69E-04	4.3E-05	1.03E-03	3.6E-05	9.92E-04	4.0E-05
750	9.48E-04	3.6E-05	9.96E-04	3.1E-05	9.65E-04	3.4E-05
850	9.31E-04	3.0E-05	9.73E-04	2.7E-05	9.46E-04	3.0E-05
950	9.18E-04	2.6E-05	9.55E-04	2.4E-05	9.29E-04	2.7E-05
1050	9.07E-04	2.2E-05	9.39E-04	2.1E-05	9.16E-04	2.4E-05

Shear rate 1/s	Shear Stress					
	Milli-Q Water		mTeSR		DMEM + 10% FBS	
	Average	Stand. Dev.	Average	Stand. Dev.	Average	Stand. Dev.
0	0.00E+00		0.00E+00		0.00E+00	
50	3.84E-02	3.3E-03	3.81E-02	4.8E-04	1.06E-01	3.7E-02
150	1.07E-01	3.8E-03	1.13E-01	1.4E-03	2.05E-01	4.4E-02
250	1.76E-01	4.3E-03	1.88E-01	2.4E-03	2.90E-01	4.3E-02
350	2.45E-01	4.8E-03	2.63E-01	3.3E-03	3.69E-01	4.0E-02
450	3.13E-01	6.1E-03	3.38E-01	4.0E-03	4.45E-01	3.6E-02
550	3.82E-01	8.2E-03	4.13E-01	4.7E-03	5.21E-01	3.5E-02
650	4.52E-01	1.0E-02	4.88E-01	5.5E-03	5.97E-01	3.4E-02
750	5.21E-01	1.3E-02	5.63E-01	6.0E-03	6.73E-01	3.4E-02
850	5.91E-01	1.5E-02	6.38E-01	6.9E-03	7.48E-01	3.3E-02
950	6.61E-01	1.7E-02	7.12E-01	8.6E-03	8.24E-01	3.3E-02
1050	7.30E-01	1.9E-02	7.87E-01	9.3E-03	8.99E-01	3.3E-02

Shear rate 1/s	Shear Stress					
	DMEM/F12 + 20% KOSR		Osteo Media		Osteo-Control	
	Average	Stand. Dev.	Average	Stand. Dev.	Average	Stand. Dev.
0	0.00E+00		0.00E+00		0.00E+00	
50	1.07E-01	2.5E-02	1.44E-01	2.6E-02	1.34E-01	2.7E-02
150	2.07E-01	2.8E-02	2.47E-01	2.4E-02	2.35E-01	2.8E-02
250	2.97E-01	2.9E-02	3.35E-01	2.3E-02	3.22E-01	2.8E-02
350	3.82E-01	3.0E-02	4.20E-01	2.3E-02	4.04E-01	2.7E-02
450	4.66E-01	3.0E-02	5.03E-01	2.3E-02	4.85E-01	2.7E-02
550	5.49E-01	2.9E-02	5.86E-01	2.3E-02	5.65E-01	2.6E-02
650	6.30E-01	2.8E-02	6.67E-01	2.3E-02	6.45E-01	2.6E-02
750	7.11E-01	2.7E-02	7.47E-01	2.3E-02	7.24E-01	2.6E-02
850	7.91E-01	2.6E-02	8.27E-01	2.3E-02	8.04E-01	2.5E-02
950	8.72E-01	2.4E-02	9.07E-01	2.3E-02	8.83E-01	2.5E-02
1050	9.52E-01	2.3E-02	9.86E-01	2.3E-02	9.62E-01	2.5E-02

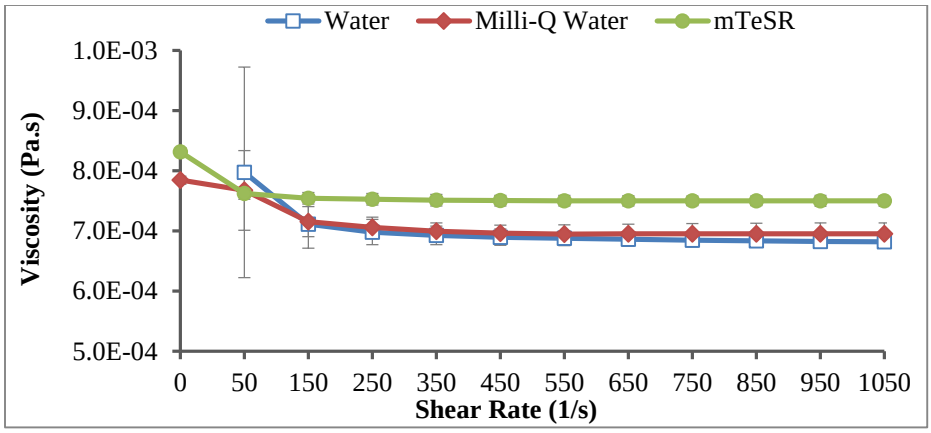
Water
Milli-Q Water
mTeSR
Viscosity (Pa.s)
1.0E-03
9.0E-04
8.0E-04
7.0E-04
6.0E-04
5.0E-04
0
50
150
250
350
450
550
650
750
850
950
1050
Shear Rate (1/s)

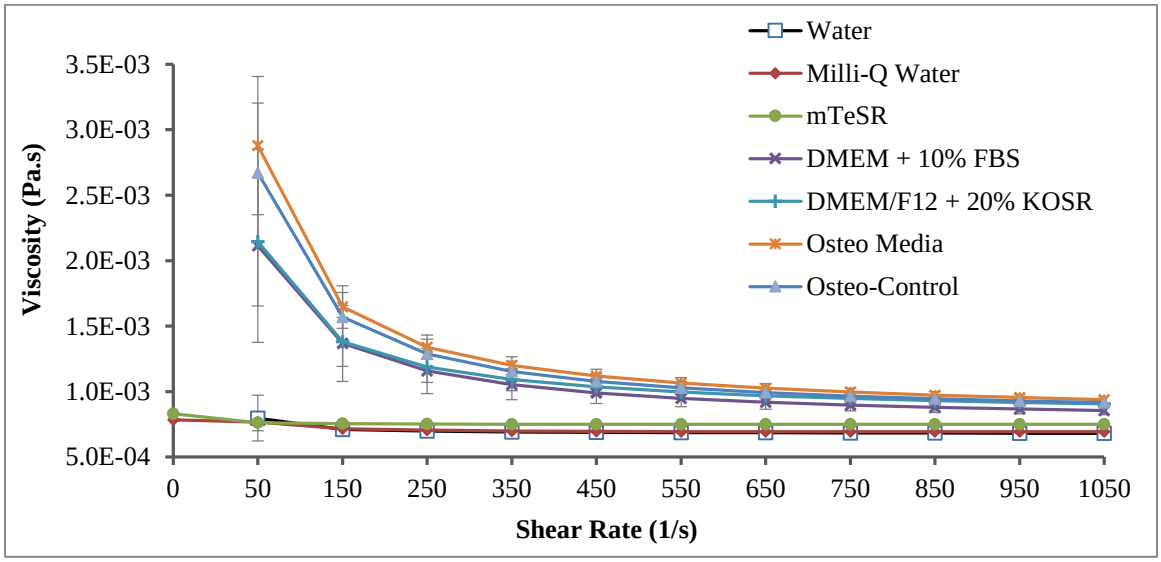
Water
Milli-Q Water
mTeSR
DMEM + 10% FBS
DMEM/F12 + 20% KOSR
Osteo Media
Osteo-Control
Viscosity (Pa.s)
3.5E-03
3.0E-03
2.5E-03
2.0E-03
1.5E-03
1.0E-03
5.0E-04
0
50
150
250
350
450
550
650
750
850
950
1050
Shear Rate (1/s)

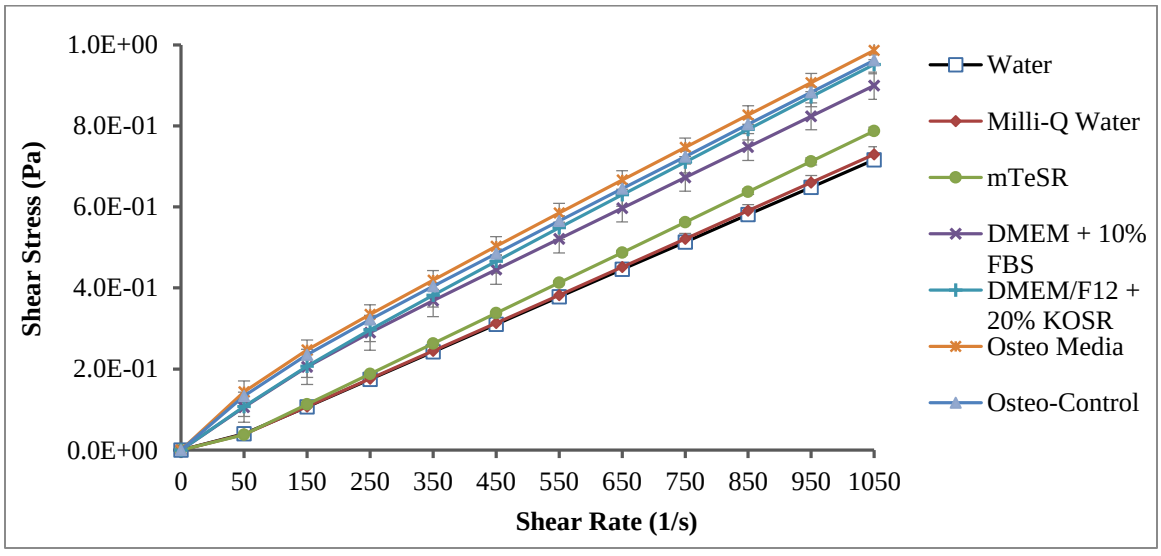
Shear Stress (Pa)
1.0E+00
8.0E-01
6.0E-01
4.0E-01
2.0E-01
0.0E+00
0
50
150
250
350
450
550
650
750
850
950
1050
Shear Rate (1/s)
Water
Milli-Q Water
mTeSR
DMEM + 10% FBS
DMEM/F12 + 20% KOSR
Osteo Media
Osteo-Control

Appendix C

Table S1. Antibodies for flow cytometry (FC), immunocytochemistry (ICC) and Western blot (WB)

Antibody	Source	Dilution
OCT4	Abcam, ab19857	1:200 (FC), 1:100 (ICC)
TRA-1-60	Invitrogen, 14880	1:200 (FC), 1:100 (ICC)
SSEA4	BD Pharmingen, 561565	1:200 (FC)
NANOG	Abcam, ab80892	1:100 (ICC)
Brachyury	R&D Systems AF2085	1:200 (FC)
α-actinin	Sigma-Aldrich, A7811	1:800 (FC), 1:500 (ICC)
Troponin I (cTnI)	Abcam, ab47003	1:100 (FC),
Troponin T (cTnT)	ThermoFisher, MS-295-P	1:200 (FC), 1:100 (ICC)
Myosin light chain 2a (MLC2a)	Synaptic Systems, 311 011	1:100 (ICC)
ACTIN	Abcam, ab8226	1:5000 (WB)
AKT	Cell Signaling Technology, 4691	1:2000 (WB)
p-AKT S473	Cell Signaling Technology, 9271	1:2000 (WB)
JNK1/2	Abcam, ab112501	1:2000 (WB)
p-JNK1/2 T135T137	Abcam, ab131499	1:2000 (WB)
ERK	Cell Signaling, 9102	1:2000 (WB)
p-ERK T202/Y204	Cell Signaling, 9101	1:2000 (WB)
CTNNB1	Life Technologies, 138400	1:1000 (WB)
Donkey Anti-Rabbit IgG	Abcam, ab150065 (Alexa Fluor 488)	1:500 (FC & ICC)
Donkey Anti-Mouse IgG	Abcam, ab150109 (Alexa Fluor 488) Invitrogen, A-21203 (Alexa Fluor 594)	1:500 (FC & ICC)
Goat Anti-Rat IgM	Invitrogen, A-21213 (Alexa Fluor 594)	1:500 (FC & ICC)
Anti-mouse IgG, HRP-linked IgG	Cell Signaling Technology, 7076	1:2000 (WB)
Anti-rabbit IgG, HRP-linked IgG	Cell Signaling Technology, 7074	1:2000 (WB)
Rabbit IgG	R&D Systems, AB-105-C	1:200 (FC), 1:100 (ICC)
Mouse IgG	Santa Cruz, sc-2025	1:200 (FC)

Table S2. RT-PCR genes

GENE	**TaqMan**
GAPDH	Hs02758991_g1
POU5F1 (OCT4)	HS00742896_s1
NANOG	Hs04260366_g1
SOX2	Hs01053049_s1
SOX17	Hs00751752_s1
GOOSECOID (GSC)	Hs009006630_g1
PAX6	Hs00240871_m1
Brachyury (T)	Hs00610080_m1
MYH6	Hs01101425_m1
MYH7	Hs01110632_m1